

THE UNIVERSITY OF CHICAGO

A HEDGEHOG-FGF SIGNALING CASCADE PATTERNS THE ANTERIOR-POSTERIOR
AXIS DURING EMBRYONIC DEVELOPMENT

A DISSERTATION SUBMITTED TO
THE FACULTY OF THE DIVISION OF THE BIOLOGICAL SCIENCES
AND THE PRITZKER SCHOOL OF MEDICINE
IN CANDIDACY FOR THE DEGREE OF
DOCTOR OF PHILOSOPHY

INTERDISCIPLINARY SCIENTIST TRAINING PROGRAM:
GENETICS, GENOMICS, AND SYSTEMS BIOLOGY

BY

ALEXANDER GUZZETTA

CHICAGO, ILLINOIS

AUGUST 2019

LIST OF FIGURES.....	V
LIST OF TABLES	VI
ACKNOWLEDGEMENTS	VII
ABSTRACT	IX
CHAPTER1: INTRODUCTION	1
OVERVIEW	1
INTRODUCTION TO THE PRIMARY SIGNALING PATHWAYS THAT DICTATE THE FORMATION AND PATTERNING OF THE A-P AXIS	1
COORDINATED CELL MOVEMENTS DURING GASTRULATION DICTATE CELL FATE DETERMINATION	4
THE ROLE OF HH SIGNALING IN EARLY EMBRYONIC PATTERNING	5
THE ROLE OF HH SIGNALING IN EARLY EXTRA-EMBRYONIC PATTERNING	6
THESIS SUMMARY	6
REFERENCES	8
CHAPTER 2: MATERIALS AND METHODS.....	13
ANIMAL HUSBANDRY GENOTYPING	13
SUPEROVULATION	13
EUTHANASIA AND EMBRYO COLLECTIONS	14
LACZ STAINING	14
RIBOPROBE DESIGN	15
IN VITRO TRANSCRIPTION	15
IN SITU HYBRIDIZATION	16
TRANSCRIPTIONAL PROFILING OF EARLY EMBRYOS	17
BULK RNA-SEQ DATA ANALYSIS	17
DROP-SEQ	18
MICROFLUIDIC CO-ENCAPSULATION OF CELLS AND BARCODED BEADS.....	18
SEQUENCING	19
RNA-SEQ DATA PROCESSING.....	19
MIGRATION ASSAY IN CHICKEN EMBRYO	22
REFERENCES	24
CHAPTER 3: A HEDGEHOG-FGF SIGNALING AXIS PATTERNS ANTERIOR MESODERM DURING GASTRULATION	25
CHAPTER 3 INTRODUCTION	25
CHAPTER 3 RESULTS	28
HEDGEHOG SIGNALING IS FIRST ACTIVE IN THE ORGANIZING CENTERS OF EMBRYONIC AXIS DETERMINATION	28

DROP-SEQ REVEALS ANTERIOR MESODERM DEFICIT IN HEDGEHOG SIGNALING MUTANTS	28
HH SIGNALING IS SELECTIVELY REQUIRED FOR ANTERIOR MESODERM DEVELOPMENT ..	31
HH RECEPTION BY CARDIAC PROGENITORS IS NOT REQUIRED FOR EARLY HEART DEVELOPMENT.....	32
HH-DEPENDENT ANTERIOR MESODERM LINEAGES DO NOT DIRECTLY RECEIVE HH SIGNALING	33
TRANSCRIPTIONAL PROFILING IDENTIFIED HH-DEPENDENT TRANSCRIPTION FACTORS AND SIGNALING PATHWAYS NECESSARY FOR MESODERM MORPHOGENESIS	34
HH-DEPENDENT TFs ARE ENRICHED FOR DETERMINANTS OF MESODERM MORPHOGENESIS AND SOMITOGENESIS.....	35
TRANSCRIPTIONAL PROFILING IDENTIFIED FGF SIGNALING DOWNSTREAM OF HH SIGNALING FOR ANTERIOR MESODERM MORPHOGENESIS.....	36
GASTRULATION CELL MIGRATION DEFECTS CAUSED BY HH PATHWAY ANTAGONISM ARE RESCUED BY FGF4	36
CHAPTER 3 DISCUSSION	38
REFERENCES.....	41
CHAPTER 4: HH SIGNALING IS REQUIRED FOR PROPER ERYTHROCYTE DIFFERENTIATION FROM HEMOGENIC PRECURSORS	68
CHAPTER 4 INTRODUCTION	68
INTRODUCTION TO HEMATOPOIESIS	68
THE ROLE OF HH SIGNALING IN BLOOD DEVELOPMENT	70
CHAPTER 4 RESULTS	72
TRANSCRIPTION OF BLOOD GENES IS SEVERELY DISRUPTED IN HH MUTANTS AFTER ORGANOGENESIS	72
SCRNA-SEQ OF HH MUTANT MESODERM REVEALS A PROPORTIONAL SHIFT FROM EMBRYONIC BLOOD TO HEMOGENIC PRECURSOR POPULATIONS	73
HH SIGNALING IS INVOLVED IN BLOOD PRECURSOR DEVELOPMENT FOR BOTH FIRST AND SECOND WAVE HEMOPOIESIS	74
CHAPTER 4 DISCUSSION	77
REFERENCES.....	80
CHAPTER 5: SYNTHESIS AND FUTURE DIRECTIONS	89
A NEW ROLE FOR HH SIGNALING IN A-P PATTERNING	89
MUCH OF A-P AXIS DETERMINATION AND PATTERNING IS DETERMINED BY EMBRYONIC ORGANIZERS.....	89
THE NODAL AND HH PATHWAYS HAVE SHARED FUNCTION IN A-P PATTERNING.....	92
DIFFERENTIAL ROLES FOR HH SIGNALING IN EMBRYONIC AND EXTRAEMBRYONIC MESODERM DEVELOPMENT.....	94
THE ROLE OF HH SIGNALING IN BLOOD AND ENDOTHELIAL DEVELOPMENT	95

ALTERNATIVE LINKS BETWEEN HH SIGNALING, ENDOTHELIAL DEVELOPMENT, AND ERYTHROCYTE DIFFERENTIATION.	97
CONCLUSION AND FUTURE DIRECTIONS	98
REFERENCES.....	101

LIST OF FIGURES

FIG. 3.1. SINGLE CELL RNA-SEQ IDENTIFIES HH-DEPENDENT SELECTIVE DEFECTS TO ANTERIOR MESODERM PROGENITOR POPULATIONS.	48
FIG. 3.2: HH SIGNALING IS REQUIRED FOR ANTERIOR MESODERM MORPHOGENESIS.....	50
FIG. 3.3: ANTERIOR MESODERM LINEAGES DO NOT RECEIVE HH SIGNALING DURING GASTRULATION.	52
FIG. 3.4: DISRUPTION OF HH SIGNALING CAUSES MAJOR DISRUPTIONS IN GENETIC PATHWAYS FOR MESODERM DEVELOPMENT.....	53
FIG. 3.5: TARGETED PATHWAY ANALYSIS REVEALS WIDESPREAD DYSFUNCTION OF NASCENT MESODERM AND FGF PATHWAYS.....	55
FIG. 3.6. HH SIGNALING IS REQUIRED FOR ANTERIOR CELL MIGRATION DURING GASTRULATION UPSTREAM OF THE FGF PATHWAY.	57
FIG. 3.7: MIDLINE HH SIGNALING FROM THE NODE DRIVES AN FGF PATHWAY FOR ANTERIOR MESODERM MORPHOGENESIS.	59
FIG. S3.1. CONSISTENT GENE AND UMI COUNTS ARE OBSERVED BETWEEN DROP-SEQ REPLICATES.	60
FIG. S3.2. DROP-SEQ ASSAY DETECTS ALL MESP1-DERIVED LINEAGES FROM MESP1CRE-SORTED CELLS.	61
FIG. S3.3. RE-CLUSTERING OF EMBRYONIC MESODERM IDENTIFIES ALL MESODERMAL SUB-LINEAGES BY CANONICAL MARKER EXPRESSION.....	62
FIG. S3.4. MESODERM CELL DISTRIBUTION IS HIGHLY CONSISTENT BETWEEN REPLICATES.	63
FIG. S3.5. PSEUDO-BULK CORRELATION ANALYSIS BETWEEN EMBRYONIC MESODERM AND EXTANT SCRNA-SEQ DATASETS.....	64
FIG. S3.6. UMAP PLOTS WITH NON-BATCH-CORRECTED SCRNA-SEQ DATA.	65
FIG. S3.7: CONDITIONAL REMOVAL OF SMO REVEALS THAT HH SIGNALING IS NOT REQUIRED IN SPECIFIED CARDIAC PRECURSORS FOR PROPER HEART DEVELOPMENT. .	66
FIG. 4.1. HH MUTANTS REVEAL AN ABSENCE OF BLOOD GENE EXPRESSION AFTER ORGANOGENESIS.	82
FIG. 4.2. SCRNA-SEQ OF MESP1-GLI3R MUTANT MESODERM DURING ORGANOGENESIS REVEALS INCREASE IN ENDOTHELIAL POPULATIONS AT THE EXPENSE OF BLOOD:	84
FIG. 4.3. SPECIFIC SUB-LINEAGES FOR BLOOD DEVELOPMENT ARE IDENTIFIED BY EXPRESSION OF CANONICAL MARKERS.....	86
FIG. S4.1. TRANSVERSE EMBRYO SECTION DISPLAYING ISH FOR GFP EXPRESSED UNDER A HH-DEPENDENT REPORTER ALLELE.....	88

LIST OF TABLES

TABLE S3.1: FATE MAP QUANTIFICATION FOR HH-RECEIVING CELLS DURING GASTRULATION SHOWS SPARSE AND STOCHASTIC CONTRIBUTION TO EARLY CARDIAC STRUCTURES.	67
---	----

ACKNOWLEDGEMENTS

This thesis is a product of scholarly work involving many members of the Moskowitz laboratory. Foremost, I would like to thank my mentor, Dr. Ivan Moskowitz, for the freedom and independence to pursue this project to its completion. I would also like to thank my thesis committee including Dr. Marcelo Nobrega, Dr. Marcus Clark, and especially my thesis committee chair Dr. Robert Ho for intellectual support throughout my graduate career. I would like to also thank Drs. Andrew Hoffmann and Junghun Kweon who helped form the foundation on which this work was based. I would like to thank past and present members of the lab including Dr. Jeffrey Steimle, Dr. Chul Kim, Dr. Michael Broman, Dr. Rajiv Nadadur, Kaitlyn Shen, Margaret Gadek, Jessica Jacobs-Li, Dr. Ariel Rydeen, Dr. Kohta Ikegami, Dr. Ozzana Burnicka-Turek, Sonja Lazarevic, Linsin Smith, Dr. Holly Yang, and Carlos Perez-Cervantes for support, reagents, and general help.

I would like to give a special thank you to Dr. Megan Rowton who helped me gain my footing in the world of developmental biology when I first joined the laboratory. Many of the original experiments that established the direction of my thesis work were aided by her generous help and support. I would also like to thank my previous undergraduate student Mervenaz Koska for her exceptional work and years-long technical and intellectual contributions to this project. I would also like to thank my current undergraduate student, Hunter Hidalgo, for his dedication and experimental support. It has been a great privilege to work with all of the talented scientists in the Moskowitz laboratory these past five years.

A portion of this work resulted from fruitful collaboration with scientists outside of the laboratory which I would like to specifically acknowledge. I would like to thank Dr. Sebastian Pott and Gurasees Bajaj for contributing to the Drop-seq Analysis. I would like to thank the Basu lab

including Dr. Oni Basu, Heather Eckhart, Rebecca Back, Stephanie Lozano, Dr. Susan Olalken for experimental support for the Drop-seq assays. I would also like to thank Drs. Michael Bressan and Anne Moon for contributing valuable embryology experience and experimental support to this project.

I would also like to thank the administrative support provided to me by the Medical Scientist Training Program in addition to the GGSB and DRSB graduate programs for their valuable funding and programming support throughout my graduate career.

I am especially grateful to several excellent teachers I had during my pre-graduate education who helped inspire me to pursue a career in science. These include: my High School A.P Biology teacher Wayne Garabedian who introduced me to the wider world of the biological sciences; my Advanced Science Topics Teachers Keri Wagnon and Bill vonFelton, who provided valuable mentorship for my state science fair project; and my undergraduate research mentor Dr. Alejandro Calderon-Urrea, who gave me the opportunity to begin my wet lab career and eventually achieve my goal of entering graduate school.

I would also like to thank my parents Susan Coleman Guzzetta and Dr. Richard Guzzetta who have given me constant support and guidance throughout my life—especially during my PhD work. Finally, I would like to thank my wife and partner, Deanna Arsala. She has been my guiding light for as long as I can remember and has been a constant source of support and motivation for everything I do. She has not only supported me as a partner but has also contributed feedback and much needed editorial support over the past five years. I owe much of my past and continued success to her.

ABSTRACT

The anterior-posterior (A-P) axis of the vertebrate body plan is established during gastrulation, as mesoderm is progressively generated and patterned by signaling from the posterior midline through the node and primitive streak. In this thesis, I describe a novel role for midline Hedgehog (Hh) signaling in the patterning of mesoderm lineages across the A-P axis. Single-cell transcriptome analysis of Hh-deficient mesoderm revealed selective deficits in anterior mesoderm populations that later translate to physical defects to anterior embryonic structures including the first pharyngeal arch, heart, and anterior somites. I found that Hh-dependent anterior mesoderm defects were cell non-autonomous to Hh-signal reception. Transcriptional profiling of Hh-deficient mesoderm during gastrulation revealed disruptions to both transcriptional patterning of the mesoderm and a key FGF signaling pathway for mesoderm migration. Finally, cellular migration during gastrulation was decreased by Hh pathway antagonism and could be restored by addition of FGF4 protein. Together, my findings define a novel midline Hh-FGF signaling axis during gastrulation required for A-P embryonic patterning.

Additionally, I observed a separate role for Hh signaling in the patterning of extraembryonic tissues involved in early blood formation. Hh-deficient mesoderm showed a severe downregulation of blood transcripts at E8.5 and an upregulation of endothelial genes. ScRNAseq confirmed that Hh mutants displayed sparse erythrocyte contribution and increased contribution to both hemogenic and non-hemogenic endothelium. Single-cell gene expression analysis revealed that Hh mutants showed proportional enrichment of hemogenic precursors that arise from both first and second wave hematopoiesis. This challenges the prevailing model which states that Hh mutations cause blood defects through a primary insufficiency of hemogenic

precursor development from nascent mesoderm. Rather, Hh mutants form sufficient hemogenic precursors but later experience impaired ability to differentiate into functional erythrocytes.

CHAPTER1: INTRODUCTION

Overview

One of the major intersections between classical biology and human congenital disease is developmental biology. A primary goal of this field is to discover links between the ontogeny of embryonic defects and the cellular and molecular mechanisms underpinning tissue formation. The embryonic origins of congenital defects are wide-ranging and include disruption across all key developmental processes including: lineage specification, proliferation, migration, differentiation, and embryonic patterning (1-5). The roles of signaling molecules are particularly important to this process as they allow a method of communication between cells during early development to induce cell fates and coordinated morphogenetic movements. In this thesis I will address novel mechanisms by which the Hedgehog (Hh) signaling affects early embryogenesis in two developmental contexts. First I investigate its role in the patterning of the anterior-posterior (A-P) embryonic axis and second, I interrogate its role in guiding blood development in the extraembryonic membranes.

Introduction to the primary signaling pathways that dictate the formation and patterning of the A-P axis

The first axis patterning event in the embryo is induced by TFG- β signaling, primarily through *Bmp4*, and determines the proximal-distal embryonic axis with respect to the maternal interface (6). Shortly thereafter, symmetry is broken across the A-P axis through combinatorial signaling from TFG- β , Fibroblast growth factor (FGF), and Wnt pathways at the posterior embryonic pole (7-15). This initiates the formation of an embryonic cleft in the posterior midline

of the embryo called the primitive streak through which cells migrate during gastrulation to form both embryonic mesoderm and endoderm lineages.

Mutations to the inductive TFG- β superfamily member *Bmp4* produces various phenotypes including the absence of mesoderm generation (6). Addition of Activin A and BMP4 have also been shown to be sufficient to induce various mesoderm lineages in time and dose-dependent manners from both embryonic stem cell-derived embryoid bodies and cultured epiblast cells (16). Although complete disruptions to the Nodal signaling pathway results in mesoderm agenesis (17-20), mild to moderate pathway disruptions result in anterior-selective defects (21). One study attempted to address the mechanism by which Nodal selectively patterns the anterior mesoderm through the generation of a chimeric embryo for *Nodal*. Although many *Nodal* mutants show anterior-selective defects, *Nodal*^{-/-} clones preferentially populated the anterior, rather than the posterior portion of the embryo after gastrulation (22). This counterintuitive result is further complicated by the fact that *Nodal*^{-/-} clones may receive NODAL from neighboring *Nodal*^{+/+} clones in chimeric embryos.

The canonical Wnt signaling pathway is both necessary and sufficient to generate embryonic mesoderm. *Wnt3*^{-/-} mutants, which have no Wnt signaling activity, fail to generate mesoderm (13) and, conversely, small molecule Wnt pathway activation induces mesoderm formation from pluripotent stem cells (23). Wnt signaling also plays a key, underappreciated role in A-P patterning as hypomorphic mutations to its canonical downstream transcription coactivator, β -catenin, results in an absence of anterior mesoderm fates (24). Unlike the *Nodal* pathway there is a dearth of genetic reagents in mammals to generate allelic series across major pathway components for early Wnt signaling which may reveal subtler influences. In zebrafish, activation of canonical Wnt signaling through addition of WNT3A during early gastrulation increases the

anterior mesoderm population of the cardiac field but inhibits crescent formation when added at later stages (25). Conversely, addition of a Wnt antagonist DKK1 reveals the opposite effect where it inhibits cardiac field formation when added early in gastrulation yet expands it when added at later stages of gastrulation(25). Although these experiments do not provide a precise mechanism to explain Wnt signaling's role in A-P patterning, they demonstrate that both the amount and timing of Wnt pathway activation determine cell behavior across the AP axis.

One signaling pathway that has a clear mechanism for the patterning of mesoderm is the FGF pathway. Although FGF activation has been shown to specify mesoderm (10, 26, 27), its primary role in early development is to control the deployment and coordinated migration of mesoderm precursors from the posterior embryonic pole to the anterior embryonic pole (10, 28). In mice, genetic disruption in the FGF pathway during gastrulation leads to phenotypes ranging from peri-implantation lethality in *Fgf4* null mutants which fail to form trophectoderm (29), to severe reductions in mesoderm generation as is the case in *Fgf8* and *FgfR1* mutants (10, 28). The FGF pathway has also been shown to play an active role in coordinating cell movements during gastrulation through both chemotaxis and downregulation of extracellular matrix proteins, such as EPCAM and through glycosaminoglycans (30-32). Direct effects of FGF ligands on chemotaxis-mediated cell migration has also been observed in chicken embryo explants using FGF4 and FGF8 ligands (32). The effect of FGF signaling on coordinated migration are particularly important as one of the strongest factors in lineage determination is the cellular context of post-migration cells in the embryo shortly after gastrulation (33, 34). This context is especially important for anterior mesoderm lineages which require a more robust migratory pathway to traverse the embryo in its entirety through the process of gastrulation (14).

Coordinated cell movements during gastrulation dictate cell fate determination

In mice, mesoderm migration occurs during gastrulation between embryonic day 6.5 (E6.5) and E7.5 as posterior epiblast cells migrate from the distal/posterior to the anterior/proximal embryonic axis (33-37). Lineage fate maps of the early gastrula reveal that the initial spatiotemporal location of epiblast cells has strong determinism on presumptive cell fate (33, 34). At E6.5, the first cells to migrate from the nascent streak exclusively populate the extraembryonic mesoderm which resides within the membranes of the yolk sac and are responsible for both the formation of endothelial and hemogenic cells (33). During the mid-streak stage, cells originating in the proximal streak continue to give rise to extraembryonic tissues while distal streak cells contribute to the anterior-most lineages of the embryonic mesoderm including the cranial, pharyngeal, cardiac, and somitic mesoderm (33, 34). Finally, cells that ingress through the primitive streak during late gastrulation at E7.5 demonstrate extraembryonic contribution to the allantois and posterior mesoderm from the proximal and distal streak respectively (33).

Despite the stereotyped nature of developmental trajectories *in situ*, cells continue to maintain high levels of multipotency throughout the end of gastrulation. This was demonstrated through orthotopic cell transplantation which removed cells from the cardiac field cells of late-gastrulation embryos and placed them back into the early primitive streak of early gastrulation embryos (34). Transplanted cells were more likely to adopt both the migratory trajectory and identity of their neighbors rather than their original fate trajectory. Conversely, pre-ingression epiblast cells can be induced towards cardiac fates when transplanted directly to the presumptive cardiac field (34). Although the source and nature of these signals are not well understood, many studies have shown the importance of antagonism towards the Wnt and TGF- β pathways from the anterior extraembryonic endoderm in directing cardiac cell fates (38-40).

Shortly after gastrulation ends, the embryo begins a process called organogenesis where the fates of cells across the embryo become rapidly restricted as tissues begin to differentiate (41). The first obvious sign of lineage-specific differentiation is at the onset of organogenesis—where specialized embryonic structures begin express genes related to tissue function in addition to cell fate determinants. During this developmental stage, the consequences to A-P axis patterning present themselves as selective defects in the development of either anterior or posterior organ systems. Classic hallmarks for disrupted anterior lineage formation include the disruption of head, heart, and pharyngeal mesoderm development while early posterior defects typically present themselves as truncations to the nascent tailbud (9, 42-45). In summary, the signaling pathways that control mesoderm formation at the primitive streak have undue influence on the eventual anterior-posterior pattern of early embryos.

The role of Hh signaling in early embryonic patterning

Although the role of Hh signaling in embryonic patterning has been well studied, its role in A-P axis patterning has not been previously described. The Hh pathway was first identified in a classic genetic screen in *Drosophila melanogaster* to determine factors responsible for A-P polarity within the segmented insect body plan (46). Decades later, Hh signaling has been shown to be necessary for patterning a large portion of mammalian tissues throughout development including the central nervous system, limbs, lungs, cartilage, teeth, hair, and heart (47-63). However, the role of Hh signaling in axis patterning has only been studied with respect to the left-right (L-R) axis determination from the Hh pathway activity in the node (64-68). In the work presented in chapter 3 of this thesis, I identified a previously unappreciated role for Hh signaling within the node for A-P axis determination.

The role of Hh signaling in early extra-embryonic patterning

Hh signaling also has a well-known role in patterning the early extraembryonic mesoderm through organizing vascular endothelium development in the yolk sac (69-73). Mutations to Hh signaling also cause defects to embryonic erythrocyte development which occurs in the yolk sac mesoderm (72). During early blood development, it is known that blood and endothelium development are closely linked as their progenitors express similar genes and form from extraembryonic mesoderm in the yolk sac (74). In first wave hematopoiesis, blood progenitors are mesenchymal cells which express both endothelial and hemogenic genes while second wave hematopoiesis occurs from yolk sac endothelium with hemogenic potential (74). Due to the requirement for Hh signaling in both blood and endothelial development, and the fact that blood cells develop from endothelial precursors, the current consensus in the field is that the role of Hh signaling in blood development is secondary to its role in endothelial development (69). However, in chapter 4 of this thesis, I provide evidence that both hemogenic and non-hemogenic endothelial cell specification is maintained in Hh mutants while only erythrocyte development is perturbed. This suggests a novel mechanism for Hh signaling in erythrocyte development where disruptions to Hh signaling block developmental transition from endothelial hemogenic precursors to mature erythrocytes.

Thesis Summary

In Chapter 3, I demonstrated a novel role for Hh signaling in directing mammalian A-P axis patterning. I found that reductions to Hh signaling in the early mesoderm leads to both a paucity of anterior mesoderm progenitors prior to organogenesis and later leads to anterior-

selective defects in anterior mesoderm derivatives. I also found that anterior lineages do not directly receive Hh signaling. Through transcriptional profiling Hh-deficient embryonic mesoderm shortly after the initiation of Hh signaling, I found disruptions to genetic pathways for the patterning and migration of nascent mesoderm. Furthermore, through the utilization of an *ex vivo* chicken model for gastrulation, I showed that Hh-dependent cell migration during gastrulation was likely responsible for the deficit in anterior mesoderm lineage disruption in Hh mutants.

In Chapter 4, I investigated the role of Hh signaling in early hematopoiesis. Unlike chapter 3, where I discuss the effect of Hh signaling on primarily embryonic mesoderm lineages, blood development occurs primarily within the extraembryonic membranes. First, I identified time and context-specific defects to two of the first phases in hematopoiesis by single cell RNA-seq (scRNA-seq). Specifically, I found that in both developmental contexts, Hh mutant cells are enriched in hemogenic precursor lineages at the expense of mature erythrocyte differentiation. This portion of the thesis directly contradicts the current model for the Hh pathway's role in blood development where it was previously thought that disruptions to Hh signaling inhibited erythrocyte development through the depletion of hemogenic precursors.

REFERENCES

1. Olson EN (2004) A decade of discoveries in cardiac biology. *Nat Med* 10(5):467-474.
2. Olson EN (2006) Gene regulatory networks in the evolution and development of the heart. *Science* 313(5795):1922-1927.
3. Srivastava D (2006) Making or breaking the heart: from lineage determination to morphogenesis. *Cell* 126(6):1037-1048.
4. Dunwoodie SL (2007) Combinatorial signaling in the heart orchestrates cardiac induction, lineage specification and chamber formation. *Semin Cell Dev Biol* 18(1):54-66.
5. Bruneau BG (2008) The developmental genetics of congenital heart disease. *Nature* 451(7181):943-948.
6. Winnier G, Blessing M, Labosky PA, & Hogan BL (1995) Bone morphogenetic protein-4 is required for mesoderm formation and patterning in the mouse. *Genes Dev* 9(17):2105-2116.
7. Lescroart F, *et al.* (2018) Defining the earliest step of cardiovascular lineage segregation by single-cell RNA-seq. *Science* 359(6380):1177-1181.
8. Tam PP & Loebel DA (2007) Gene function in mouse embryogenesis: get set for gastrulation. *Nat Rev Genet* 8(5):368-381.
9. Robb L & Tam PP (2004) Gastrula organiser and embryonic patterning in the mouse. *Semin Cell Dev Biol* 15(5):543-554.
10. Ciruna B & Rossant J (2001) FGF signaling regulates mesoderm cell fate specification and morphogenetic movement at the primitive streak. *Developmental Cell* 1(1):37-49.
11. Shi YQ, Katsev S, Cai C, & Evans S (2000) BMP signaling is required for heart formation in vertebrates. *Developmental Biology* 224(2):226-237.
12. Beppu H, *et al.* (2000) BMP type II receptor is required for gastrulation and early development of mouse embryos. *Dev Biol* 221(1):249-258.
13. Liu P, *et al.* (1999) Requirement for Wnt3 in vertebrate axis formation. *Nat Genet* 22(4):361-365.
14. Tam PP & Behringer RR (1997) Mouse gastrulation: the formation of a mammalian body plan. *Mech Dev* 68(1-2):3-25.
15. Rossant J, Ciruna B, & Partanen J (1997) FGF signaling in mouse gastrulation and anteroposterior patterning. *Cold Spring Harb Symp Quant Biol* 62:127-133.
16. Kattman SJ, *et al.* (2011) Stage-specific optimization of activin/nodal and BMP signaling promotes cardiac differentiation of mouse and human pluripotent stem cell lines. *Cell Stem Cell* 8(2):228-240.
17. Conlon FL, *et al.* (1994) A primary requirement for nodal in the formation and maintenance of the primitive streak in the mouse. *Development* 120(7):1919-1928.
18. Conlon FL, Barth KS, & Robertson EJ (1991) A novel retrovirally induced embryonic lethal mutation in the mouse: assessment of the developmental fate of embryonic stem cells homozygous for the 413.d proviral integration. *Development* 111(4):969-981.

19. Iannaccone PM, Zhou X, Khokha M, Boucher D, & Kuehn MR (1992) Insertional mutation of a gene involved in growth regulation of the early mouse embryo. *Dev Dyn* 194(3):198-208.
20. Zhou X, Sasaki H, Lowe L, Hogan BL, & Kuehn MR (1993) Nodal is a novel TGF-beta-like gene expressed in the mouse node during gastrulation. *Nature* 361(6412):543-547.
21. Xu C, Liguori G, Persico MG, & Adamson ED (1999) Abrogation of the Cripto gene in mouse leads to failure of postgastrulation morphogenesis and lack of differentiation of cardiomyocytes. *Development* 126(3):483-494.
22. Lu CC & Robertson EJ (2004) Multiple roles for Nodal in the epiblast of the mouse embryo in the establishment of anterior-posterior patterning. *Dev Biol* 273(1):149-159.
23. Burridge PW, *et al.* (2014) Chemically defined generation of human cardiomyocytes. *Nat Methods* 11(8):855-860.
24. Haegel H, *et al.* (1995) Lack of beta-catenin affects mouse development at gastrulation. *Development* 121(11):3529-3537.
25. Ueno S, *et al.* (2007) Biphasic role for Wnt/beta-catenin signaling in cardiac specification in zebrafish and embryonic stem cells. *Proc Natl Acad Sci U S A* 104(23):9685-9690.
26. Fletcher RB & Harland RM (2008) The role of FGF signaling in the establishment and maintenance of mesodermal gene expression in *Xenopus*. *Dev Dyn* 237(5):1243-1254.
27. Barron M, Gao M, & Lough J (2000) Requirement for BMP and FGF signaling during cardiogenic induction in non-precardiac mesoderm is specific, transient, and cooperative. *Dev Dyn* 218(2):383-393.
28. Sun X, Meyers EN, Lewandoski M, & Martin GR (1999) Targeted disruption of *Fgf8* causes failure of cell migration in the gastrulating mouse embryo. *Gene Dev* 13(14):1834-1846.
29. Tanaka S, Kunath T, Hadjantonakis AK, Nagy A, & Rossant J (1998) Promotion of trophoblast stem cell proliferation by FGF4. *Science* 282(5396):2072-2075.
30. Ciruna B & Rossant J (2001) FGF signaling regulates mesoderm cell fate specification and morphogenetic movement at the primitive streak. *Dev Cell* 1(1):37-49.
31. Sun X, Meyers EN, Lewandoski M, & Martin GR (1999) Targeted disruption of *Fgf8* causes failure of cell migration in the gastrulating mouse embryo. *Genes Dev* 13(14):1834-1846.
32. Yang XS, Dormann D, Munsterberg AE, & Weijer CJ (2002) Cell movement patterns during gastrulation in the chick are controlled by chemotaxis mediated by positive and negative FGF4 and FGF8. *Developmental Cell* 3(3):425-437.
33. Kinder SJ, *et al.* (1999) The orderly allocation of mesodermal cells to the extraembryonic structures and the anteroposterior axis during gastrulation of the mouse embryo. *Development* 126(21):4691-4701.
34. Tam PP, Parameswaran M, Kinder SJ, & Weinberger RP (1997) The allocation of epiblast cells to the embryonic heart and other mesodermal lineages: the role of ingression and tissue movement during gastrulation. *Development* 124(9):1631-1642.

35. Singh BN, *et al.* (2018) A conserved HH-Gli1-Mycn network regulates heart regeneration from newt to human. *Nat Commun* 9(1):4237.
36. Parameswaran M & Tam PP (1995) Regionalisation of cell fate and morphogenetic movement of the mesoderm during mouse gastrulation. *Dev Genet* 17(1):16-28.
37. Lawson KA, Meneses JJ, & Pedersen RA (1991) Clonal analysis of epiblast fate during germ layer formation in the mouse embryo. *Development* 113(3):891-911.
38. Brown K, *et al.* (2010) eXtraembryonic ENdoderm (XEN) stem cells produce factors that activate heart formation. *PLoS One* 5(10):e13446.
39. Liu W, Brown K, Legros S, & Foley AC (2012) Nodal mutant eXtraembryonic ENdoderm (XEN) stem cells upregulate markers for the anterior visceral endoderm and impact the timing of cardiac differentiation in mouse embryoid bodies. *Biol Open* 1(3):208-219.
40. Niakan KK, Schrode N, Cho LT, & Hadjantonakis AK (2013) Derivation of extraembryonic endoderm stem (XEN) cells from mouse embryos and embryonic stem cells. *Nat Protoc* 8(6):1028-1041.
41. Ibarra-Soria X, *et al.* (2018) Defining murine organogenesis at single-cell resolution reveals a role for the leukotriene pathway in regulating blood progenitor formation. *Nat Cell Biol* 20(2):127-134.
42. Cunningham TJ, *et al.* (2017) Id genes are essential for early heart formation. *Genes Dev* 31(13):1325-1338.
43. Arnold SJ & Robertson EJ (2009) Making a commitment: cell lineage allocation and axis patterning in the early mouse embryo. *Nat Rev Mol Cell Biol* 10(2):91-103.
44. Lu CC, Brennan J, & Robertson EJ (2001) From fertilization to gastrulation: axis formation in the mouse embryo. *Curr Opin Genet Dev* 11(4):384-392.
45. Ding J, *et al.* (1998) Cripto is required for correct orientation of the anterior-posterior axis in the mouse embryo. *Nature* 395(6703):702-707.
46. Nusslein-Volhard C & Wieschaus E (1980) Mutations affecting segment number and polarity in *Drosophila*. *Nature* 287(5785):795-801.
47. Rowton M, *et al.* (2018) Hedgehog signaling controls progenitor differentiation timing during heart development. *bioRxiv*.
48. Tickle C & Towers M (2017) Sonic Hedgehog Signaling in Limb Development. *Front Cell Dev Biol* 5:14.
49. Briscoe J & Therond PP (2013) The mechanisms of Hedgehog signalling and its roles in development and disease. *Nat Rev Mol Cell Biol* 14(7):416-429.
50. Robbins DJ, Fei DL, & Riobo NA (2012) The Hedgehog signal transduction network. *Sci Signal* 5(246):re6.
51. Balaskas N, *et al.* (2012) Gene regulatory logic for reading the Sonic Hedgehog signaling gradient in the vertebrate neural tube. *Cell* 148(1-2):273-284.
52. Hoffmann AD, Peterson MA, Friedland-Little JM, Anderson SA, & Moskowitz IP (2009) sonic hedgehog is required in pulmonary endoderm for atrial septation. *Development* 136(10):1761-1770.

53. Goddeeris MM, *et al.* (2008) Intracardiac septation requires hedgehog-dependent cellular contributions from outside the heart. *Development* 135(10):1887-1895.
54. Ingham PW & Placzek M (2006) Orchestrating ontogenesis: variations on a theme by sonic hedgehog. *Nat Rev Genet* 7(11):841-850.
55. Yamagishi C, *et al.* (2006) Sonic hedgehog is essential for first pharyngeal arch development. *Pediatr Res* 59(3):349-354.
56. Harfe BD, *et al.* (2004) Evidence for an expansion-based temporal Shh gradient in specifying vertebrate digit identities. *Cell* 118(4):517-528.
57. Scherz PJ, Harfe BD, McMahon AP, & Tabin CJ (2004) The limb bud Shh-Fgf feedback loop is terminated by expansion of former ZPA cells. *Science* 305(5682):396-399.
58. St-Jacques B, Hammerschmidt M, & McMahon AP (1999) Indian hedgehog signaling regulates proliferation and differentiation of chondrocytes and is essential for bone formation. *Genes Dev* 13(16):2072-2086.
59. Wechsler-Reya RJ & Scott MP (1999) Control of neuronal precursor proliferation in the cerebellum by Sonic Hedgehog. *Neuron* 22(1):103-114.
60. St-Jacques B, *et al.* (1998) Sonic hedgehog signaling is essential for hair development. *Curr Biol* 8(19):1058-1068.
61. Amthor H, Christ B, Weil M, & Patel K (1998) The importance of timing differentiation during limb muscle development. *Curr Biol* 8(11):642-652.
62. Pepicelli CV, Lewis PM, & McMahon AP (1998) Sonic hedgehog regulates branching morphogenesis in the mammalian lung. *Curr Biol* 8(19):1083-1086.
63. Lee J, Platt KA, Censullo P, & Ruiz i Altaba A (1997) Gli1 is a target of Sonic hedgehog that induces ventral neural tube development. *Development* 124(13):2537-2552.
64. Gao L, *et al.* (2018) Large Cardiac Muscle Patches Engineered From Human Induced-Pluripotent Stem Cell-Derived Cardiac Cells Improve Recovery From Myocardial Infarction in Swine. *Circulation* 137(16):1712-1730.
65. Zhang XM, Ramalho-Santos M, & McMahon AP (2001) Smoothed mutants reveal redundant roles for Shh and Ihh signaling including regulation of L/R symmetry by the mouse node. *Cell* 106(2):781-792.
66. Monsoro-Burq A & Le Douarin NM (2001) BMP4 plays a key role in left-right patterning in chick embryos by maintaining Sonic Hedgehog asymmetry. *Mol Cell* 7(4):789-799.
67. Tsukui T, *et al.* (1999) Multiple left-right asymmetry defects in Shh(-/-) mutant mice unveil a convergence of the shh and retinoic acid pathways in the control of Lefty-1. *Proc Natl Acad Sci U S A* 96(20):11376-11381.
68. Meyers EN & Martin GR (1999) Differences in left-right axis pathways in mouse and chick: functions of FGF8 and SHH. *Science* 285(5426):403-406.
69. Kim PG, *et al.* (2013) Signaling axis involving Hedgehog, Notch, and Scl promotes the embryonic endothelial-to-hematopoietic transition. *Proc Natl Acad Sci U S A* 110(2):E141-150.

70. Gering M & Patient R (2005) Hedgehog signaling is required for adult blood stem cell formation in zebrafish embryos. *Dev Cell* 8(3):389-400.
71. Vokes SA, *et al.* (2004) Hedgehog signaling is essential for endothelial tube formation during vasculogenesis. *Development* 131(17):4371-4380.
72. Byrd N, *et al.* (2002) Hedgehog is required for murine yolk sac angiogenesis. *Development* 129(2):361-372.
73. Dyer MA, Farrington SM, Mohn D, Munday JR, & Baron MH (2001) Indian hedgehog activates hematopoiesis and vasculogenesis and can respecify prospective neurectodermal cell fate in the mouse embryo. *Development* 128(10):1717-1730.
74. Lacaud G & Kouskoff V (2017) Hemangioblast, hemogenic endothelium, and primitive versus definitive hematopoiesis. *Exp Hematol* 49:19-24.

CHAPTER 2: MATERIALS AND METHODS

Animal husbandry genotyping

All animals were housed in a barrier facility at the University of Chicago Animal Resource Center. Mice were genotyped by PCR using genomic DNA extracted by incubating tail clips or embryonic tissue in a 50mM NaOH solution at 98°C for 45 minutes; prior to genotyping, crude DNA extracts were neutralized with a 10mM Tris-HCL pH 8 solution. Genotyping protocols were based on the conditions the Jackson Laboratory provided corresponding to each locus, including primer sequences and thermocycler conditions.

Superovulation

For large-scale mouse timed pregnancies 21-35 days old female mice were injected intraperitoneally (IP) with 5 units of pregnant mares serum (PMS) (EMD Chemicals) in 0.9% saline between noon and 4 PM. 46-48 hours after the PMS injection, mice received a second IP injection with 5 units of human chorionic gonadotropin (HCG) (Sigma). Immediately after injection females were placed into the cages of stud males, 8 weeks of age or older. The noon of the day a vaginal plug was observed was designated E0.5. For all other embryo collections, female mice of 6-16 weeks were housed with stud males of 8 weeks or older until the detection of a vaginal plug at noon the next day (E0.5). For lineage tracing experiments, mice were treated with 2 mg of tamoxifen (MP Biomedicals) mixed in a 2:1 ratio with progesterone by (Sigma) intraperitoneal injection.

Euthanasia and embryo collections

These studies were performed using embryos harvested from pregnant dams by terminal dissection. Females were euthanized by CO₂ asphyxiation, followed by cervical dislocation. After this, careful dissections of embryos ranging from E7.5 to E10.5 were performed in phosphate-buffered saline (1xPBS). Specimens were incubated in 4% paraformaldehyde (4% PFA):PBST overnight and consequently dehydrated with washes containing 50% Methanol (MeOH):PBST followed by two washes in 100% MeOH and stored at -20°C until processed for ISH. Slightly different protocols were followed for LacZ staining, RNA-Seq and ATAC-seq experiments following dissection, which will be described below.

LacZ staining

For LacZ staining experiments, embryos were fixed in 4% PFA for 20 minutes with gentle rocking at 4 °C. Embryos were washed 3 times for 5 minutes in 1X PBS. They were then incubated overnight at 37°C with staining solution. Staining solutions were comprised of 5ml of 1x PBS, 1.5ml of 5M NaCl, 50µl of 1M MgCl₂, 1.5 ml of 10% TX-100, 500 µl of 0.5M Potassium ferricyanide, 500 µl of 0.5M Potassium ferrocyanide in 50 ml of total volume. X-gal solution (100mg/ml in DMF) (RPI Corp) stored in -20°C in light-impermeable containers was added at a concentration of 1:100 immediately prior to staining. In the morning, the embryos were washed three times with 1xPBS and re-fixed in 4% PFA for one hour at room temperature. They were washed again following fixation, stored in 1xPBS and imaged with Leica MZ 16F microscope.

Riboprobe design

Probe templates were amplified using primers for partial cDNA sequences. Transcript mRNA templates were taken from the NCBI refseq. Primers were designed to amplify partial cDNAs between 400-1000 base pairs long, with 45-55% GC content. On the 5' end of the downstream (antisense) primer, the sequence 5'-CTAATACGACTCACTATAGGGAGA-3' was added. This served as the minimal promoter site for T7 to increase the efficiency of the transcription reaction. The PCR product was ran on a 0.8% TAE gel and amplicons of the correct predicted sizes were isolated using QIAquick gel extraction kit (Qiagen). For the genes that PCR primers failed to reliably amplify off of cDNA templates, we utilized the commercially available Gibson assembly service (gBlocks) provided by Integrated DNA Technologies. 440 base pairs from mRNA sequences were chosen to design the gBlock, with paired gateway sites comprised of an Attb1 (GGGGACAAGTTTGTACAAAAAAGCAGGC) site upstream and Attb2-(GACCCAGCTTTCTTGTACAAAGTGGTCCCC) site downstream of the gBlock fragment. gBlock fragments were cloned into pDonor using BP clonase (Invitrogen). The reaction components were incubated 3 hours at room temperature. 1µl of ProK was added and the mix was incubated for 10 min at 37°C to stop the reaction. Gateway clones were then transformed into competent dh5α bacteria (Invitrogen). Plasmids were then isolated and clones were validated by Sanger sequencing performed at the University of Chicago Sequence Facility.

In vitro transcription

In vitro transcription of dioxigenin-labeled riboprobe was performed with 1 µg linearized plasmid template or 200 ng PCR template acquired as described in the steps above. 2 µl 10x

transcription buffer (Ambion), 2 μ l 10x Dig labeling mix (Roche) and 2 μ l T7 (Thermo), T3 (Roche) or SP6 (Ambion) RNA polymerase in 20 μ l reactions. The mixture was incubated at least for 2 hours at 37°C. To stop the reaction, 1 μ l TURBO DNase I (Ambion) was added and the mix was incubated at 37°C for 15 minutes. IVT reactions were brought to 50 μ l in volume and precipitated by addition of 5 μ l of 3M NaOAc pH5.2, and 125 μ l of 100% EtOH and incubation at -20 °C overnight.

In situ hybridization

MeOH-dehydrated embryos were rehydrated in the following series: 75% MeOH, 50% MeOH, 25% MeOH in 1x PBST with 5-minute washes. Embryos were permeabilized with 1 μ l per 4 ml ProK (Invitrogen) for 1 minute at 37°C. Specimens were then incubated in glycine, post-fixed in 0.2% glutaraldehyde/4% paraformaldehyde and hybridized overnight at 65 °C in solution containing 50% formamide, 5X SSC, 1% SDS, 0.5 mg/ml tRNA (Gibco), 0.5 mg/ml Heparin (Sigma), and 100 ng/ml antisense riboprobe. Post-hybridization, embryos were washed in solution containing 50% formamide, 4X SSC and 1% SDS at 65°C, followed by washes in solution containing 500mM NaCl, 10 mM Tris 7.5 and 0.1% Tween-20. Embryos were incubated in 100 μ g/ml RNase A (Sigma) for 30 minutes at 37 °C. The embryos were then washed in MABTL made with 100mM Maleic Acid (Sigma) pH7.5, 150 mM NaCl, 0.1% Tween-20, 2mM Levamisole (Sigma), and blocked in 10% sheep serum (Sigma) and 2% Boehringer Mannheim Blocking Reagent (Roche) in MABTL. Alkaline phosphatase-conjugated anti-dioxigenin FAB (Roche) fragments were then added to a solution of 1% sheep serum and 2% Boehringer Mannheim Blocking Reagent in MABTL allow for detection of the probe. Embryos were then washed at least 10 times in MABTL remove non-specific antibody binding. The next day, the embryos were

washed in NTMTL made with 100mM NaCl, 100mM Tris, pH 9.5, 50 mM MgCl₂, 0.1% Tween-20 and 2mM levamisole, and then placed into color reaction with BM purple (Roche) between 4 hours and overnight at room temperature. When the color reaction was completed, the embryos were washed in PBST and post-fixed in 4% PFA. The embryos then went through washes of glycerol gradient and stored in 80% glycerol at 4°C for easier handling later during imaging.

Transcriptional Profiling of Early Embryos

Embryos used for bulk transcriptome profiling were dissected at E7.5 in 1x PBS, pooled with their littermates and dissociated with TrypLE reagent for 5 minutes at 37°C shaking at 1,400rpm in a Fisher Thermomixer followed by inactivation by addition of 10% FBS. Cells were spun down at 800 x g for 5 minutes and re-suspended in 10% FBS with a Near-IR dead dye (Life Technologies) for 30 minutes prior to sorting in order to assess cell viability. 1000 live cells were sorted directly into cell lysis buffer from either the tdTomato or YFP channel for biological replicates of wild type and mutant cells respectively. cDNAs libraries were generated using SMARTer Ultra Low RNA Kit for Illumina sequencing (Clontech) and sequencing libraries were constructed using Nextera XT DNA Library Preparation Kit (Illumina). Quality control was performed both after cDNA synthesis and library preparation using Bioanalyzer (Agilent). RNA-seq Libraries were sequenced on the HiSeq2500 in the University of Chicago Functional Genomics Facility.

Bulk RNA-seq Data Analysis

FASTQ files were aligned to the mm9 *mus musculus* genome using TopHat running standard parameters. FeatureCounts in SubRead package were used to generate read counts from

the aligned bam files and subsequently analyzed using edgeR for differential expression. Significantly differentially expressed genes were identified using a Benjamini-Hochberg (1) corrected statistical thresholds of $FDR \leq 0.10$. Differentially expressed genes were also used to identify associated gene ontology (GO) terms using Panther classification system (2).

Drop-seq

Microfluidic Co-encapsulation of Cells and Barcoded Beads

For **Drop-seq**, 2 mL of cells at 100,000 cells/mL in PBS-BSA was loaded in a 3 mL syringe (BD, #309657). A 125 μm Drop-seq microfluidic device was used for droplet generation (3). DNA barcoded beads (ChemGenes, Macosko-2011-10(V+)) were washed, filtered, and suspended in Drop-seq lysis buffer, at 120,000 beads/mL and kept in suspension under constant stirring using a magnetic tumble stirrer and flea magnet (V&P Scientific, VP 710 Series, VP 782N-3-150). Beads and cells were co-flowed into the device, each at 4 mL/hr, along with a surfactant-oil mix (BioRad, #1864006) at 16 mL/hr that was loaded into a 10 mL syringe (BD, #302995) and used as the outer carrier oil phase. Reverse emulsions droplets were generated at ~ 2000 drops/sec and collected in two batches of 15 minutes each in 50 mL tubes (Genesee Scientific, #28-106). After collection, the standard Drop-seq protocol for bead recovery, washing, and reverse transcription was followed (3). After washes and DNaseI treatment as per Drop-seq protocol (3), cDNA amplification was performed on 75,000 RNA-DNA barcode bead conjugates in a 96-well plate (Genesee Scientific, #24-302) loaded at 5000 beads per well, for a total of 15-35 wells and amplified for 14 PCR cycles using template switching (3). Post-PCR cleanup was performed by removing the STAMPs (Single Transcriptome Attached to Micro-Particles) (3) and pooling the supernatant from the wells together into a single 1.7 mL tube (Genesee Scientific, #22-281LR) along with 0.6X Ampure XP

beads (Beckman Coulter, #A63880). After adding the Ampure beads to the PCR product, the tube was incubated at room temperature for 2 minutes on a thermomixer (Eppendorf Thermomixer C, #5382000023) set to 1250 rpm, and for another 2 minutes on bench for stationary incubation. Next, the tube was placed on a magnet, and 4X 80% ethanol washes were performed with 1 mL ethanol added in each wash. cDNA was eluted in 150 μ L of water and the concentration and library size were measured using Qubit 3 fluorometer (Thermo Fisher) and BioAnalyzer High Sensitivity Chip (Agilent, #5067-4626). A BioAnalyzer trace is provided in Figure 5C as an example of the amplified transcriptome obtained from a typical Drop-seq run. 450 pg of the cDNA library was used in Nextera Library prep, instead of 650 pg as suggested in the Drop-seq protocol (3) to obtain Nextera libraries between 300 – 600 bp.

Sequencing

Sample libraries were loaded at \sim 1.5 pM concentration and sequenced on an Illumina NextSeq 500 using the NextSeq 75 cycle v3 kits for paired-end sequencing. 20 bp were sequenced for Read 1, 60 bp for Read 2 using Custom Read 1 primer, GCCTGTCCGCGGAAGCAGTGGTATCAACGCAGAGTAC (3), according to manufacturer's instructions. Illumina PhiX Control v3 Library was added at 5% of the total loading concentration for all sequencing runs. Each sample was sequenced on 1 or 2 lanes to a total of \sim 350 – 600 million reads.

RNA-Seq Data Processing

Each sequencing run produced paired-end reads, with one pair representing the 12 bp cell barcode and 8 bp unique molecular identifier (UMI), and the second pair representing a 60 bp mRNA

fragment (3). We utilized a pipeline (4) based on Snakemake (5) that processed raw sequencing data to produce an expression matrix corresponding to the UMI of each gene in each cell (github.com/aselewa/dropseq_pipeline). Briefly, the pipeline initially performs *FastQC* to obtain a report of read quality. Next, it creates a whitelist of cell barcodes using *umi_tools* (6) (version 0.5.3), based on the expected cell number per run (set to 7500 cells for this study). Next the cell barcode and UMI are extracted from read 1, and added to the name string of read 2 which represents the sequenced cDNA. This FASTQ file contains only the cell barcodes found in the whitelist. Finally, the protocol trims the ends of reads to remove polyA sequences and adaptors using *cutadapt* (7) (version 1.15). The tagged and trimmed FASTQ file is aligned to the mouse reference genome (version GRCm38/mm10) using the *STAR* (8) aligner (version 2.5.3). We used *featureCounts* (9) (version 1.6.0) to assign each aligned read to a gene on the genome. Gene annotations were based on GENCODE mV15 (10). We used the *count* function from *umi_tools* (6) to create a count matrix representing the frequency of each feature in the BAM file.

Further data processing and analyses were performed using the software tool *Seurat* (Version3) (11). Samples were imported separately and only cell barcodes with at least 1000 and less than 6000 UMIs were retained. In addition, cells with a high proportion of UMIs mapping to mitochondrial genes were removed (<5%). Data were normalized by scaling the total UMI count of each cell to 10,000 followed by log transformation (*NormalizeData*). For subsequent analyses, we selected the 2000 most variable features using *FindVariableFeatures* with default options. The datasets were combined by first identifying integration anchors (*FindIntegrationAnchors*) and then integrated (*IntegrateData*) using default settings and the first 50 PCs for both procedures. In addition to two wildtype and two mutant samples we included a mixed sample in this run. While we were not able to assign a genotype to cells from this sample we reasoned that the combined

processing will minimize technical variation and help detection of cell types by increasing the total number of analyzed cells. This sample was used for initial integration only. Before dimensionality reduction, data were scaled using *ScaleData*. We used *RunPCA* to calculate the first 70 PCs. Only the first 45 appeared to represent significant signal and were used for further analyses. We used Uniform Manifold Approximation and Projection (UMAP) (12) applying *RunUMAP* with default settings to further reduce dimensionality. In order to cluster cells we generated the neighborhood graph using *FindNeighbors* with *n.neighbors* set to 20. Data were clustered using *FindClusters* with the resolution parameter set to 1.2. We found that this resolution was optimal in yielding a high number of clusters while maintaining biological interpretability. Marker genes for each cluster were identified using *FindAllMarkers* with default settings and clusters were annotated based on known marker genes and comparisons with published data (13). Based on these annotations, we subset the dataset into embryonic-derived mesoderm. We recalculated UMAP and the neighborhood graph on the subset for better visual representation and improved clustering. As before, we obtained best clustering results with resolution parameter 1.2. However, similar resolution led only to marginally different results. Marker gene and cell type identification was performed as described above. We assessed the manually identified cell types by comparison to a single cell atlas of mouse gastrulation and early embryogenesis (13). To this end we obtained the processed data generated in Pijuan-Sala (13). We generated pseudo-bulk data for both datasets by combining the UMI counts for each gene per cluster. Data were normalized by scaling each cluster to 10,000 and log transformation. To assess similarity between our clusters and the published clusters we obtained the pair-wise correlation between all clusters (Fig. S5).

To assess differences between wildtype and mutant cells we calculated the proportion of cells in a given cluster of the total cells represented by that genotype. Proportions were plotted as

bar graphs. In addition, we verified that these differences were observed for both replicates. These analyses allowed us to establish differences in cellular proportions between wildtype and mutant samples in multiple clusters. However, as a change in proportion of one cluster necessarily affects the proportion of cells in other clusters, these observations alone are not sufficient to establish the directionality and primary cell type of change.

We used the data integration procedure described in Stuart et al. (11) to correct for technical differences between samples. However, this procedure could potentially ‘overcorrect’ the data, removing differences between cells of different genotypes. To assess the potential magnitude of this effect we performed the same analyses without correction. As expected, these analyses showed some differences to the corrected analyses and the difference between the genotypes were more profound. However, cluster annotations were very similar and thus the resulting interpretation remained unchanged (Fig. S6). Importantly, in some instances the integrated data allowed for the unambiguous identification of expected cell types (e.g. pSHF) while we were unable to achieve the same resolution in the uncorrected dataset.

Migration Assay in Chicken Embryo

Chick embryos were isolated at HH stage 2/3 and cultured according to the technique described by (Chapman – Improved method for Chick whole-embryo culture using a filter paper carrier – Dev Dyn 2001). DiI and DiO (ThermoFisher Scientific) were applied to the lateral aspect of the primitive streak using a Femotjet pressure injector and Injectman micromanipulator (Eppendorf) as described in (Bressan et al. Science, 2013). Following 16 hrs of incubation embryos were photographed on a Lecia M165 FC fluorescent stereo microscope using a Hamamatsu Orca-flash 4.0 camera. Anterior/Posterior spread was quantified using ImageJ

software (v2.0.0). Briefly, the center-of-mass for all fluorescent particles present within the embryonic area pellucida was calculated and this position was normalized to the posterior extent of the embryonic midline. For Hh inhibition studies, Cyclopamine (sigmaaldrich) was dissolved in 45% cyclodextrin (sigmaaldrich) Pannet/Compton's saline at concentrations described in the text. 500ul of Cyclopamine solution was then added to each embryo. For FGF rescue experiments, Heparin-agarose beads (sigmaaldrich) were soaked for 1hr at room temperature in either 1mg/ml BSA or FGF4 (R&D). Beads were then implanted between the epiblast and hypoblast of HH st 2/3 embryos as depicted in Figure 6 just prior to treatment with 25uM Cyclopamine.

REFERENCES

1. Benjamini Y & Hochberg Y (1995) Controlling the False Discovery Rate - a Practical and Powerful Approach to Multiple Testing. *J Roy Stat Soc B Met* 57(1):289-300.
2. Mi H, *et al.* (2017) PANTHER version 11: expanded annotation data from Gene Ontology and Reactome pathways, and data analysis tool enhancements. *Nucleic Acids Res* 45(D1):D183-D189.
3. Macosko EZ, *et al.* (2015) Highly Parallel Genome-wide Expression Profiling of Individual Cells Using Nanoliter Droplets. *Cell* 161(5):1202-1214.
4. Selewa A, *et al.* (2019) Systematic Comparison of High-throughput Single-Cell and Single-Nucleus Transcriptomes during Cardiomyocyte Differentiation. *bioRxiv*:585901.
5. Koster J & Rahmann S (2018) Snakemake-a scalable bioinformatics workflow engine. *Bioinformatics* 34(20):3600.
6. Smith T, Heger A, & Sudbery I (2017) UMI-tools: modeling sequencing errors in Unique Molecular Identifiers to improve quantification accuracy. *Genome Res* 27(3):491-499.
7. Martin M (2011) Cutadapt removes adapter sequences from high-throughput sequencing reads. *EMBnet. journal* 17(1):10-12.
8. Dobin A, *et al.* (2013) STAR: ultrafast universal RNA-seq aligner. *Bioinformatics* 29(1):15-21.
9. Liao Y, Smyth GK, & Shi W (2014) featureCounts: an efficient general purpose program for assigning sequence reads to genomic features. *Bioinformatics* 30(7):923-930.
10. Frankish A, *et al.* (2019) GENCODE reference annotation for the human and mouse genomes. *Nucleic Acids Res* 47(D1):D766-D773.
11. Stuart T, *et al.* (2019) Comprehensive Integration of Single-Cell Data. *Cell* 177(7):1888-1902 e1821.
12. Becht E, *et al.* (2018) Dimensionality reduction for visualizing single-cell data using UMAP. *Nat Biotechnol.*
13. Pijuan-Sala B, *et al.* (2019) A single-cell molecular map of mouse gastrulation and early organogenesis. *Nature* 566(7745):490-495.

CHAPTER 3: A HEDGEHOG-FGF SIGNALING AXIS PATTERNS ANTERIOR MESODERM DURING GASTRULATION

Chapter 3 Introduction

One of the first challenges during metazoan development is the establishment of embryonic axes through symmetry breaking (1-4). In triploblastic organisms, the anterior-posterior (A-P) axis is established through a process called gastrulation. In amniotes, gastrulation begins with the emergence of a cleft at the posterior embryonic pole called the primitive streak, through which cells migrate, are specified to mesoderm or endoderm, and subsequently patterned as they move towards the anterior embryonic pole (1, 3-6). Gastrulation is initiated and mediated by signaling pathways localized at the posterior embryonic midline including the Nodal, Fibroblast Growth Factor (FGF), Wnt, and Bone Morphogenic Protein (BMP) families which control A-P patterning by directing the anteriorward migration of nascent mesoderm (7-12).

The Hedgehog (Hh) signaling pathway is known to pattern tissues derived from all three germ layers in most metazoans (13, 14). Hh signaling was first described in a classic forward genetic screen for genes that determine A-P segment polarity during early *Drosophila melanogaster* development (15). Hh pathway activation in mammals is initiated by the binding of Hh ligands, *Shh*, *Ihh* or *Dhh*, to *Ptch1*—relieving its inhibition on Smoothed (*Smo*), which induces nuclear translocation of full-length Gli2/3 transcription factors (TFs) to promote Hh target gene transcription (16, 17). Conversely, the absence of Hh signaling triggers proteolysis and truncation of Gli2/3 proteins to their repressive isoforms Gli2R/3R (17, 18). Hh signaling works to pattern a diverse array of structures including the *Drosophila* wing disc (19), cnidarian pharyngeal musculature (20), tetrapod forelimb (21-24), vertebrate central nervous system (25-27) and heart

(28-30). However, it has not been previously implicated in patterning the early A-P axis in vertebrates.

Removal of all Hh signaling through germline deletion of *Smo* in mice, revealed an essential role for the Hh pathway in early mammalian development (31). *Smo*^{-/-} embryos exhibit cardiac and somitic defects, absence of the anterior dorsal aorta, and fail to establish left-right (L-R) axis asymmetry (31, 32). Furthermore, treatment of zebrafish embryos with a small molecule *Smo* antagonist during early, but not late, gastrulation resulted in cardiac hypoplasia—suggesting that Hh signaling is essential during early embryogenesis for mesoderm lineage formation (33). Whereas *Shh* is the only Hh ligand necessary for L-R axis patterning in mammals (34), compound *Shh*^{-/-};*Ihh*^{-/-} mutants produce phenotypes indistinguishable from *Smo*^{-/-} mutants(31). This suggests an important but poorly understood role for redundant *Shh* and *Ihh* signaling during early embryogenesis independent of L-R patterning.

We investigated the role of Hh signaling in the early mesoderm and found that the pathway is first active within the node at E7.25 which is a critical midline organizing structure that determines both L-R and A-P axis patterning. We studied the consequence of early disruptions to midline Hh signaling on the mesoderm through single cell RNA-seq (scRNA-seq) by profiling wild type (Wt) and Hh-mutant (Mut) mesoderm at the onset of organogenesis and identified a deficiency in anterior mesoderm lineages specific to Hh-Mut embryos. Mesoderm-intrinsic and germline Hh pathway mutants had selective defects to anterior mesoderm-derived structures including the heart, pharyngeal arch, and anterior, but not posterior somites—which was consistent with a requirement for Hh signaling for anterior mesoderm development. Surprisingly, the affected anterior mesoderm lineages did not directly receive Hh signaling during early development. Through transcriptional profiling of Hh-deficient mesoderm during gastrulation, we found severe

disruptions to mesoderm patterning and to an FGF mesoderm migratory pathway. To determine whether Hh signaling played a direct role in mesoderm migration, we added a small molecule Hh pathway inhibitor to chicken embryos and observed a substantial migratory defect to anterior mesoderm. Lastly, we demonstrate that Hh signaling is upstream of FGF signaling for mesoderm migration as the addition of FGF4 protein could rescue Hh-dependent migratory defects. Together, these observations identify a novel Hh-dependent midline signaling axis responsible for patterning embryonic mesoderm across the A-P axis.

Chapter 3 Results

Hedgehog signaling is first active in the organizing centers of embryonic axis determination

In order to study the role of early Hh pathway activity on mesoderm development, we first set out to identify the earliest tissue to receive Hh signaling using a *Ptch1*^{LacZ} reporter allele (35). No evidence of *Ptch1* reporter activity was observed prior to E7.0 (Fig. 3.1A) but becomes apparent in the node at E7.25, consistent with previous reports (Fig. 3.1A)(36). At E8.25, *Ptch1* reporter activity expands to the notochord (Fig. 3.1A) and shortly thereafter appears throughout the neural floorplate, somites, dorsal aorta and the SHF at E8.5 (Fig. 3.1A). These observations indicate that Hh signaling is first active in the node and notochord which are critical embryonic midline structures that determine embryonic axis patterning (37-39). The node is especially important in determining both L-R and A-P patterning of the mesoderm by mediating midline signaling at the distal-most aspect of the primitive streak.

Based on the importance of signaling from the node on mesoderm development, we assessed the direct role of Hh signaling within the mesoderm by driving expression of a dominant-negative transcriptional repressor, Gli3R in the nascent mesoderm using *Mesp1*^{Cre} (40, 41). We observed severe head and heart tube defects in *Mesp1*^{Cre/+};R26^{Gli3R-IRES-Venus/+} (*Mesp1*^{Cre}-*Gli3R*) (23) mutants which phenocopied the majority of defects characteristic of *Smo*^{-/-} mutants (Fig. 3.1B). This result suggested that Hh signaling from the midline plays a primary role in early mesoderm development.

Drop-seq reveals anterior mesoderm deficit in Hedgehog signaling mutants

To examine the consequence of disrupting mesoderm-intrinsic Hh signaling, we performed single-cell RNA-seq (Drop-seq)(42) on cells isolated by fluorescence activated cell sorting

(FACS) from mutant (*Mesp1^{Cre}-Gli3R*) and control *Mesp1^{Cre/+};R26^{tdTomato}* (*Mesp1^{Cre}-tdTomato*)(43) embryos at the onset of organogenesis (E8.25)(44, 45)(Fig. 3.1C). We jointly processed and analyzed 9,843 *R26-tdTomato* and 10,663 *R26-Gli3R* cells from two biological replicates and observed similar gene detection across replicates (Fig. S3.1). Using unsupervised clustering to identify distinct cell populations (46, 47) we assigned cells to either embryonic mesoderm lineages (44%; 8,937/20,506) or hepatic stellate cells, blood and vasculature lineages which mostly originate from extraembryonic tissues (56%, 11,569/20,506)(Fig 1D, Fig. S3.2 and Table S1)(48). Focusing our analysis on the embryonic mesoderm, we identified all expected *Mesp1^{Cre}*-derived lineages in both mutant and control embryos using a combination of canonical marker gene detection and integration with extant scRNA-seq datasets (Fig. S3.3, Fig. S3.4 and Fig. S3.5)(40, 41, 49, 50). When projected onto two dimensions using Uniform Manifold Approximation and Projection (UMAP), the proximity between clusters roughly recapitulated developmental relationships (Fig. 3.1E) with and without batch correction (Fig. S3.6). Specifically, we identified that the majority of embryonic mesoderm cells contributed to mesenchyme (4,619, 51.7%, dark blue) followed by: cardiac (1109, 12.4%, orange), lateral plate (887, 9.92%, grey-blue), allantoic (734, 8.21%, pale orange), somitic (641, 7.17%, light-green), pharyngeal (433, 4.85%, dark-green), cranial (311, 3.48%, red) and intermediate (203, 2.27%, salmon) mesoderm lineages (Fig. 3.1E, Fig. S3.3, and Fig. S3.4).

Expression of *Gli3R* significantly altered the distribution of *Mesp1^{Cre}*-derived cells (Fig. 3.1F). Specifically, we observed a selective deficiency in the proportional contribution of cells to anterior mesoderm lineages including cranial, pharyngeal and somitic mesoderm (Fig. 3.1G). Cranial mesoderm, marked by *Otx2* expression (51), is the anterior-most mesoderm lineage and demonstrated the most pronounced deficiency where there was more than four-fold reduction in

lineage contribution from mutant *Mesp1-Gli3R* cells (1.33% of cells) compared to *Mesp1-tdTomato* controls (6.06%). Somitic mesoderm, which is marked by *Meox1* and *Tcf15* (52, 53) and contributes to the development of the anterior-most somites at E8.25, was reduced in mutants by nearly three-fold (3.82% vs 11.2%). Finally, pharyngeal mesoderm, marked by *Col2a1* and *Sox9* (51, 52), demonstrated nearly 2-fold reduction within mutants (3.43% vs 6.53%). Therefore, multiple independent anterior mesoderm lineages demonstrated a deficiency in *Mesp1^{Cre}*-derived cell contributions after expression of the Hh-pathway transcriptional repressor, *Gli3R*.

Interestingly the cardiac lineage derives from the anterior mesoderm, was severely malformed in *Mesp1-Gli3R* embryos—yet does not show obvious proportional reduction in cell contribution. To investigate this further we analyzed this lineage in isolation which was comprised of three distinct sub-clusters: differentiated cardiomyocytes marked by *Tnnt2* and *Myh6* (54, 55) and two cardiac progenitor clusters comprised of a cardiac progenitor pool called the second heart field (SHF) which is located anatomically dorsal to the heart tube (56, 57). The SHF can be divided anatomically into anterior (aSHF) and posterior (pSHF) regions which express distinct transcripts where the aSHF is defined by *Fgf10* and *Isl1* expression (Fig. 3.1 *H* and *I*) (58) while the pSHF is defined by *Wnt2* and *Tbx5* expression (Fig. 3.1 *H* and *I*) (59, 60). Within the SHF populations, mutant embryos contribute proportionally less cells to the aSHF (57.3%) compared to controls (73.9%)(Fig. 3.1*J*). To directly test whether Hh mutants exhibited decreased aSHF cellularity (??), we performed a genetic fate map using a Cre (*Mef2c^{AHF-Cre}*) that primarily marks cells within the aSHF (61). We analyzed the aSHF progenitor pool in *Smo^{+/+}* and *Smo^{-/-}* backgrounds using *Mef2c^{AHF-Cre}* and a Cre-dependent lacZ reporter (*R26R*)(62). We observed a substantial reduction of the aSHF in *Mef2c^{AHF-Cre};R26R^{c/+};Smo^{-/-}* mutants compared to *Mef2c^{AHF-Cre};R26R^{c/+};Smo^{+/+}* controls at E9.5, when the aSHF is normally well established (Fig 3.1*J*). These data suggest that

reduction in Hh signaling cause anterior-selective defects within the cardiac lineage, just as the embryo as a whole shows a deficiency of anterior lineages in *Mesp1-Gli3R* embryos.

Hh signaling is selectively required for anterior mesoderm development

Overall, Drop-seq analysis suggested that anterior mesoderm lineages were selectively reduced in Hh mutants during organogenesis. We hypothesized that this disruption would culminate in anterior-specific phenotypic defects later in development. Anterior embryonic mesoderm lineages arise during gastrulation when undifferentiated epiblast cells migrate through a transient structure known as the primitive streak (1, 3-5, 63). The earliest cells to contribute to the embryo enter the streak during early to mid-streak stage and migrate furthest towards the anterior embryonic pole (4, 5) where they subsequently differentiate into specific lineages including, from anterior to posterior, pharyngeal mesoderm, cardiac mesoderm, and anterior somitic mesoderm (Fig. 3.2A). We directly analyzed the development of anterior mesoderm-derived structures in both mesoderm-intrinsic and germline Hh pathway mutants. Mesoderm-intrinsic Hh mutants, including *Mesp1^{Cre/+};Smo^{f/-}* (41, 64) and *Mesp1-Gli3R* embryos, exhibited cardiac and first pharyngeal arch hypoplasia compared to *Mesp1^{Cre/+};Smo^{f/+}* controls (Fig. 3.2B and C). Although the anterior-most somites in mesoderm-intrinsic Hh mutants were positioned normally, they exhibited severe morphologic defects and failed to compact (Fig. 3.2 E and G) which was in contrast to the anterior somites which were relatively similar to *Mesp1^{Cre/+};Smo^{f/+}* controls (Fig. 3.2E and G). Germline removal of *Smo* resulted in the most severe anterior defects including agenesis of the first pharyngeal arch and previously published cardiac defects (Fig 3.2J)(31). *Smo^{-/-}* mutants also revealed a complete absence of the anterior-most somites, which were replaced by loosely packed mesenchyme (Fig. 2M). In contrast, removal of *Shh* resulted in

cardiac chamber and somite development indistinguishable from Wt controls (Fig. 3.2 H-K) (65). These results demonstrated that severely reduced Hh signaling, by *Smo* but not *Shh* mutation, selectively affected the development of anterior mesoderm (31).

Hh reception by cardiac progenitors is not required for early heart development

Due to the selective role of Hh signaling in anterior-specific mesoderm development, we hypothesized that anterior lineages would autonomously require intact Hh pathway function. To test this in the cardiovascular lineage we conditionally removed *Smo* from the earliest specified cardiac precursors using *Nkx2.5^{Cre}* (66). Surprisingly, no phenotypic abnormality was observed in *Nkx2.5^{Cre/+};Smo^{f/-}* embryos (Fig. S3.7B) compared to *Nkx2.5^{Cre/+};Smo^{f/-}* controls (Fig. S3.7A) at E9.5. To rule-out insufficiency of *Nkx2.5^{Cre}* to functionally delete *Smo* in cardiac progenitors we analyzed *Nkx2.5^{Cre/+};Smo^{f/-}* embryos later in development where Hh signaling is required within the Nkx2-5 sub-domain of the SHF for atrioventricular septum development (30, 67). At E14.5, *Nkx2.5^{Cre/+};Smo^{f/-}* displayed completely penetrant atrioventricular septal defects (AVSDs) (Fig. S3.7D) compared to normal morphology observed in *Nkx2.5^{Cre/+};Smo^{f/+}* littermate controls (Fig. S3.7C). Additionally, genetic fate mapping of *Nkx2.5^{Cre}* expression revealed no Hedgehog dependence. We observed identical fate maps between *Nkx2.5^{Cre/+};Smo^{f/-};R26R^{c/+}* mutants and *Nkx2.5^{Cre/+};Smo^{f/-};R26R^{c/+}* controls where both genotypes demonstrated robust staining throughout the cardiac chambers and SHF (Fig. S3.7 E and F). These data suggested that Hh signaling was either not cell-autonomously required for cardiac development or required for cardiac development in early pre-cardiac mesoderm prior to specification.

Hh-dependent anterior mesoderm lineages do not directly receive Hh signaling

To ask whether anterior mesoderm lineages receive Hh signaling at any point during early development, we utilized an inducible CreERT2 knock-in allele at the *Gli1* locus (*Gli1*^{CreERT2})(68) to mark Hh-receiving cells and their decedents in a tamoxifen (TM)-dependent manner. TM was administered between E5.5 to E8.5 in *Gli1*^{Cre/+};*R26R*^{c/c} embryos which were analyzed at E9.5 (Fig. 3.3A). We observed a near-absence of marked cells when TM was administered one day preceding gastrulation at E5.5 (Fig 3.3A)—suggesting that Hh signaling is not active in embryonic mesoderm immediately prior to gastrulation. Administration of TM during early gastrulation at either E6.5, or late gastrulation at E7.5, resulted in robust X-gal staining throughout the neural tube and lateral mesenchyme; notably, few to no positive clones appeared in the pharyngeal mesoderm, somite bodies, or heart (Fig 3.3A). TM administered shortly after gastrulation at E8.5 demonstrated much more prevalent staining in the ventral neural tube and paraxial mesoderm but anterior mesoderm lineages remained unmarked (Fig. 3.3A). TM administration at both E6.5 and E7.5 did not result in the marking of anterior mesoderm lineages, although a higher proportion of stained cells within previously marked lineages was observed (Fig 3.3B). Serially sectioned embryos revealed a near-absence of labeled clones in the pharyngeal mesoderm and somite bodies (Fig 3.3C). In contrast to the heart itself, which had few to no labeled clones throughout several litters analyzed (Table S1, Fig 3.3D), SHF cells were robustly labeled—providing a positive control for a lineage with known Hh signaling activity (Fig. 3.3D)(30, 67, 69). These results suggested that Hh signaling is required for anterior lineage development in a cell non-autonomous manner.

Transcriptional profiling identified Hh-dependent transcription factors and signaling pathways necessary for mesoderm morphogenesis

To search for candidate Hh-dependent genes capable of acting through cell non-autonomous mechanisms, we performed RNA-seq on *Mesp1-Gli3R* mutants late during gastrulation at E7.5. We utilized a Cre-dependent dual color system to separate red fluorophore-expressing wild type (*Mesp1-Tomato*), from yellow fluorophore-expressing Hh mutant (*Mesp1-Gli3R*) *Mesp1*^{Cre}-labeled cells by FACS in order to generate three biological replicates of litter-matched RNA-seq samples (Fig. 3.4A). We observed consistent differential expression profiles between biological replicates and identified 190 dysregulated genes by mRNA-seq (FDR ≤ 0.10) and (Fig. 3.4B). We observed a consistent enrichment of genes expressed in the posterior midline—especially those important for mesoderm development including: *Wnt3a*, *Mesogenin*, *Fgf4*, and *Fgf8* (8, 70-74). Furthermore, we identified downregulation of genes essential for both mesoderm induction and anterior-posterior axis patterning, including Brachyury (*T*), *FoxA2*, and *Tdgf1* (Crypto) (10, 37, 38, 73, 75). Gene Ontology (GO) analysis for all downregulated genes (FDR < 0.10) (Fig. 3.4D) identified terms related to processes essential for mesoderm morphogenesis, such as paraxial mesoderm and cardiac development—highlighted by the GO term for Mesoderm Development (GO:0007498) (FDR <0.3) (Fig. 3.4E) in addition to previously described Hh-dependent processes such as L-R patterning, and lung morphogenesis (31, 34, 76). *Bmp4*, which has been shown to be antagonized by positive Hh signaling in multiple contexts (77, 78), was one of the few upregulated mesoderm determinants. In agreement with our earlier finding that Hh signaling does not directly signal to cardiac precursors, we did not observe dysregulation of genes implicated in cardiac specification such as *Gata4* *Tbx5* or *Nkx2.5* (Fig. 4C) (79).

Hh-dependent TFs are enriched for determinants of mesoderm morphogenesis and somitogenesis.

GO analysis for Hh-dependent TFs identified somitogenesis and paraxial mesoderm as the most highly represented terms (Fig. 3.5A). Genes disrupted within the GO term for somitogenesis (GO:0001756)(FDR <0.3) reveal downregulation of transcription factors that are important to both somite development alone (*Hes7*, *Tcf15*, *Dll3*, *Ripply2*)(80-84) and factors that are jointly responsible for gastrulation and somite development (*Msgn1*, *Tbx6*, *Mesp2*, *FoxA2*, *T*, and *Smad3*)(37, 38, 74, 75, 85)(Fig. 3.5B). Using RNA *in situ* hybridization, we analyzed the spatial expression patterns for key genes responsible for shared paraxial and general mesoderm development (*Tbx6*, *Msgn1*, and *Mesp2*) along with *Dll3*, a gene responsible primarily for somitogenesis. *Tbx6*, which is critical for L/R patterning and mesoderm formation (74, 85-87), is lost from all but the most distal mesoderm expression domains (Fig. 3.5C). *Msgn1*, which is a master regulator of pre-somitic mesoderm development (73, 74), lost expression in the majority of paraxial mesoderm and only maintained medial posterior expression—proximal to the primitive streak (Fig. 3.5C). *Mesp2*, which is crucial for both nascent mesoderm development for somite-psm boundary determination (88), prematurely lost expression in the posterior streak while maintaining nascent somite boundary expression. In summary, all three shared mesoderm-somite program genes demonstrated significantly reduced expression near the posterior primitive streak (Fig. 3.5C).

Transcriptional profiling identified FGF signaling downstream of Hh signaling for anterior mesoderm morphogenesis

Anterior mesoderm lineages require an intact Hh pathway within the mesoderm despite not receiving direct Hh signaling. Due to the indirect nature of this mechanism, we hypothesized that a secondary signaling pathway downstream of Hh signaling was directly responsible for anterior mesoderm development. To identify candidate pathways, we performed GO analysis for downregulated genes classified as either signal ligands or ligand receptors in the Fantom consortium database (89) (Fig. 3.5D). The FGF pathway comprised the top candidate using this approach and differential expression for genes in the GO category “FGF Receptor signaling pathway” (GO:0008543) revealed a striking pattern of downregulation among all included FGF ligands (FDR \leq 0.30) (Fig. 3.5E). Specifically, *Fgf4* and *Fgf8* share posterior expression domains in the primitive streak and both lose much of their posterior-lateral expression in Hh mutants (Fig 3.5F). Studies in early mammalian development have shown that the FGF pathway directs the migration of nascent mesoderm towards the anterior embryonic pole (72, 90-92) and *Fgf4* and *Fgf8* are uniquely important for this process (8, 70-72). Given the quantitative and spatial reduction in the expression of these ligands in the primitive streak, we hypothesized that Hh signaling lies upstream of an FGF signaling pathway for mesoderm migration.

Gastrulation cell migration defects caused by Hh pathway antagonism are rescued by FGF4

To directly assess whether impaired Hh signaling disrupts mesoderm migration, we utilized a chicken embryonic model of gastrulation. Mesoderm migration was tracked by adding either DiI (red) and DiO (green) fluorescent lipophilic dyes on each side of the primitive streak in

Hamburger-Hamilton (93) stage 3 chick embryos (Fig. 3.6A). Embryos treated with DMSO vehicle demonstrated classic anterior-lateral movement of labeled cells consistent with well-established fate and migration maps of nascent mesoderm (Fig. 3.6B) (72, 94, 95) which could be quantified (Fig. 3.6C). We observed a dose-response of nascent mesoderm migration to the Hh signaling antagonist cyclopamine (96) (Fig. 3.6F) where embryos treated with 25 μ M cyclopamine demonstrated a marked reduction in directional migration (Fig. 3.6D) whereas embryos treated with 50 μ M or higher concentrations of cyclopamine demonstrated migratory defects compounded with widespread phenotypic disruptions including greatly reduced overall embryo size (Fig. 3.6E). These experiments demonstrated that A-P cell migration during gastrulation was hindered by Hh pathway inhibition (Fig. 3.6F).

To test whether FGF-directed cell migration was downstream of the Hh pathway, we placed beads coated with either a BSA control or FGF4 protein on opposite sides of the anterior midline in 25 μ M-cyclopamine-treated HH4-stage chick embryos (Fig. 3.6G). We determined and quantified migration by monitoring the anterior excursion of DiO or DiI labeled regions of the primitive streak over a 16 hr period of gastrulation. Importantly, labeled cells that gastrulated on the same side as FGF4-coated beads showed a statistically significant increase in anterior-posterior spread when compared with cells migrating through the contralateral side of the primitive streak (towards control beads coated with BSA) (N=11; ttest pValue=0.0057; Fig. 3.6H and I). These data suggest that the migratory defects resulting from cyclopamine treatment could be rescued by FGF4 and provide evidence that Hh signaling is required upstream of FGF signaling for anterior mesoderm development through morphogenetic movements at the primitive streak during gastrulation.

Chapter 3 Discussion

The mechanism by which embryos pattern tissues across their axes has fascinated developmental biologists since the founding of embryology. The A-P axis is the most complex—establishing the template for the distribution of all embryonic structures. A-P patterning is executed in two stages—the first stage is the initiation of TGF- β signaling to establish the rotation of the distal embryonic axis towards the nascent anterior embryonic pole (97). The second phase involves the concurrent specification of mesoderm and anteriorward cell migration through the newly formed primitive streak at the posterior embryonic through midline Nodal, FGF, Wnt, and BMP pathway expression (7-12, 98). Cells fated to form extraembryonic tissues are the first to migrate through the early streak and are followed by the anterior embryonic mesoderm lineages such as the cardiac, cranial, pharyngeal, and anterior somitic mesoderm precursors during the mid-streak stage (99). Although the Hh pathway is critical to the patterning of diverse tissues across multiple organisms, its role in patterning the early A-P axis has not been previously described.

In this study, we provide evidence that midline Hh signaling acts upstream of an FGF-migratory pathway for anterior mesoderm development during gastrulation. Although the FGF pathway can function as a mitogen, its primary role during gastrulation is to direct coordinated cell migration through matrix remodeling and chemotaxis (92, 100)—particularly through the action of FGF4 and FGF8 which function as potent chemotactic signals (72). For example, severe gastrulation defects observed in *Fgfr1*^{-/-} embryos, which FGF4/8 signal through (101), can be phenotypically rescued by restoring cell migration through downregulation of the cell-adhesion molecule, EPCAM (102). The expression of *Fgf4* and *Fgf8* ligands are particularly important patterning distal structures in diverse contexts. *Fgf8* germline hypomorph mutants reveal anterior-specific defects across multiple organ systems—including hypoplasia of the pharyngeal

mesoderm, cardiovascular lineages, and selective anterior truncation of the zygomatic arch (103, 104). *Fgf4/8* conditional deletions within the late-streak posterior mesoderm reveal widespread somite defects distal to the posterior source of *Fgf4/8* expression (70, 71). The anterior-specific defects we observed in mutant embryos where Hh signaling was disturbed in the primitive streak echo phenotypes produced by perturbations to FGF signaling in the streak where tissues distal to the signaling event are either absent or reduced. Because we established the FGF pathway as a downstream component of Hh signaling for cell migration during gastrulation, it is possible that a major role of the Hh pathway in early development is to modulate anterior mesoderm migration through control of *Fgf4/8* expression at the streak.

Hh signaling may also be an integral part of a broader gene regulatory network within the embryonic midline for anterior mesoderm development. Surprisingly, the vast majority of mutations that drive anterior-specific phenotypes during early mouse development are confined to the Nodal pathway (6). Furthermore, a recent pathway controlled by *toddler-appelin* signaling was shown to pattern anterior mesoderm solely through dictating cell migration downstream of Nodal signaling (105, 106). In mammals, while there exists modest evidence for direct cross-activation between the Hh and *Nodal* pathways during early development (31, 107-109), our mutants present phenotypes common to mild and moderate perturbations to early *Nodal* expression without direct downregulation of *Nodal* expression itself. We did however observe a critical network of shared target genes downstream of Nodal and Hh signaling, including *FoxA2*, *T*, *Tdgfl*, and *Fgf4*—all of which are involved in A-P axis patterning (10, 37, 38, 75, 110). This shared gene set suggests that the Hh and Nodal pathways coordinately regulate downstream genes necessary for mesoderm morphogenesis through gastrulation.

Removal of redundant Hh signals in the early embryo through either double knockout of *Shh* and *Ihh* or knockout of *Smo* uncovers a previously uncharacterized role for Hh signaling in A-P axis patterning. Hh signaling within the node functions to drive sufficient midline FGF signaling from the primitive streak for proper anterior mesoderm allocation (Fig. 3.7A). Disruption to Hh signaling during this period diminishes expression of migratory FGF midline signals which subsequently leads to defects in A-P patterning through a deficit in anterior mesoderm contribution (Fig. 3.7B). Furthermore, extant mutants in the literature, which show commonality of phenotype with Hh mutants also share a commonality of expression domains within midline node and primitive streak compartments in addition to shared downstream genes for mesoderm morphogenesis. This suggests that the migratory Hh-FGF signaling pathway described in this study may describe a broader mechanism by which signaling pathways in the embryonic midline control A-P axis patterning through mesoderm allocation.

REFERENCES

1. Tam PP & Behringer RR (1997) Mouse gastrulation: the formation of a mammalian body plan. *Mech Dev* 68(1-2):3-25.
2. Garcia-Martinez V & Schoenwolf GC (1993) Primitive-streak origin of the cardiovascular system in avian embryos. *Dev Biol* 159(2):706-719.
3. Lawson KA, Meneses JJ, & Pedersen RA (1991) Clonal analysis of epiblast fate during germ layer formation in the mouse embryo. *Development* 113(3):891-911.
4. Tam PP, Parameswaran M, Kinder SJ, & Weinberger RP (1997) The allocation of epiblast cells to the embryonic heart and other mesodermal lineages: the role of ingression and tissue movement during gastrulation. *Development* 124(9):1631-1642.
5. Parameswaran M & Tam PP (1995) Regionalisation of cell fate and morphogenetic movement of the mesoderm during mouse gastrulation. *Dev Genet* 17(1):16-28.
6. Tam PP & Loebel DA (2007) Gene function in mouse embryogenesis: get set for gastrulation. *Nat Rev Genet* 8(5):368-381.
7. Liu P, *et al.* (1999) Requirement for Wnt3 in vertebrate axis formation. *Nat Genet* 22(4):361-365.
8. Sun X, Meyers EN, Lewandoski M, & Martin GR (1999) Targeted disruption of Fgf8 causes failure of cell migration in the gastrulating mouse embryo. *Genes Dev* 13(14):1834-1846.
9. Xu C, Liguori G, Persico MG, & Adamson ED (1999) Abrogation of the Cripto gene in mouse leads to failure of postgastrulation morphogenesis and lack of differentiation of cardiomyocytes. *Development* 126(3):483-494.
10. Ding J, *et al.* (1998) Cripto is required for correct orientation of the anterior-posterior axis in the mouse embryo. *Nature* 395(6703):702-707.
11. Rossant J, Ciruna B, & Partanen J (1997) FGF signaling in mouse gastrulation and anteroposterior patterning. *Cold Spring Harb Symp Quant Biol* 62:127-133.
12. Winnier G, Blessing M, Labosky PA, & Hogan BL (1995) Bone morphogenetic protein-4 is required for mesoderm formation and patterning in the mouse. *Genes Dev* 9(17):2105-2116.
13. Irimia M, *et al.* (2012) Comparative genomics of the Hedgehog loci in chordates and the origins of Shh regulatory novelties. *Sci Rep* 2:433.
14. Ingham PW & Placzek M (2006) Orchestrating ontogenesis: variations on a theme by sonic hedgehog. *Nat Rev Genet* 7(11):841-850.
15. Nusslein-Volhard C & Wieschaus E (1980) Mutations affecting segment number and polarity in *Drosophila*. *Nature* 287(5785):795-801.
16. Briscoe J & Therond PP (2013) The mechanisms of Hedgehog signalling and its roles in development and disease. *Nat Rev Mol Cell Biol* 14(7):416-429.

17. Robbins DJ, Fei DL, & Riobo NA (2012) The Hedgehog signal transduction network. *Sci Signal* 5(246):re6.
18. Falkenstein KN & Vokes SA (2014) Transcriptional regulation of graded Hedgehog signaling. *Semin Cell Dev Biol* 33:73-80.
19. Tabata T & Kornberg TB (1994) Hedgehog is a signaling protein with a key role in patterning Drosophila imaginal discs. *Cell* 76(1):89-102.
20. Walton KD, Warner J, Hertzler PH, & McClay DR (2009) Hedgehog signaling patterns mesoderm in the sea urchin. *Dev Biol* 331(1):26-37.
21. Tickle C & Towers M (2017) Sonic Hedgehog Signaling in Limb Development. *Front Cell Dev Biol* 5:14.
22. Bowers M, *et al.* (2012) Limb anterior-posterior polarity integrates activator and repressor functions of GLI2 as well as GLI3. *Dev Biol* 370(1):110-124.
23. Vokes SA, Ji H, Wong WH, & McMahon AP (2008) A genome-scale analysis of the cis-regulatory circuitry underlying sonic hedgehog-mediated patterning of the mammalian limb. *Genes Dev* 22(19):2651-2663.
24. Scherz PJ, Harfe BD, McMahon AP, & Tabin CJ (2004) The limb bud Shh-Fgf feedback loop is terminated by expansion of former ZPA cells. *Science* 305(5682):396-399.
25. Balaskas N, *et al.* (2012) Gene regulatory logic for reading the Sonic Hedgehog signaling gradient in the vertebrate neural tube. *Cell* 148(1-2):273-284.
26. Wechsler-Reya RJ & Scott MP (1999) Control of neuronal precursor proliferation in the cerebellum by Sonic Hedgehog. *Neuron* 22(1):103-114.
27. Lee J, Platt KA, Censullo P, & Ruiz i Altaba A (1997) Gli1 is a target of Sonic hedgehog that induces ventral neural tube development. *Development* 124(13):2537-2552.
28. Hoffmann AD, *et al.* (2014) Foxf genes integrate tbx5 and hedgehog pathways in the second heart field for cardiac septation. *PLoS Genet* 10(10):e1004604.
29. Xie L, *et al.* (2012) Tbx5-hedgehog molecular networks are essential in the second heart field for atrial septation. *Dev Cell* 23(2):280-291.
30. Hoffmann AD, Peterson MA, Friedland-Little JM, Anderson SA, & Moskowitz IP (2009) sonic hedgehog is required in pulmonary endoderm for atrial septation. *Development* 136(10):1761-1770.
31. Zhang XM, Ramalho-Santos M, & McMahon AP (2001) Smoothed mutants reveal redundant roles for Shh and Ihh signaling including regulation of L/R symmetry by the mouse node. *Cell* 106(2):781-792.
32. Vokes SA, *et al.* (2004) Hedgehog signaling is essential for endothelial tube formation during vasculogenesis. *Development* 131(17):4371-4380.
33. Thomas NA, Koudijs M, van Eeden FJ, Joyner AL, & Yelon D (2008) Hedgehog signaling plays a cell-autonomous role in maximizing cardiac developmental potential. *Development* 135(22):3789-3799.

34. Tsukui T, *et al.* (1999) Multiple left-right asymmetry defects in Shh(-/-) mutant mice unveil a convergence of the shh and retinoic acid pathways in the control of Lefty-1. *Proc Natl Acad Sci U S A* 96(20):11376-11381.
35. Goodrich LV, Milenkovic L, Higgins KM, & Scott MP (1997) Altered neural cell fates and medulloblastoma in mouse patched mutants. *Science* 277(5329):1109-1113.
36. Daane JM & Downs KM (2011) Hedgehog signaling in the posterior region of the mouse gastrula suggests manifold roles in the fetal-umbilical connection and posterior morphogenesis. *Dev Dyn* 240(9):2175-2193.
37. Ang SL & Rossant J (1994) HNF-3 beta is essential for node and notochord formation in mouse development. *Cell* 78(4):561-574.
38. Weinstein DC, *et al.* (1994) The winged-helix transcription factor HNF-3 beta is required for notochord development in the mouse embryo. *Cell* 78(4):575-588.
39. Hart AH, *et al.* (2002) Mix11 is required for axial mesendoderm morphogenesis and patterning in the murine embryo. *Development* 129(15):3597-3608.
40. Saga Y, Kitajima S, & Miyagawa-Tomita S (2000) Mesp1 expression is the earliest sign of cardiovascular development. *Trends Cardiovas Med* 10(8):345-352.
41. Saga Y, *et al.* (1999) MesP1 is expressed in the heart precursor cells and required for the formation of a single heart tube. *Development* 126(15):3437-3447.
42. Macosko EZ, *et al.* (2015) Highly Parallel Genome-wide Expression Profiling of Individual Cells Using Nanoliter Droplets. *Cell* 161(5):1202-1214.
43. Madisen L, *et al.* (2010) A robust and high-throughput Cre reporting and characterization system for the whole mouse brain. *Nat Neurosci* 13(1):133-140.
44. Kaufman MH & Bard JB (1999) *The anatomical basis of mouse development* (Gulf Professional Publishing).
45. Ibarra-Soria X, *et al.* (2018) Defining murine organogenesis at single-cell resolution reveals a role for the leukotriene pathway in regulating blood progenitor formation. *Nat Cell Biol* 20(2):127-134.
46. Stuart T, *et al.* (2018) Comprehensive integration of single cell data. *bioRxiv*:460147.
47. Butler A, Hoffman P, Smibert P, Papalexi E, & Satija R (2018) Integrating single-cell transcriptomic data across different conditions, technologies, and species. *Nat Biotechnol* 36(5):411-420.
48. Yoder MC (2014) Inducing definitive hematopoiesis in a dish. *Nat Biotechnol* 32(6):539-541.
49. Devine WP, Wythe JD, George M, Koshiba-Takeuchi K, & Bruneau BG (2014) Early patterning and specification of cardiac progenitors in gastrulating mesoderm. *Elife* 3.
50. Lescroart F, *et al.* (2014) Early lineage restriction in temporally distinct populations of Mesp1 progenitors during mammalian heart development. *Nat Cell Biol* 16(9):829-840.

51. Ang SL, Conlon RA, Jin O, & Rossant J (1994) Positive and negative signals from mesoderm regulate the expression of mouse *Otx2* in ectoderm explants. *Development* 120(10):2979-2989.
52. Reijntjes S, Stricker S, & Mankoo BS (2007) A comparative analysis of *Meox1* and *Meox2* in the developing somites and limbs of the chick embryo. *Int J Dev Biol* 51(8):753-759.
53. Blonar MA, *et al.* (1995) *Mesol1*, a basic-helix-loop-helix protein involved in mammalian presomitic mesoderm development. *Proc Natl Acad Sci U S A* 92(13):5870-5874.
54. Wang Q, Reiter RS, Huang QQ, Jin JP, & Lin JJ (2001) Comparative studies on the expression patterns of three troponin T genes during mouse development. *Anat Rec* 263(1):72-84.
55. Ruiz JC, Conlon FL, & Robertson EJ (1994) Identification of novel protein kinases expressed in the myocardium of the developing mouse heart. *Mech Dev* 48(3):153-164.
56. Kelly RG (2012) The second heart field. *Curr Top Dev Biol* 100:33-65.
57. Buckingham M, Meilhac S, & Zaffran S (2005) Building the mammalian heart from two sources of myocardial cells. *Nat Rev Genet* 6(11):826-835.
58. Watanabe Y, *et al.* (2012) Fibroblast growth factor 10 gene regulation in the second heart field by *Tbx1*, *Nkx2-5*, and *Islet1* reveals a genetic switch for down-regulation in the myocardium. *Proc Natl Acad Sci U S A* 109(45):18273-18280.
59. Francou A, *et al.* (2013) Second heart field cardiac progenitor cells in the early mouse embryo. *Biochim Biophys Acta* 1833(4):795-798.
60. Vincent SD & Buckingham ME (2010) How to make a heart: the origin and regulation of cardiac progenitor cells. *Curr Top Dev Biol* 90:1-41.
61. Verzi MP, McCulley DJ, De Val S, Dodou E, & Black BL (2005) The right ventricle, outflow tract, and ventricular septum comprise a restricted expression domain within the secondary/anterior heart field. *Developmental Biology* 287(1):134-145.
62. Soriano P (1999) Generalized *lacZ* expression with the ROSA26 Cre reporter strain. *Nat Genet* 21(1):70-71.
63. Singh BN, *et al.* (2018) A conserved HH-Gli1-Mycn network regulates heart regeneration from newt to human. *Nat Commun* 9(1):4237.
64. Long F, Zhang XM, Karp S, Yang Y, & McMahon AP (2001) Genetic manipulation of hedgehog signaling in the endochondral skeleton reveals a direct role in the regulation of chondrocyte proliferation. *Development* 128(24):5099-5108.
65. Yamagishi C, *et al.* (2006) Sonic hedgehog is essential for first pharyngeal arch development. *Pediatr Res* 59(3):349-354.
66. Biben C, *et al.* (2000) Cardiac septal and valvular dysmorphogenesis in mice heterozygous for mutations in the homeobox gene *Nkx2-5*. *Circ Res* 87(10):888-895.

67. Goddeeris MM, *et al.* (2008) Intracardiac septation requires hedgehog-dependent cellular contributions from outside the heart. *Development* 135(10):1887-1895.
68. Ahn S & Joyner AL (2004) Dynamic changes in the response of cells to positive hedgehog signaling during mouse limb patterning. *Cell* 118(4):505-516.
69. Dyer LA & Kirby ML (2009) Sonic hedgehog maintains proliferation in secondary heart field progenitors and is required for normal arterial pole formation. *Dev Biol* 330(2):305-317.
70. Boulet AM & Capecchi MR (2012) Signaling by FGF4 and FGF8 is required for axial elongation of the mouse embryo. *Developmental Biology* 371(2):235-245.
71. Naiche LA, Holder N, & Lewandoski M (2011) FGF4 and FGF8 comprise the wavefront activity that controls somitogenesis. *P Natl Acad Sci USA* 108(10):4018-4023.
72. Yang XS, Dormann D, Munsterberg AE, & Weijer CJ (2002) Cell movement patterns during gastrulation in the chick are controlled by chemotaxis mediated by positive and negative FGF4 and FGF8. *Developmental Cell* 3(3):425-437.
73. Chalamalasetty RB, *et al.* (2014) Mesogenin 1 is a master regulator of paraxial presomitic mesoderm differentiation. *Development* 141(22):4285-4297.
74. Nowotschin S, Ferrer-Vaquero A, Concepcion D, Papaioannou VE, & Hadjantonakis AK (2012) Interaction of Wnt3a, Msn1 and Tbx6 in neural versus paraxial mesoderm lineage commitment and paraxial mesoderm differentiation in the mouse embryo. *Dev Biol* 367(1):1-14.
75. Beddington RSP, Rashbass P, & Wilson V (1992) Brachyury - a Gene Affecting Mouse Gastrulation and Early Organogenesis. *Development*:157-165.
76. Pepicelli CV, Lewis PM, & McMahon AP (1998) Sonic hedgehog regulates branching morphogenesis in the mammalian lung. *Curr Biol* 8(19):1083-1086.
77. Monsoro-Burq A & Le Douarin NM (2001) BMP4 plays a key role in left-right patterning in chick embryos by maintaining Sonic Hedgehog asymmetry. *Mol Cell* 7(4):789-799.
78. Watanabe Y, Duprez D, Monsoro-Burq AH, Vincent C, & Le Douarin NM (1998) Two domains in vertebral development: antagonistic regulation by SHH and BMP4 proteins. *Development* 125(14):2631-2639.
79. Olson EN (2006) Gene regulatory networks in the evolution and development of the heart. *Science* 313(5795):1922-1927.
80. Sewell W, *et al.* (2009) Cyclical expression of the Notch/Wnt regulator Nrarp requires modulation by Dll3 in somitogenesis. *Dev Biol* 329(2):400-409.
81. Rowton M, *et al.* (2013) Regulation of mesenchymal-to-epithelial transition by PARAXIS during somitogenesis. *Dev Dyn* 242(11):1332-1344.
82. Burgess R, Rawls A, Brown D, Bradley A, & Olson EN (1996) Requirement of the paraxis gene for somite formation and musculoskeletal patterning. *Nature* 384(6609):570-573.

83. Chan T, *et al.* (2007) Ripply2 is essential for precise somite formation during mouse early development. *FEBS Lett* 581(14):2691-2696.
84. Bessho Y, *et al.* (2001) Dynamic expression and essential functions of Hes7 in somite segmentation. *Genes Dev* 15(20):2642-2647.
85. Chapman DL & Papaioannou VE (1998) Three neural tubes in mouse embryos with mutations in the T-box gene Tbx6. *Nature* 391(6668):695-697.
86. Concepcion D, Hamada H, & Papaioannou VE (2018) Tbx6 controls left-right asymmetry through regulation of Gdf1. *Biol Open* 7(5).
87. Hadjantonakis AK, Pisano E, & Papaioannou VE (2008) Tbx6 regulates left/right patterning in mouse embryos through effects on nodal cilia and perinodal signaling. *PLoS One* 3(6):e2511.
88. Morimoto M, Takahashi Y, Endo M, & Saga Y (2005) The Mesp2 transcription factor establishes segmental borders by suppressing Notch activity. *Nature* 435(7040):354-359.
89. Ramilowski JA, *et al.* (2015) A draft network of ligand-receptor-mediated multicellular signalling in human. *Nat Commun* 6:7866.
90. Ciruna B & Rossant J (2001) FGF signaling regulates mesoderm cell fate specification and morphogenetic movement at the primitive streak. *Developmental Cell* 1(1):37-49.
91. Boilly B, Vercoutter-Edouart AS, Hondermarck H, Nurcombe V, & Le Bourhis X (2000) FGF signals for cell proliferation and migration through different pathways. *Cytokine Growth Factor Rev* 11(4):295-302.
92. Sun X, Meyers EN, Lewandoski M, & Martin GR (1999) Targeted disruption of Fgf8 causes failure of cell migration in the gastrulating mouse embryo. *Gene Dev* 13(14):1834-1846.
93. Hamburger V & Hamilton HL (1951) A series of normal stages in the development of the chick embryo. *J Morphol* 88(1):49-92.
94. Redkar A, Montgomery M, & Litvin J (2001) Fate map of early avian cardiac progenitor cells. *Development* 128(12):2269-2279.
95. Bressan M, Liu G, & Mikawa T (2013) Early mesodermal cues assign avian cardiac pacemaker fate potential in a tertiary heart field. *Science* 340(6133):744-748.
96. Chen JK, Taipale J, Cooper MK, & Beachy PA (2002) Inhibition of Hedgehog signaling by direct binding of cyclopamine to Smoothened. *Genes Dev* 16(21):2743-2748.
97. Lu CC, Brennan J, & Robertson EJ (2001) From fertilization to gastrulation: axis formation in the mouse embryo. *Curr Opin Genet Dev* 11(4):384-392.
98. Arnold SJ & Robertson EJ (2009) Making a commitment: cell lineage allocation and axis patterning in the early mouse embryo. *Nat Rev Mol Cell Biol* 10(2):91-103.
99. Kinder SJ, *et al.* (1999) The orderly allocation of mesodermal cells to the extraembryonic structures and the anteroposterior axis during gastrulation of the mouse embryo. *Development* 126(21):4691-4701.

100. Garcia-Garcia MJ & Anderson KV (2003) Essential role of glycosaminoglycans in Fgf signaling during mouse gastrulation. *Cell* 114(6):727-737.
101. Zhang X, *et al.* (2006) Receptor specificity of the fibroblast growth factor family. The complete mammalian FGF family. *J Biol Chem* 281(23):15694-15700.
102. Ciruna B & Rossant J (2001) FGF signaling regulates mesoderm cell fate specification and morphogenetic movement at the primitive streak. *Dev Cell* 1(1):37-49.
103. Abu-Issa R, Smyth G, Smoak I, Yamamura K, & Meyers EN (2002) Fgf8 is required for pharyngeal arch and cardiovascular development in the mouse. *Development* 129(19):4613-4625.
104. Frank DU, *et al.* (2002) An Fgf8 mouse mutant phenocopies human 22q11 deletion syndrome. *Development* 129(19):4591-4603.
105. Norris ML, *et al.* (2017) Toddler signaling regulates mesodermal cell migration downstream of Nodal signaling. *Elife* 6.
106. Pauli A, *et al.* (2014) Toddler: an embryonic signal that promotes cell movement via Apelin receptors. *Science* 343(6172):1248636.
107. Yamamoto M, *et al.* (2001) The transcription factor FoxH1 (FAST) mediates Nodal signaling during anterior-posterior patterning and node formation in the mouse. *Genes Dev* 15(10):1242-1256.
108. Lu CC & Robertson EJ (2004) Multiple roles for Nodal in the epiblast of the mouse embryo in the establishment of anterior-posterior patterning. *Dev Biol* 273(1):149-159.
109. Morsut L, *et al.* (2010) Negative control of Smad activity by ectodermin/Tiflgamma patterns the mammalian embryo. *Development* 137(15):2571-2578.
110. Tanaka S, Kunath T, Hadjantonakis AK, Nagy A, & Rossant J (1998) Promotion of trophoblast stem cell proliferation by FGF4. *Science* 282(5396):2072-2075.

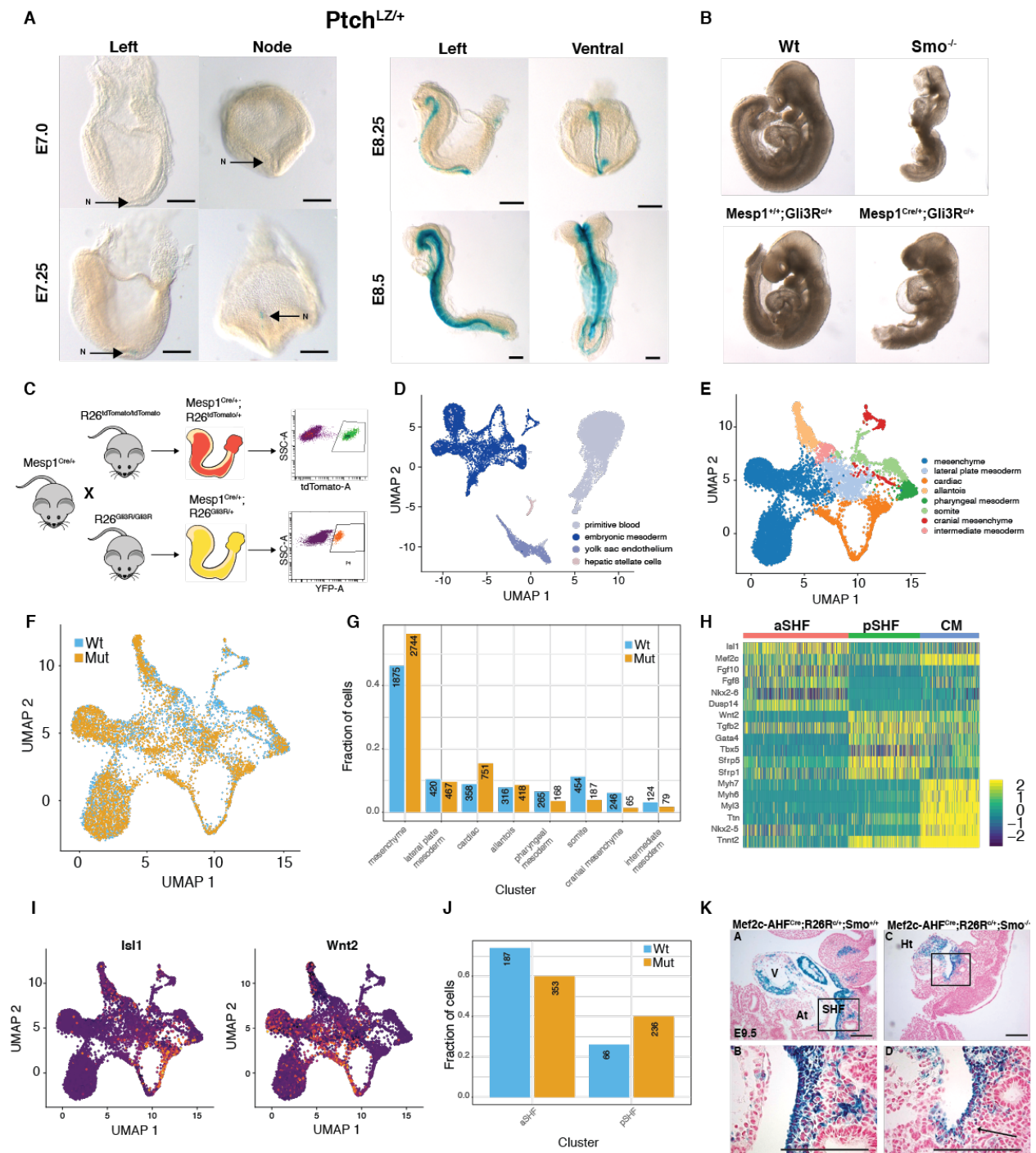


Fig. 3.1. Single cell RNA-seq identifies Hh-dependent selective defects to anterior mesoderm progenitor populations. (A) *Ptch^{LZ}* marks Hh receiving cells during early development between E7.0 (top-left) and E8.5 (bottom-right). (B) Whole-mount sagittal views of Hh-mutant embryos

(Fig. 3.1, Continued)

comparing defects observed between *Smo*^{-/-} mutants (top-right) and *Mesp1*^{Cre/+}*R26*^{Gli3R} mutants (bottom-right). (C) Schematic of experimental setup for collecting mutant (*R26-Gli3R*) and wild type (*R26-tdTomato*) *Mesp1*^{Cre}-labeled cells by FACS for single-cell RNA-seq. (D) Uniform manifold approximation and projection (UMAP) for all *R26-tdTomato* and *R26-Gli3R* cells used in this study. Extra embryonic mesoderm and blood were colored grey and light blue, while embryonic mesoderm lineages are shaded in dark blue. (E) UMAP representation of embryonic-derived mesoderm lineages where cells are colored by their cell type annotation with labels provided on the side of the plot. (F) UMAP for embryonic mesoderm with color segregation of control *R26-tdTomato* (blue) and mutant *R26-Gli3R* (orange) derived cells. (G) Column graph representing the proportion of *R26-tdTomato* (blue) and *R26-Gli3R* (orange) cells in each annotated lineage from (E) where the number linked to each column represents absolute cell counts. (H) Heatmap of marker gene expression for aSHF (red), pSHF (green), and cardiomyocytes (blue). Expression of aSHF and pSHF markers *Isl1* and *Wnt2* (I) superimposed on UMAP clusters derived from (E). (J) Proportion of *R26-tdTomato* (blue) and *R26-Gli3R* (orange) cells across aSHF, pSHF, and CM populations. (K) Fate map aSHF-specific Cre (*Mef2c*^{AHF^{Cre}}) with a cre-dependent lacZ reporter (*R26R*) in *Smo*^{+/+} and *Smo*^{-/-} backgrounds. Images represent the posterior margin of the aSHF at low and high power in the top and bottom panels respectively. (Legend: LV=left ventricle SHF = Second Heart Field, At = Atrium, HT = Heart tube). Size bars = 200µm.

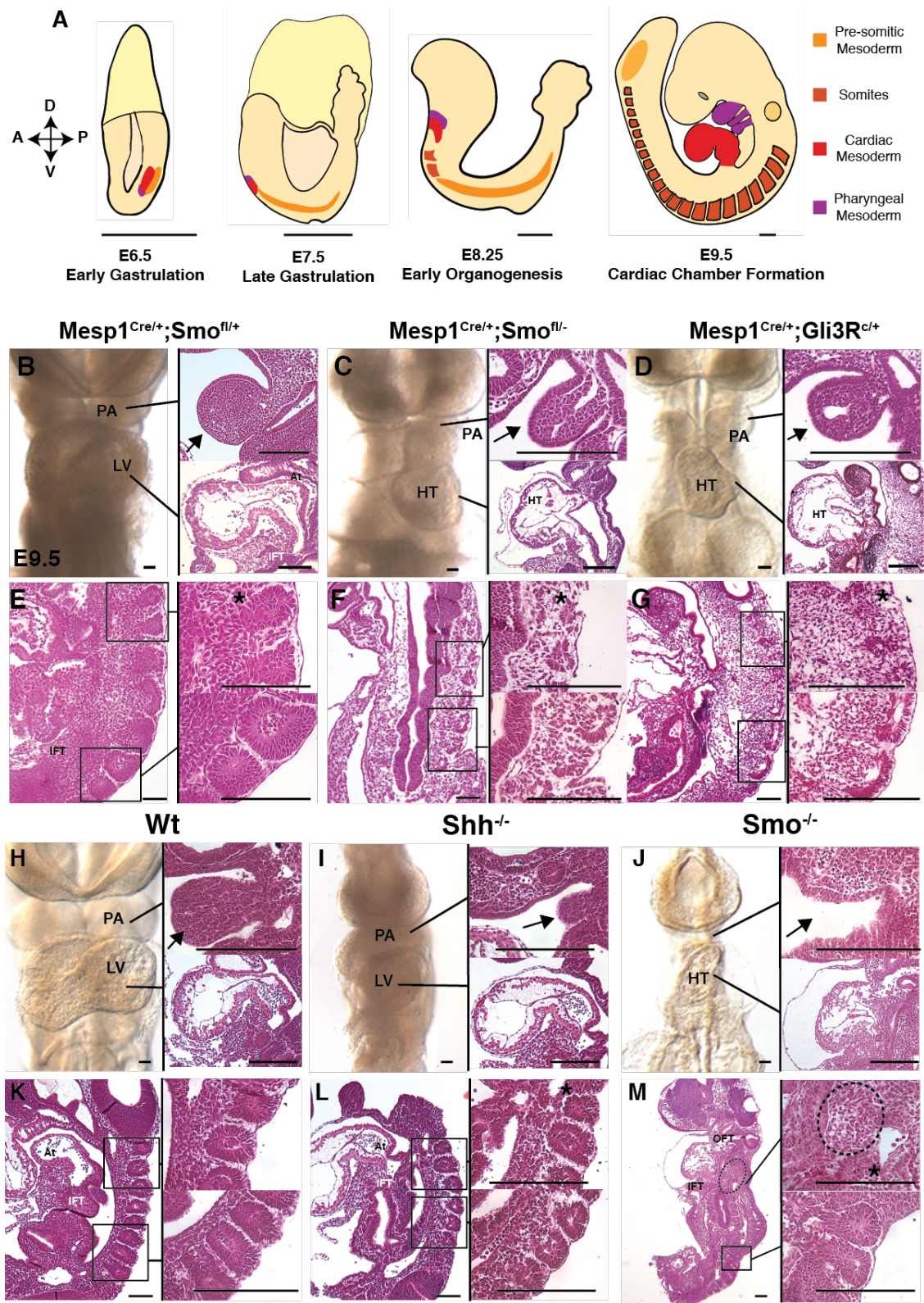


Fig. 3.2: Hh signaling is required for anterior mesoderm morphogenesis. (A) Represents a cartoon model depicting the developmental ontogeny of anterior mesoderm lineages with

(Fig. 3.2, Continued)

estimated size bars for each embryonic stage. (B-G) demonstrate phenotypic abnormalities in conditional Hh mutants, *Mesp1^{Cre/+}Smo^{f/-}* (C and F) and *Mesp1^{Cre/+};R26^{Gli3R/+}* (*Mesp1-Gli3R*) (D and G) with their respective control, *Mesp1^{Cre/+};Smo^{f/+}* (B and E) at E9.5. (H-M) Represent germline Hh pathway mutants, *Shh^{-/-}* (I and L) and *Smo^{-/-}* (J and M) and their respective Wt control (H and K) at E9.5. (B-D and H-J) Represent frontal whole-mount views of embryos (left panels) with corresponding sagittal histology sections of the pharyngeal arch (top-right panels) and heart (bottom-right panels). Black arrows link the whole mount views of the pharyngeal arch and heart to their corresponding histology section. (F-G and K-M) represent low-power sagittal histology views of both anterior and posterior somites (left panel). High power views of anterior and posterior somites are represented in the top-right panels and bottom-right panels respectively. Somite 1 is indicated by an * in each top-right panel. (Size bars = 200µm). (Legend: IFT = Inflow tract; LV = Left Ventricle; OFT = Outflow tract; At = Atrium; PA = pharyngeal arch; D = Dorsal; A = Anterior; P = Posterior; V = Ventral).

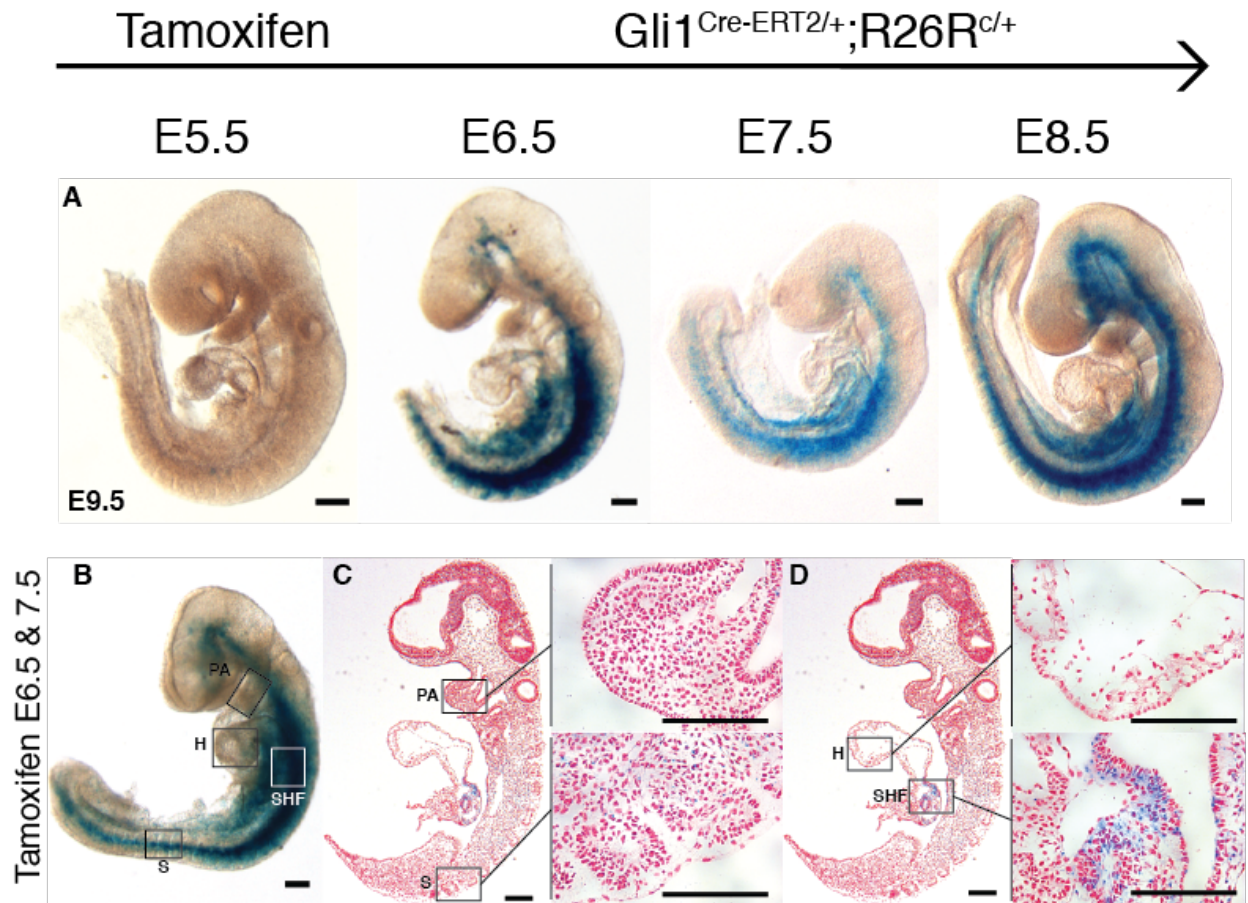


Fig. 3.3: Anterior mesoderm lineages do not receive Hh signaling during gastrulation. (A-D) Genetic-inducible fate maps for Hh-receiving cells in $Gli1^{Cre-ERT2/+}; R26R^{c/c}$ embryos. (A) Shows whole-mount left lateral views of E9.5 embryos harvested from pregnant dams given a single tamoxifen dose at the times indicated at top. (B-D) Shows whole mount (B) and sagittal sections (C and D) from embryos harvested from pregnant dams dosed with tamoxifen at both E6.5 and E7.5. (C) Sagittal sections of the pharyngeal arch at low power (left) and high-power images of the pharyngeal arch (top-right) or somite bodies (bottom-right). D) Shows sagittal views of the heart and SHF arch at low power (left) and high-power images of the left ventricle (top-right) or SHF (bottom-right). (Size bars = 200µm) (Legend: PA = Pharyngeal arch; H = heart; SHF = Second Heart Field; S = somite).

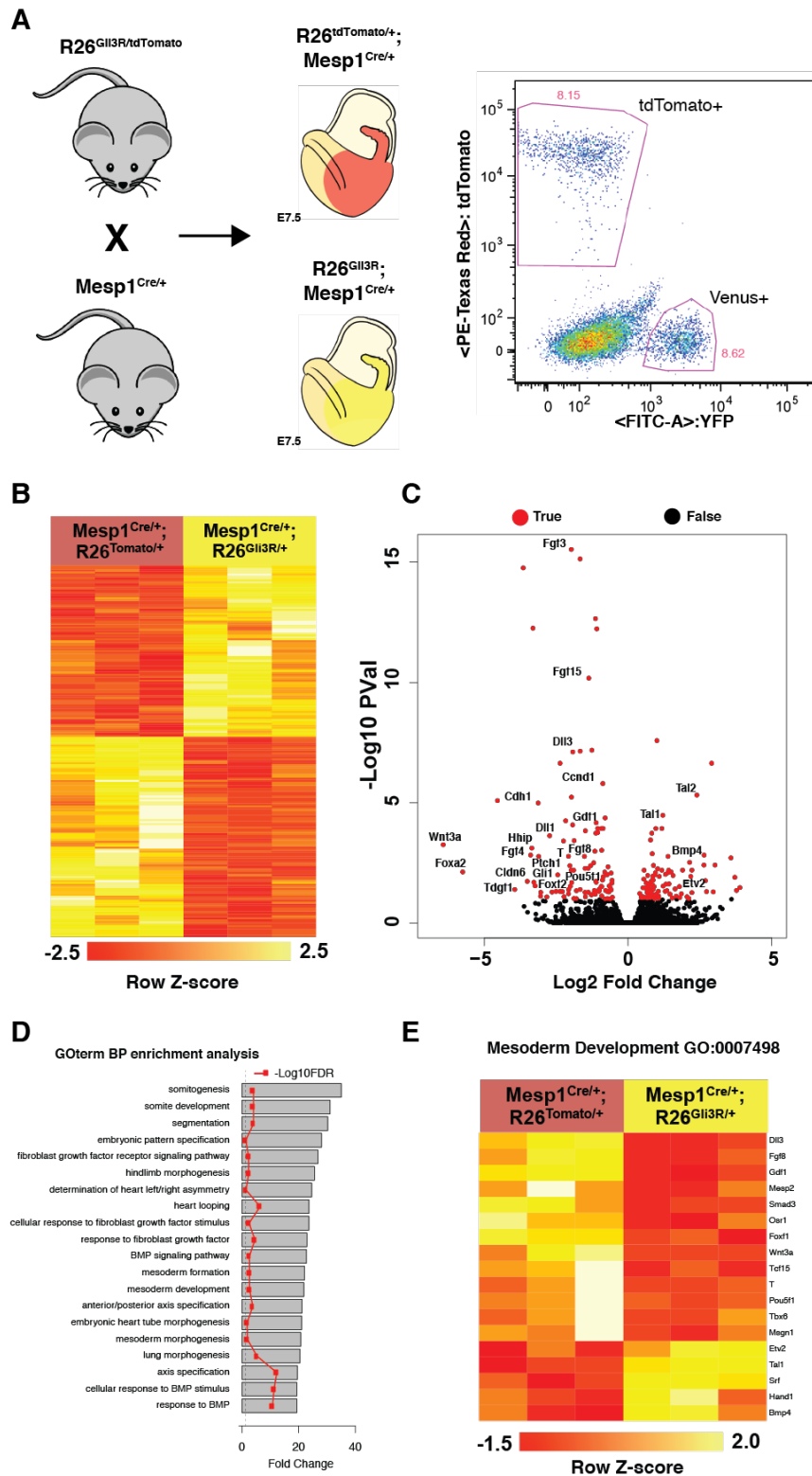


Fig. 3.4: Disruption of Hh signaling causes major disruptions in genetic pathways for mesoderm development. (A) Represents a breeding strategy to produce litter-matched controls

(Fig. 3.4, Continued)

between hedgehog mutant (*Mesp1-Gli3R*) and wild type (*Mesp1-tdTomato*) mesoderm by FACS-sorting *Mesp1^{Cre}*-marked cells by yellow and red channels respectively. (B) Z-score normalized heatmap for dysregulated genes (FDR \leq 0.10). (C) A volcano plot for dysregulated genes in Hh mutants. (D) GO analysis for genes downregulated genes in *Mesp1-Gli3R* mutants. (E) Heatmaps for all genes dysregulated under the Mesoderm Development (GO:007498) term (FDR \leq 0.30).

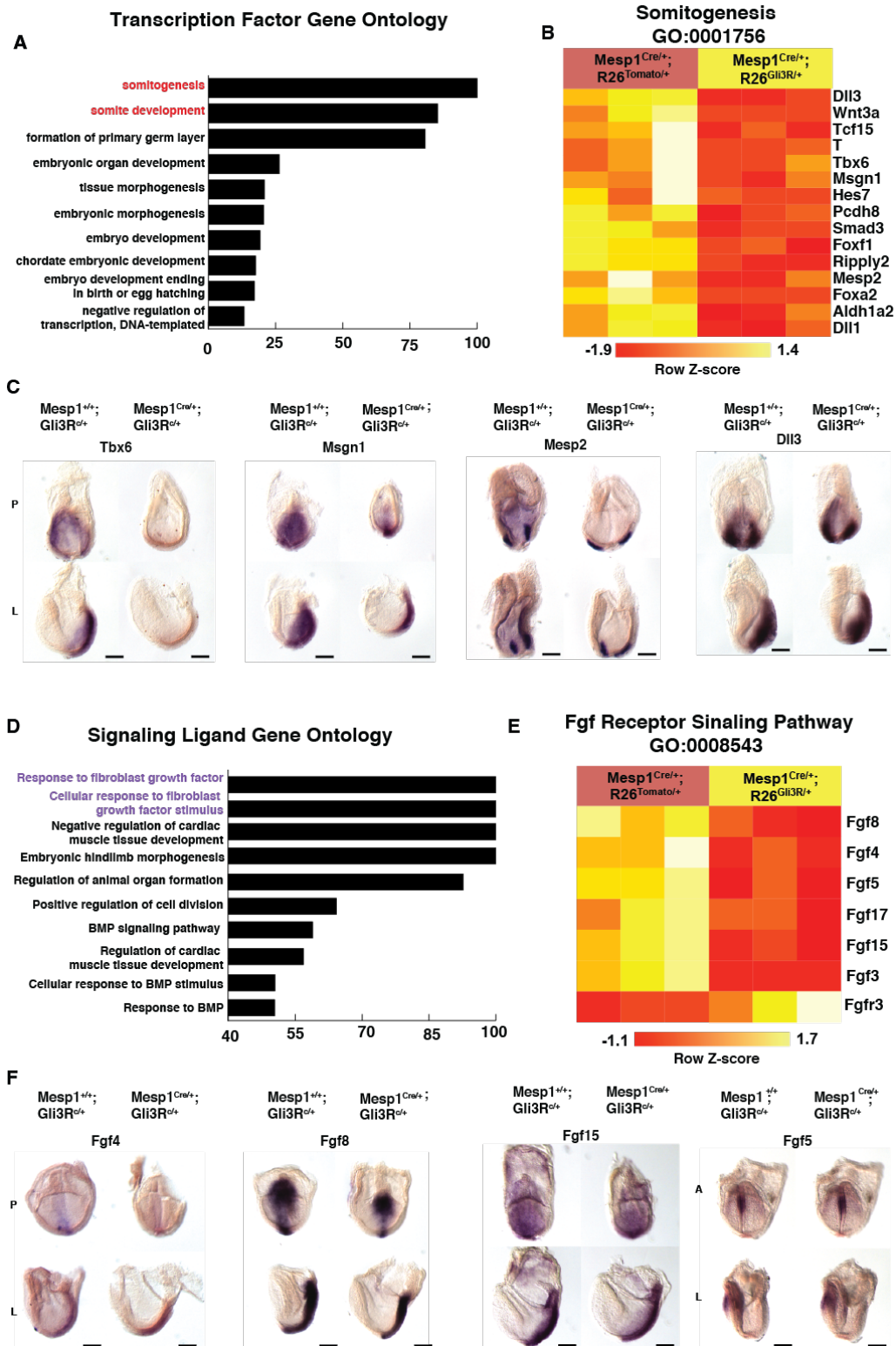


Fig. 3.5: Targeted pathway analysis reveals widespread dysfunction of nascent mesoderm and Fgf pathways. (A) GO analysis performed only on downregulated genes classified as

(Fig. 3.5, Continued)

transcription factors (B) shows a heatmap generated from dysregulated genes (FDR ≤ 0.30) overlapping with top GO term, Somitogenesis (GO:0001756). (C) ISH for the somitogenesis genes *Msgn1*, *Tbx6*, *Mesp2*, and *Dll1* in Wt ($Mesp1^{+/+};R26^{Gli3R/+}$) and Mut ($Mesp1^{Cre/+};R26^{Gli3R/+}$) embryos at E7.5. (D) GO analysis for downregulated genes classified as signaling molecules. (E) A heatmap for dysregulated genes FDR (≤ 0.30) for the top GO term, Fgf Receptor Signaling Pathway (GO:0008543). (F) ISH for FGF ligands *Fgf4*, *Fgf8*, *Fgf15*, and *Fgf5* in Wt ($Mesp1^{+/+};R26^{Gli3R/+}$) and Mut ($Mesp1^{Cre/+};R26^{Gli3R/+}$) embryos at E7.5. (Size bars = 200um).

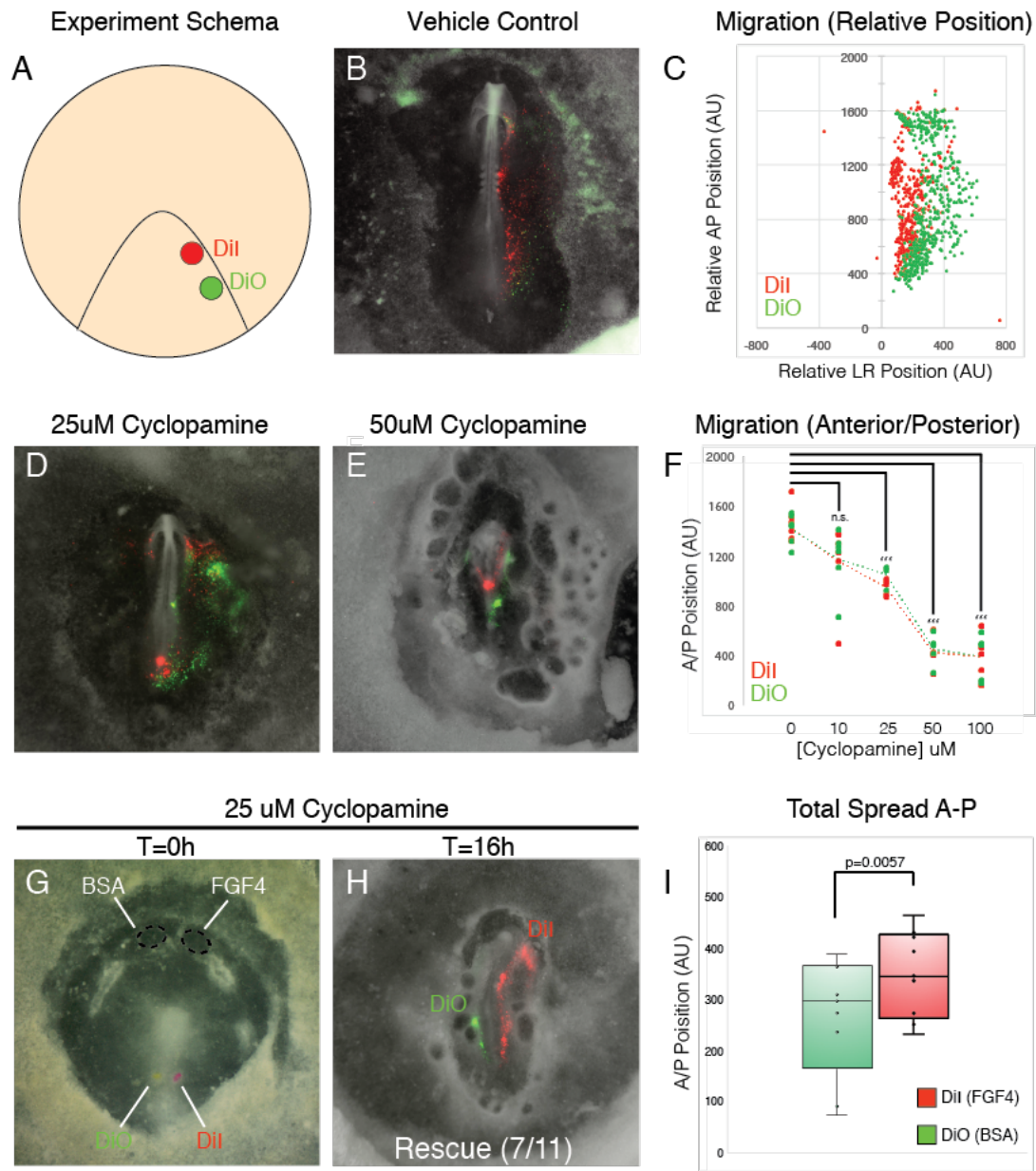


Fig. 3.6. Hh signaling is required for anterior cell migration during gastrulation upstream of the FGF pathway. (A) Demonstrates the placement of two lipophilic dye at the posterior portion of the embryo at (HH stage 3). (B and C) Demonstrates the trajectory of post-ingression mesoderm cells in vehicle control-treated chick embryos (B) which is spatially quantified in (C). (D and E) Addition of Smo antagonist Cyclopamine at 25 uM (D) and 50 μ M (E). (F) Shows quantification

(Fig. 3.6, Continued)

of inhibitory effect of cyclopamine between 10 μ M and 100 μ M. (*G-I*) Embryos treated with 25 μ M of cyclopamine had heparin beads coated with FGF4 placed towards the anterior-right pole of the embryo and BSA-coated heparin beads placed on the anterior-left portion of the embryo to serve as a contralateral control (*G*). After 16 hours of development 7/11 embryos show a marked rescue of specific directional migration on the side of the embryo with Fgf4 treatment (*H*) which was quantified to significantly differ from the control $p=0.0057$ (*I*).

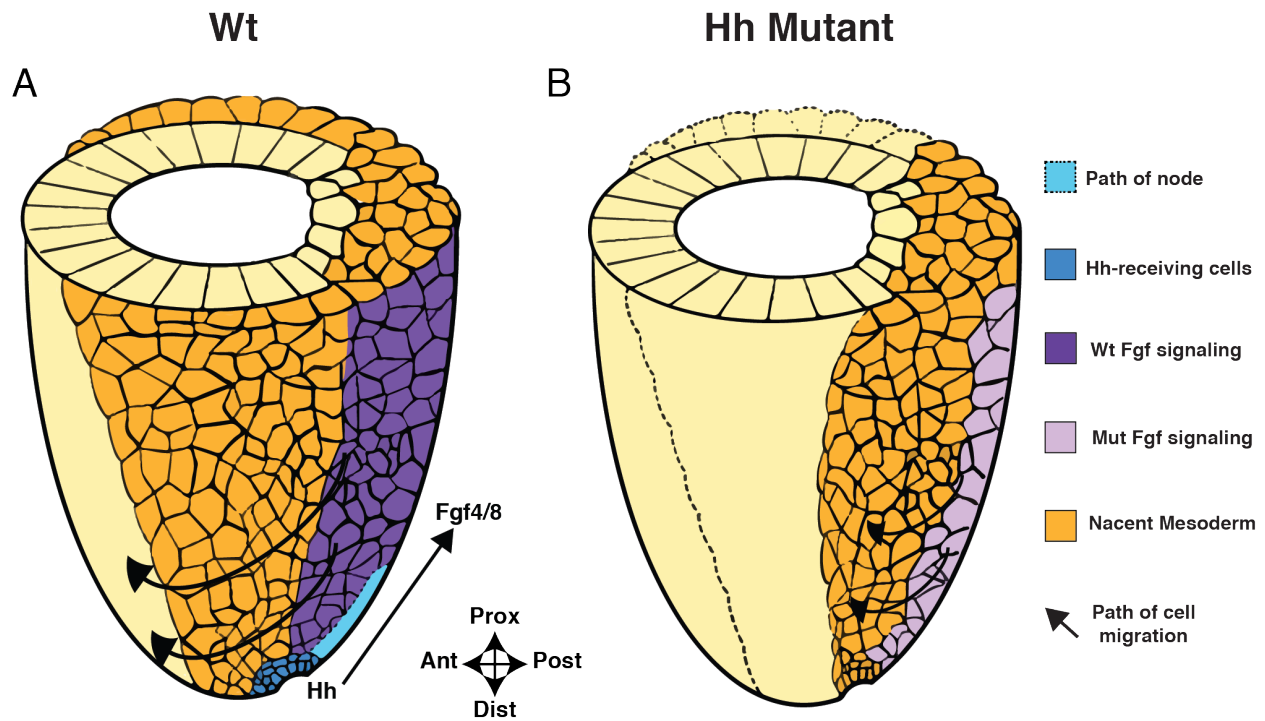


Fig. 3.7: Midline Hh signaling from the node drives an FGF pathway for anterior mesoderm morphogenesis. (*A* and *B*) Demonstrate a cartoon model for the role of Hh signaling in anterior mesoderm patterning. In (*A*) Wt Hh signaling is active early in embryonic midline in the node which is required for the full activation of a midline *Fgf4/8* signaling axis from the primitive streak which drives mesoderm migration. In (*B*) Hh pathway mutants, the FGF migratory pathway is greatly attenuated—resulting in disproportionate impacts on the migration and patterning of anterior mesoderm lineages which must migrate furthest during development. (Legend: Prox = Proximal, Dist = Distal, Ant = Anterior, Post = Posterior).

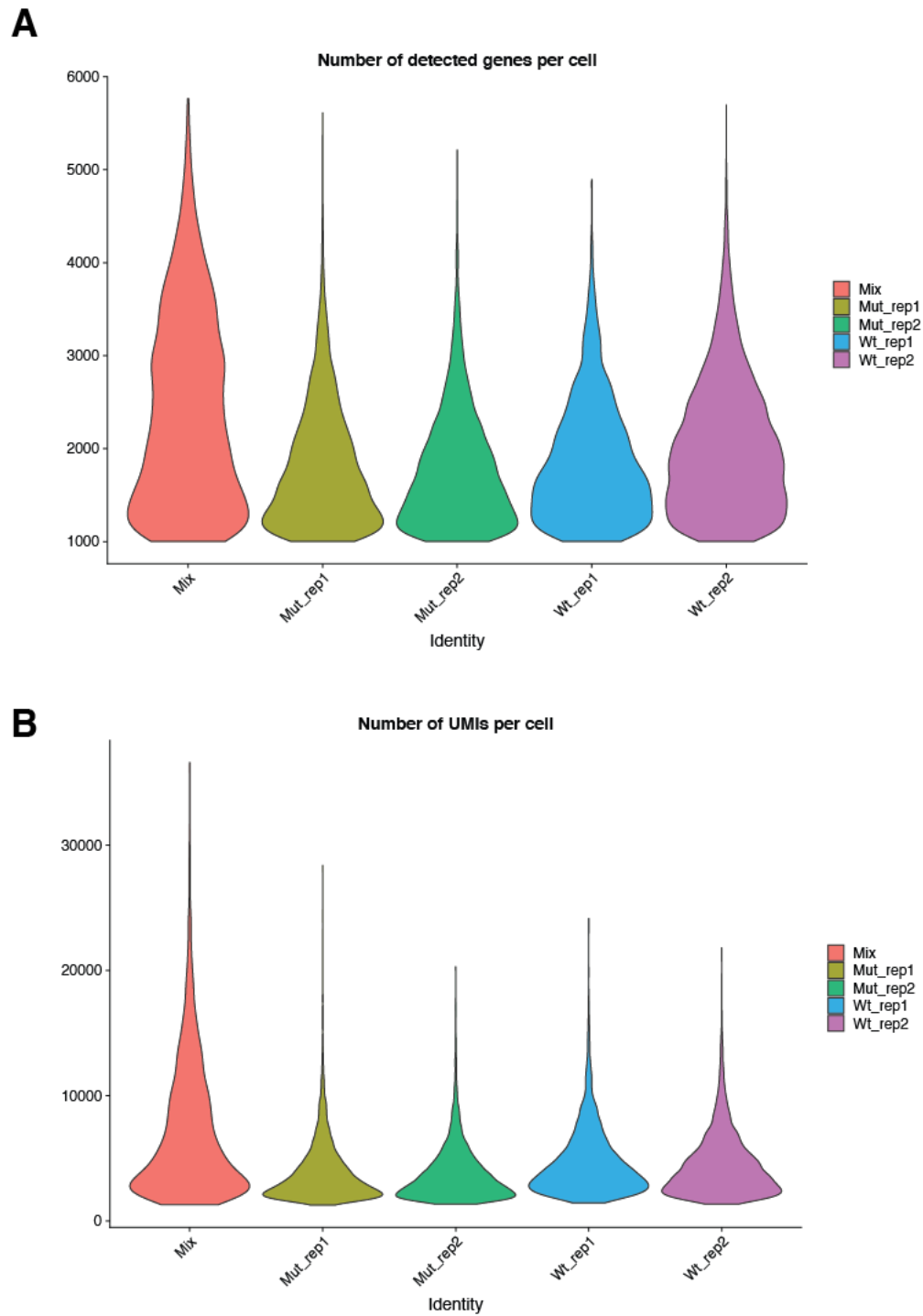


Fig. S3.1. Consistent gene and UMI counts are observed between Drop-seq replicates. (A) Violin plots for numbers of genes detected between all samples. **(B)** Violin plots for numbers of Unique Molecular Identifiers (UMIs) detected between all cell replicates.

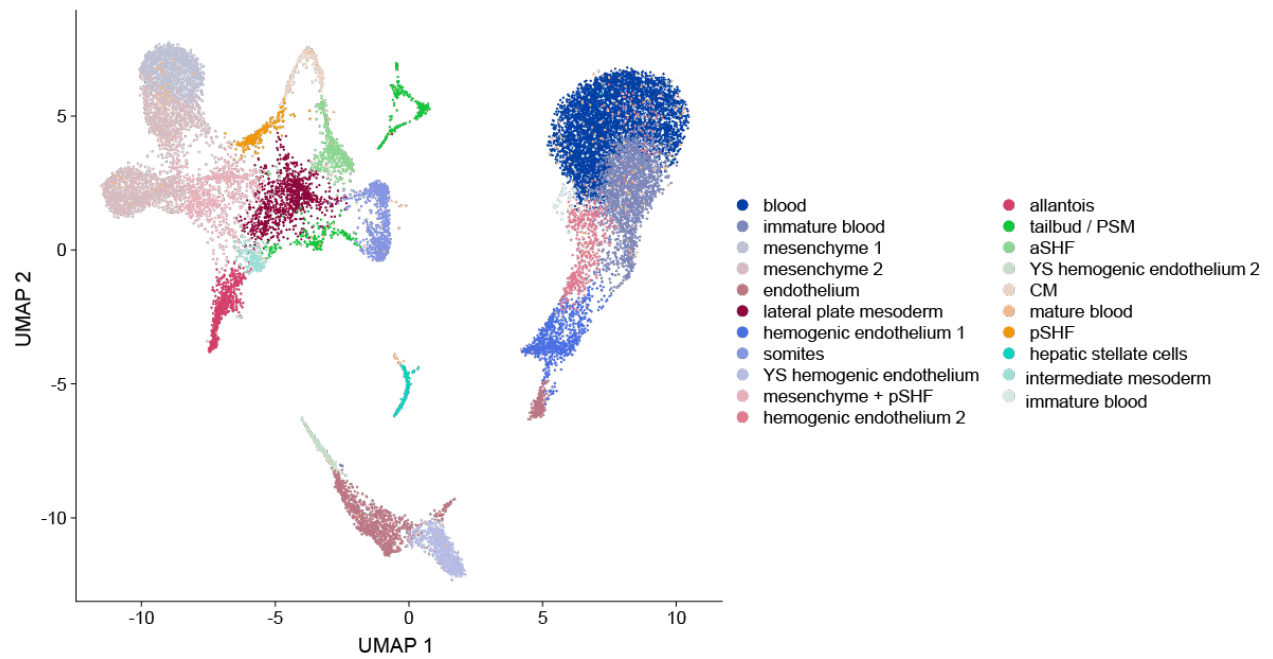


Fig. S3.2. Drop-seq Assay detects all Mesp1-derived lineages from Mesp1Cre-sorted cells.

UMAP for all cell types detected in Drop-seq assay for Mesp1^{Cre}-marked cells at E8.25.

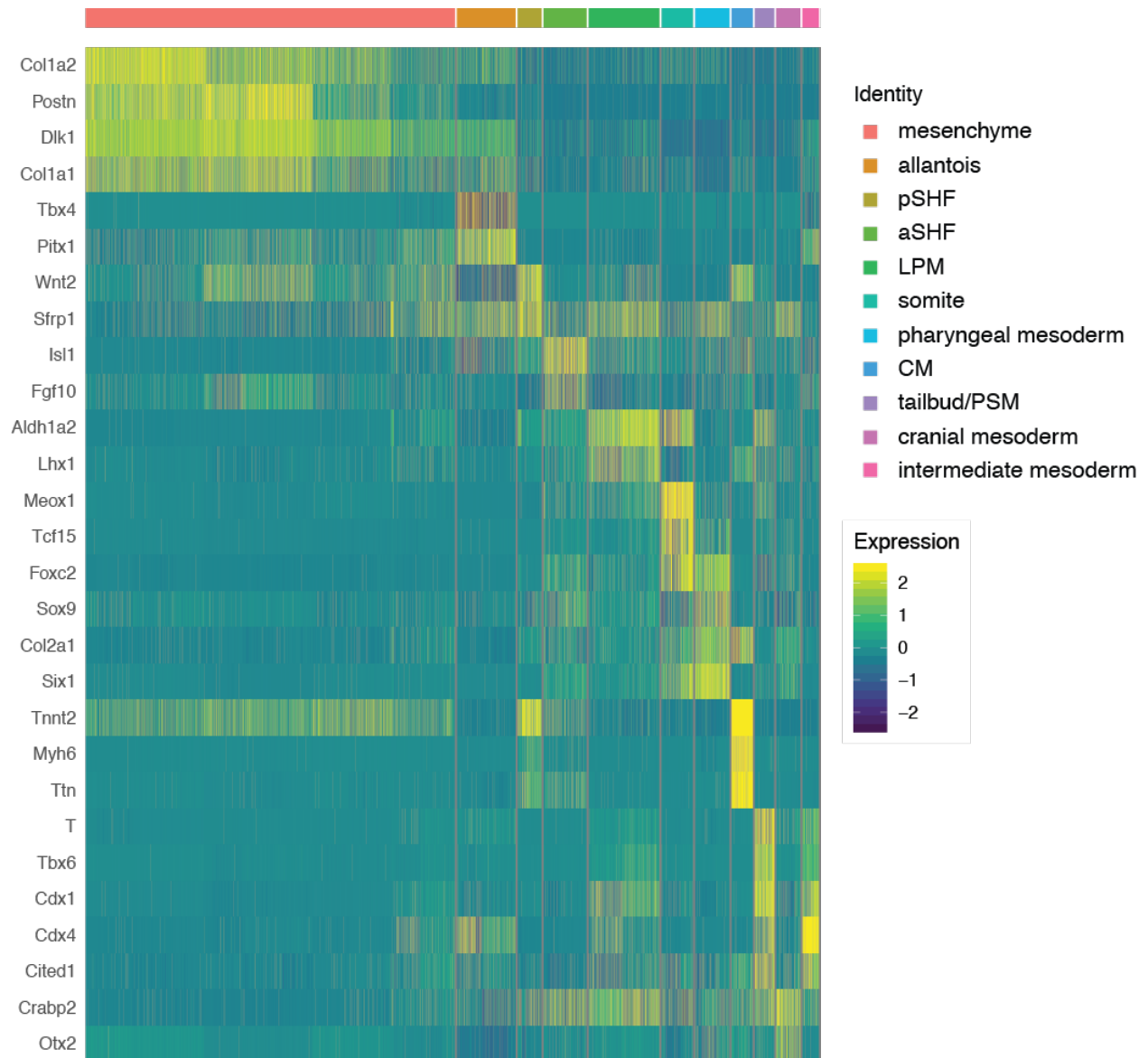


Fig. S3.3. Re-clustering of embryonic mesoderm identifies all mesodermal sub-lineages by canonical marker expression. Heatmap for the expression of canonical lineage markers in sub-clustered embryonic mesoderm.

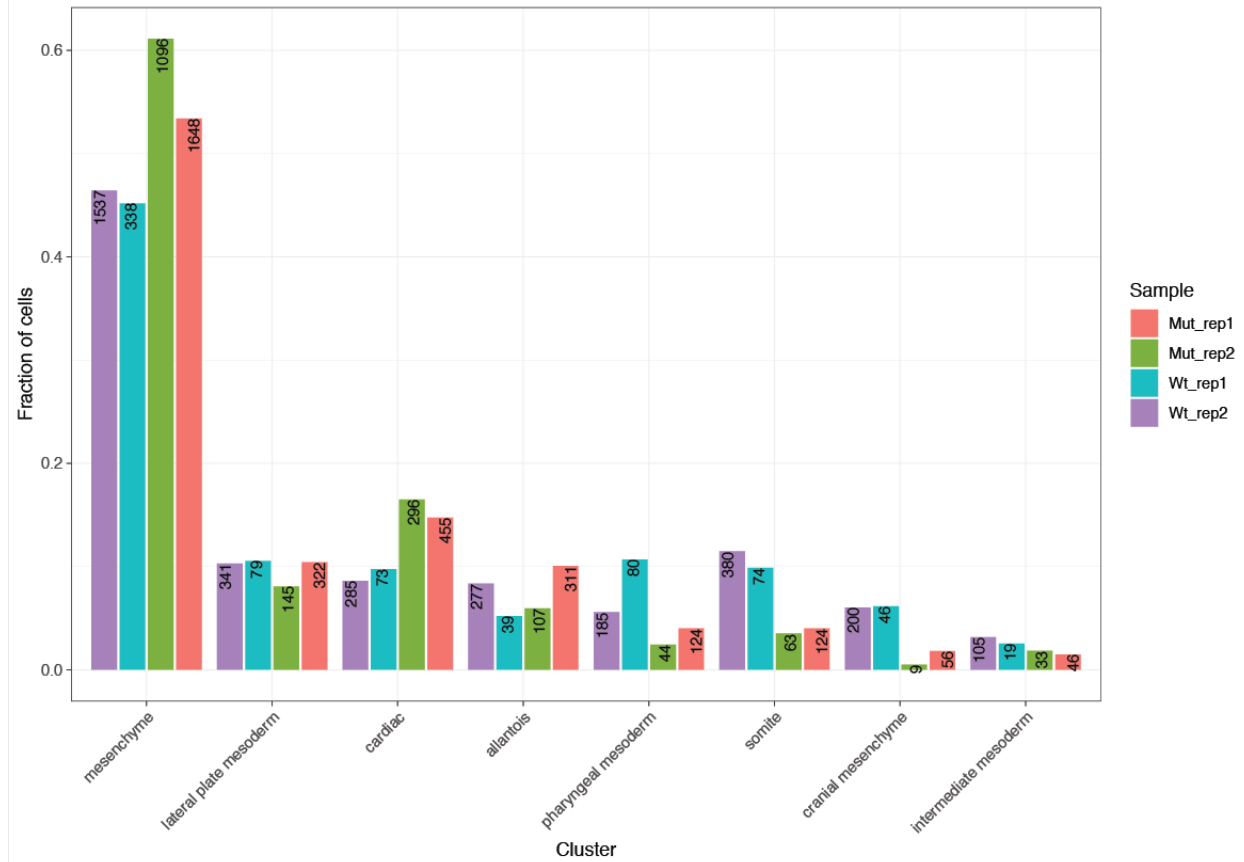


Fig. S3.4. Mesoderm cell distribution is highly consistent between replicates. Bar graph showing the proportional cell contribution to each mesoderm lineage split up by individual replicate.

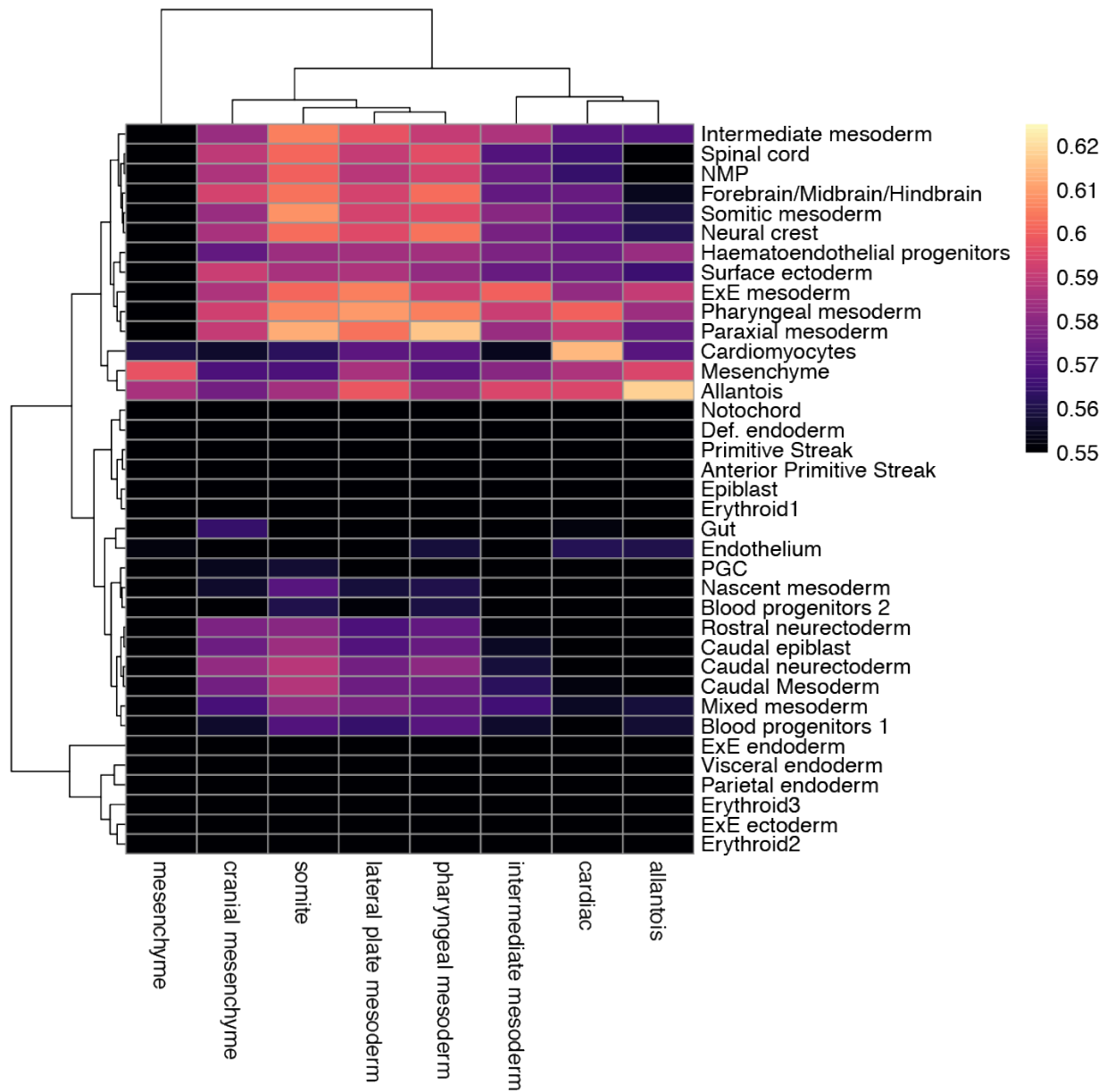


Fig. S3.5. Pseudo-bulk correlation analysis between embryonic mesoderm and extant scRNA-seq datasets. Correlation matrix comparing averaged (pseudo-bulk) RNA-seq signal in each assigned embryonic mesoderm cluster with a reference whole-embryo scRNA-seq database. The legend colors correspond to correlation values.

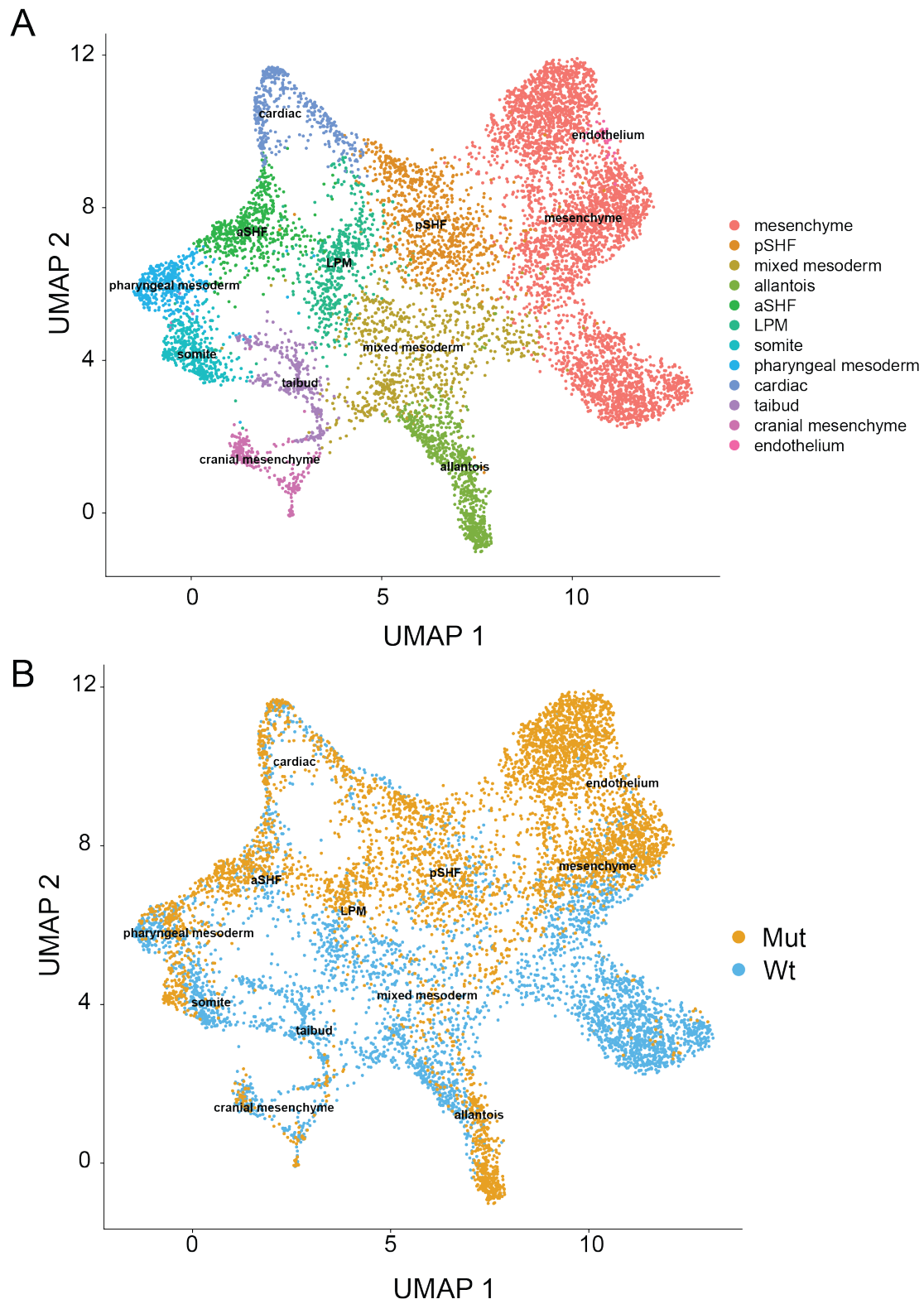


Fig. S3.6. UMAP plots with non-batch-corrected scRNA-seq data. (A and B) UMAP projections demonstrating cluster assignment (A) and genotype (B).

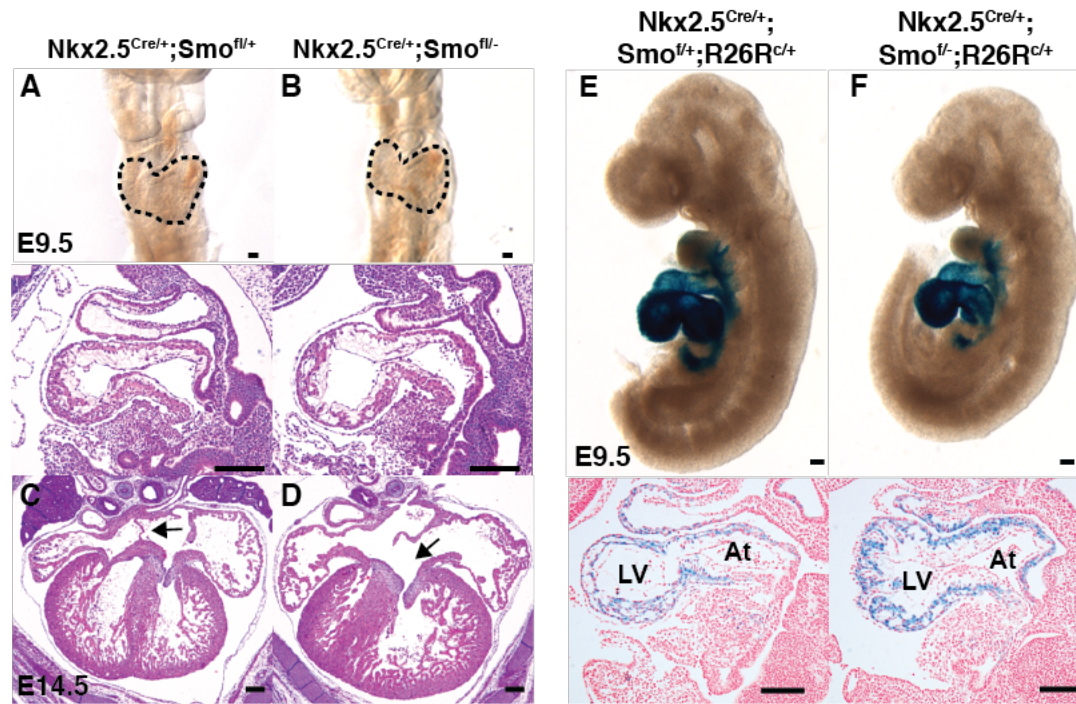


Fig. S3.7: Conditional removal of Smo reveals that Hh signaling is not required in specified cardiac precursors for proper heart development. (*A* and *B*) Shows frontal whole-mount (top panels) and sagittal histology (bottom panels) views of Conditional embryos with conditional *Smo* deletions from specified cardiac precursors in $Nkx2.5^{Cre/+};Smo^{fl/+}$ E9.5 (*B*) and $Nkx2.5^{Cre/+};Smo^{fl/+}$ controls (*A*). (*C* and *D*) show four-chambered-view histology slices of E14.5 $Nkx2.5^{Cre/+};Smo^{fl/+}$ and $Nkx2.5^{Cre/+};Smo^{fl/-}$ embryos; arrow points to the atrial septum. (*D*). (*E* and *F*) Shows sagittal whole-mount (top panels) and sagittal histology (Bottom panels) views of $Nkx2.5^{Cre}$ fate maps in $Smo^{fl/+}$ (*E*) and $Smo^{fl/-}$ (*F*) backgrounds. Blue X-gal stain marks cells that have expressed $Nkx2.5$ during development and their derivatives. (Size bars = 200µm) (LV = Left Ventricle, At = Atrium).

Tamoxifen at E6.5-E7.5
Analyzed at E9.5

	Litter 1			Litter 2			Litter 3		
	#1	#2	#3	#1	#2	#3	#1	#2	#3
IFT	5	5	4	5	5	4	5	5	4
AT	4	3	1	4	3	1	4	3	1
AVC	1	2	0	1	2	0	1	2	0
LV	1	2	1	1	2	1	1	2	1
RV	2	3	1	2	3	1	2	3	1
OFT	3	4	3	3	4	3	3	4	3

Table S3.1: Fate map quantification for Hh-receiving cells during gastrulation shows sparse and stochastic contribution to early cardiac structures. Values indicate numbers of marked clones in each cardiac structure derived from Gli1^{CreERT2} fate maps induced by tamoxifen administration at E6.5 and E7.5 in development. Key: IFT (Inflow tract), AT (common atrium), AVC (Atrioventricular canal), LV (Left Ventricle), RV (Right Ventricle, OFT (Outflow tract).

CHAPTER 4: HH SIGNALING IS REQUIRED FOR PROPER ERYTHROCYTE DIFFERENTIATION FROM HEMOGENIC PRECURSORS

Chapter 4 Introduction

Introduction to Hematopoiesis

Hematopoiesis is thought to occur in three waves during embryogenesis (1). The first wave begins near the onset of gastrulation where newly specified mesoderm migrates to the embryonic yolk sac and begins forming the first blood progenitors (1). The prevailing hypothesis is that blood is produced during this phase through an intermediate ‘hematoendothelial’ cell type that arises from the nascent mesoderm during gastrulation and expresses both hemogenic and endothelial genes. Despite expression of endothelial genes, these hematoendothelial precursors are likely not a common precursor for both blood and endothelial cells as was posited by the prediction of a hemangioblast cell (2, 3). However, angioblasts are generated during the same developmental period and give rise to the endothelial cells of the yolk sac vasculature which later participate in second wave hematopoiesis (4).

The second wave of hematopoiesis occurs in the yolk sac vasculature which is comprised of both non-hemogenic and hemogenic endothelium (5). The hemogenic endothelium undergoes an endothelial to hematopoietic (EHT) transition where it can produce multipotential erythromyeloid progenitors while non-hemogenic endothelium function solely to transport blood (5, 6). These hemogenic endothelial clusters were first described in classic embryology as ‘blood islands’ and can be defined by expression of the gene *Lyve1* (5, 7). Additionally, fate maps for *Lyve1*-expressing cells reveal an absence of primitive erythrocytes which are formed during first wave hematopoiesis—making it a specific marker for second wave hematopoietic lineages (5).

Throughout second wave hematopoiesis, the endothelial cells in the yolk sac undergo angiogenesis and remodel themselves into larger vessels and eventually join with the embryonic vasculature proximal to the onset of circulation (1, 3, 7). The connection between the embryonic and extraembryonic vasculature provides the embryo with early blood cells during the first two waves of hematopoiesis including: primitive erythrocytes cells formed during first wave hematopoiesis, megakaryocytes and tissue-resident macrophages formed from both waves, and definitive erythrocytes and erythromyeloid progenitors (EMPs) formed during second wave hematopoiesis (1).

The third wave of hematopoiesis begins around E10.5 and is localized to clusters of hemogenic endothelial cells located to the posterior region of the dorsal aorta in a region called the aorta gonad mesonephros (AGM) (6, 8). These hemogenic endothelial cells give rise to the first true hematopoietic stem cells which eventually colonize the adult bone marrow (9). Interestingly, the source of AGM hemogenic endothelium seems to largely originate from *Runx1*-expressing cells produced from the first wave of hematopoiesis (3). Ablation of this early population of *Runx1*-expressing cells during first wave hematopoiesis at E6.5 and E7.5 reduces future populations of hemogenic endothelium within the dorsal aorta and subsequently hematopoietic stem cell development to the point of causing perinatal lethal anemia (3). Although first wave hemogenic cells are incapable of directly producing mature hematopoietic stem cells, they are clearly linked to the development of AGM hemogenic endothelium and may have unappreciated roles in the generation of hematopoietic stem cells (10).

The role of Hh signaling in blood development

The role of Hh signaling in hematopoiesis has been both controversial and sparsely studied. While the Hh pathway is dispensable within adult hematopoietic stem cells for renewal and function (11), Hh signaling is critical for blood development throughout embryogenesis (10, 12, 13). *Smo*^{-/-} mutants exhibit anemia and a marked failure to remodel primitive yolk sac endothelial tubes into larger blood vessels through angiogenesis (14). The first study to provide a positive link between Hh signaling and blood demonstrated that *Ihh* was expressed within the early yolk sac endoderm and is sufficient to induce ectopic hematovascular lineage specification in the anterior epiblast (13). Additionally, *Ihh*^{-/-} mutants also display anemia yolk sac angiogenesis defects (15). Because defects within the Hh pathway disrupt both blood development and vascular remodeling through angiogenesis, it is often claimed that the disruption to angiogenesis itself is directly related to the blood development defects (16). While there is strong evidence showing Hh signaling is both necessary and sufficient for vascular remodeling, the initial specification of endothelial cells and the formation of the rudimentary yolk sac vascular bed through neovasculogenesis is preserved (15). Furthermore, endothelial disorganization in itself is likely probably not sufficient to explain the defects to blood development given the disparate developmental influences governing the hemogenic and non-hemogenic endothelium (2, 3).

The rationale that endothelial tube formation is required for both hemogenic endothelium development and subsequent blood production was used as the basis for recent *in vitro* studies (16, 17). While it is clear that inhibition of Hh signaling greatly reduces the potential for blood formation in mouse embryonic stem cell (mESCs) differentiation models, the disruption to hemogenic endothelial cells is consistently modest or negligible (16-18). In one case, cyclopamine-mediated Hh pathway inhibition increased the expression of the hemogenic

endothelial marker *Runx1* (16). This provides evidence more in favor of separate requirements for Hh signaling in blood and hemogenic endothelium development.

In summary, there is clear evidence that both endothelial tube formation and blood development are acutely disrupted in Hh mutants *in vivo*. Although it is clear that Hh signaling is required for proper blood formation *in vitro*, the presumption that this is secondary to defect in hemogenic endothelial development is tenuous. Furthermore, there has yet to be any attempt in the literature to clarify which phase of blood development is dependent upon Hh signaling. In this chapter, I will discuss my findings regarding a putative role for Hh signaling in the establishment of endothelium, hemogenic precursors, and blood during early embryonic development.

Chapter 4 Results

Transcription of blood genes is severely disrupted in Hh mutants after organogenesis

To survey the impact of early disruptions to Hh signaling on early embryonic mesoderm development, we dissociated whole E8.5 embryos and isolated *Mesp1*^{Cre}-marked cells from dominant negative Hh mutants overexpressing Gli3R in the mesoderm (*Mesp1-Gli3R*) and control (*Mesp1-tdTomato*) mesoderm using FACS. Litter-matched samples were processed for RNA-seq and the resultant differential gene expression was consistent between biological replicates with majority of significantly different genes (FDR < 0.10) being downregulated (Fig 4.1 A). Although phenotypic defects were present across all in *Mesp1-Gli3R* embryos at this stage in development, the vast majority of significantly downregulated genes were related to blood development—including a large number of embryonic hemoglobin subunits and canonical transcription factors for hematopoiesis including *Runx1* and *Gata1* (Fig. 4.1 B)(2, 3, 19). This suggested that a major effect of disruptions to early Hh signaling is a defect to erythrocyte production.

To confirm the observation that blood genes were overrepresented amongst our downregulated gene set, we performed Gene Ontology (GO) analysis. As expected, terms for blood development dominated the list generated for downregulated genes (Fig. 4.1 C). Interestingly, when we performed GO analysis for the genes upregulated in Hh mutants, terms for angiogenesis and vascular development were the most highly represented (Fig. 4.1D). This was of particular interest as disruptions to Hh signaling have classically been described as disruptive to the early endothelium (12-15). Interestingly, the downregulation of blood developmental genes was not observed at E7.5 when the first wave hemogenic precursors are produced. Overlap between downregulated genes at both E7.5 and E8.5 resulted in many classically Hh-dependent

genes such as *Ptch1* (20) and context-specific Hh-dependent genes such as *Foxf2* (Fig 4.1 E) (21). However, when genes that were downregulated in E8.5 *Mesp1-Gli3R* mutants were overlapped with genes upregulated in E7.5 *Mesp1-Gli3R* mutants I observed the inclusion of many genes for early blood and endothelial development (Fig. 4.1 F). This suggested that there may be disparate effects of hh signaling on first and second wave hematopoiesis.

scRNA-seq of Hh mutant mesoderm reveals a proportional shift from embryonic blood to hemogenic precursor populations

Although it was clear that blood development was generally disrupted in Hh mutants, it was unclear which wave of hematopoiesis was affected, and by what mechanism. To address these questions, we performed scRNA-seq on FACS-sorted *Mesp1^{Cre}*-marked cells from *Mesp1-Gli3R* (Hh signaling deficient) and *Mesp1-tdTomato* (control) embryos at E8.25, which coincides with the onset of organogenesis (Fig 4.2 A) (22). The advantage of conducting studies at this time point was that we could assay both the tail-end of 1st wave hematopoiesis and the beginning of 2nd wave hematopoiesis within the same embryos (1, 8). UMAP projections from single cells revealed that extraembryonic tissues responsible for early blood formation are the most highly represented populations (Fig 4.2 B).

We removed lineages unrelated to blood development from further analysis and re-clustered the remaining cells to gain finer resolution of blood sub-lineages. By gene expression, we identified three primary cell types consisting of either erythrocytes, hemogenic endothelium, and non-hemogenic endothelium (Fig 4.2 C). When we mapped cells by genotype, it was clear that there was a major change in the distribution of cells across different lineages (Fig 4.2 D). We plotted the proportion of cell types for each genotype and found a major relative deficit across the

observed erythrocyte population in *Mesp1-Gli3R* mutants in addition to relative enrichment of both endothelium and hemogenic endothelium (Fig. 4.2 *E*). This result was in-line with our E8.5 bulk RNA-seq which showed a relative reduction in blood transcripts in Hh mutants and a relative increase to vascular and endothelial transcripts (Fig 4.1 *A-D*). However, it is unclear whether Hh was required within pre-blood hemogenic precursors or within nascent erythrocytes. To complicate this further, hemogenic and non-hemogenic endothelium derived from both embryonic and extraembryonic mesoderm receive active Hh signaling throughout hematopoiesis (Fig 4.2 *F*)(15). Additionally, erythrocytes retain active Hh signaling well after organogenesis at E9.5—before the onset of embryonic blood production from the dorsal aorta (Fig. S4.1)—though it is unclear whether marked erythrocytes originate from first or second wave hematopoiesis.

Hh signaling is involved in blood precursor development for both first and second wave hemopoiesis

In order to understand the independent effects of Hh signaling on first and second wave hematopoiesis, we used single cell gene expression to determine the identity extraembryonic sub-lineages. We created a heatmap for canonical lineage-marker expression where the expression level of individual genes in single cells was represented by the color intensity. We noted that each cluster expressed a unique combination of genes with the exception of clusters 0-2, which represent erythrocyte populations and share nearly identical gene expression patterns (Fig. 4.3 *A*). However, the most notable aspect of the lineage distribution is the appearance of two superclusters of cells separated on the x-axis of the UMAP which represent first and second waves hematopoiesis respectively. The clusters on the right side of the UMAP comprise first wave hemogenic cells and

are marked by high *Runx1* expression while cells on the left represent the maturing yolk sac and are marked by *Lyve1* expression (5).

First wave hematopoiesis, represented by clusters 0-3 and 6, begins during gastrulation as extraembryonic mesoderm generates blood in the yolk sac through an intermediate cell that expresses both hemogenic and endothelial genes. This so-called hematoendothelial cell type, represented by Cluster 3 expresses endothelial genes such as *Tall*, *Etv2* and *Pecam1*, but not *Rhoj* (17, 23-27), in addition to genes that confer hemogenic potential such as *Gfilb*, *Runx1* and *Itga2b* (CD41)(6) (Fig 4.3 A and B). Cluster 3 hematoendothelial cells then progress through development into a transitional lineage represented by cluster 6 where precursor genes such as *Runx1* and *Gfilb* are downregulated and mature erythrocyte genes such as *Gata1* and *Hbb-y* start to become expressed (Fig 4.3 A and B)(19, 28). They then give rise to the erythrocyte population, which is almost exclusively produced by first wave hematopoiesis at this stage.

The yolk sac located on the left side of the UMAP is represented by clusters 4, 5, and 8. This supercluster shows robust expression of classic endothelial markers in at least one cluster including: *Pecam1*, *Etv2*, *Flt1*, *Tall*, and *Rhoj* (Fig 4.3 A and B). Conversely, these clusters lack expression of most hemogenic precursors including *Gata1* and *Runx1*—though they do begin to express early markers of blood differentiation including CD34, CD41 and Kit (c-kit) (Fig 4.3 A and B)(6). However, the main gene to distinguish this supercluster from first wave hemogenic precursors is *Lyve1*, which exclusively expressed in the definitive yolk sac hemogenic endothelium—the site of secondary hematopoiesis (Fig 4.3 A and B)(5).

In this study, it is clear that Hh-mutant *Mesp1-Gli3R* cells preferentially contribute to endothelial and hemogenic precursor lineages at the expense of mature erythrocytes in both first and second wave hematopoietic lineages (Fig. 4.2 E). This result is particularly striking because it

seems contrary to extant literature citing both endothelial and blood defects within the early yolk sac. This may suggest that the dysfunction to erythrocyte production in Hh mutants may be due to a failure for hemogenic endothelial precursors to properly differentiate into mature erythrocytes.

Chapter 4 Discussion

In this study, we identified that Hh mutations cause defects to hematopoiesis in the early embryo while preserving, or perhaps enhancing the development of endothelial and hemogenic endothelial precursor development. This is contrary to all current theories about the role of Hh signaling in blood development where it is widely assumed that blood defects are secondary to defects to the production of endothelium and hemogenic precursors (16).

The first studies to investigate the role of Hh signaling in early blood development were primarily concerned with the ability of Hh ligand to induce endothelial tube formation in angioblast cells and to ectopically induce hemogenic and angiogenic cell fates in the early anterior epiblast (12, 13, 15, 29). Loss of function studies in mouse embryos focused exclusively on the defects of large vessels where it is noted that vascular remodeling in the yolk sac and anterior dorsal aorta require Hh pathway activity (12, 14, 15, 29). However, it was shown that even in *Smo*^{-/-} embryos, robust expression of the endothelial-specific protein, PECAM, is observed in the yolk sac—suggesting that extraembryonic endothelial cell specification is intact (15). Additionally, it is clear by gross morphology that the primitive vascular bed of the yolk sac is appropriately formed—restricting the defect to that of vessel remodeling.

A recent *in vitro* study attempted to link the endothelial remodeling defects observed in Hh mutants to defects in blood development (16). However, although they noted clear defects to blood differentiation, they noticed only mild defects to hemogenic endothelium production. Interestingly, they were able to overcome the effects of Hh inhibition by upregulating either Scl or Delta/Notch signaling though this may speak to a rescue of EHT rather than a rescue of hemogenic endothelium production (16). Of note, they rest a large part of their model on extant literature citing developmental disruption to endothelial organization despite the fact that there is no current

linking a requirement for endothelial tube organization alone to produce blood. Furthermore, past *in vitro* models for blood development have led to improper conclusions. Notably evidence for a bipotential progenitor cell for both blood and vascular lineages, referred to as the hemangioblast, was supposedly identified *in vitro* (30, 31). Later studies demonstrated that this bipotential cell was not resident *in vivo* and was primarily a product of exogenous culture conditions which alter cellular differentiation potential (1, 30-35).

For the above reasons, it is imperative to use *in vivo* systems to study the role of Hh signaling in early blood development. Based on our transcriptional studies, it appears that both first wave hematoendothelial precursors and second wave hemogenic endothelial cells are enriched in Hh mutants at the expense of functional blood development. Firstly, this decouples the link between endothelial tube dysfunction and the specification of endothelial cells themselves. Second, this suggests that the reduction in blood is due to a failure of hemogenic endothelial cells to differentiate into mature erythrocytes rather than an underlying deficit in hemogenic endothelium production. Furthermore, the fact that E8.5 embryos demonstrate even greater reduction to blood transcripts compared to E8.25 embryos suggests that anemia persists in early Hh mutants and suggests that this defect continues through at least through second wave hematopoiesis.

Several questions remain—the first being why there is a lack of downregulated blood transcripts in E7.5 *Mesp1-Gli3R* mutants even though these cells are generated during gastrulation (Fig 4.1 *E* and *F*). It may be the case that the original specification of these progenitors from the mesoderm is intact but have reduced potential for renewal without active Hh signaling. We are also unaware of which genes are directly regulated by Hh signaling for blood differentiation. An obvious candidate is the *Vegf* pathway which has been shown to be downstream of Hh signaling

in vascular development and is responsible for assisting in both primitive and definitive hematopoiesis (10, 36). Finally, although the Hh pathway is dispensable for adult hematopoietic stem cell (HSC) function in mammals, it has never been shown whether Hh signaling is required for the initial development of HSCs during mammalian embryogenesis despite the fact that Hh signaling is required for HSC development in zebrafish (10). This will require ablation of the Hh pathway from hemogenic endothelium within either the dorsal aorta which directly produce presumptive adult HSCs or in the Runx1⁺ hematoendothelial precursors that give rise to the hemogenic endothelium in the dorsal aorta (2, 3).

REFERENCES

1. Lacaud G & Kouskoff V (2017) Hemangioblast, hemogenic endothelium, and primitive versus definitive hematopoiesis. *Exp Hematol* 49:19-24.
2. Tanaka Y, *et al.* (2012) Early ontogenic origin of the hematopoietic stem cell lineage. *Proc Natl Acad Sci U S A* 109(12):4515-4520.
3. Samokhvalov IM, Samokhvalova NI, & Nishikawa S (2007) Cell tracing shows the contribution of the yolk sac to adult haematopoiesis. *Nature* 446(7139):1056-1061.
4. Padron-Barthe L, *et al.* (2014) Clonal analysis identifies hemogenic endothelium as the source of the blood-endothelial common lineage in the mouse embryo. *Blood* 124(16):2523-2532.
5. Lee LK, *et al.* (2016) LYVE1 Marks the Divergence of Yolk Sac Definitive Hemogenic Endothelium from the Primitive Erythroid Lineage. *Cell Rep* 17(9):2286-2298.
6. Thambyrajah R, *et al.* (2016) GF11 proteins orchestrate the emergence of haematopoietic stem cells through recruitment of LSD1. *Nature Cell Biology* 18(1):21-+.
7. Ferkowicz MJ & Yoder MC (2005) Blood island formation: longstanding observations and modern interpretations. *Exp Hematol* 33(9):1041-1047.
8. Yoder MC (2014) Inducing definitive hematopoiesis in a dish. *Nat Biotechnol* 32(6):539-541.
9. Medvinsky A & Dzierzak E (1996) Definitive hematopoiesis is autonomously initiated by the AGM region. *Cell* 86(6):897-906.
10. Gering M & Patient R (2005) Hedgehog signaling is required for adult blood stem cell formation in zebrafish embryos. *Dev Cell* 8(3):389-400.
11. Gao J, *et al.* (2009) Hedgehog signaling is dispensable for adult hematopoietic stem cell function. *Cell Stem Cell* 4(6):548-558.
12. Astorga J & Carlsson P (2007) Hedgehog induction of murine vasculogenesis is mediated by Foxf1 and Bmp4. *Development* 134(20):3753-3761.
13. Dyer MA, Farrington SM, Mohn D, Munday JR, & Baron MH (2001) Indian hedgehog activates hematopoiesis and vasculogenesis and can respecify prospective neurectodermal cell fate in the mouse embryo. *Development* 128(10):1717-1730.
14. Vokes SA, *et al.* (2004) Hedgehog signaling is essential for endothelial tube formation during vasculogenesis. *Development* 131(17):4371-4380.
15. Byrd N, *et al.* (2002) Hedgehog is required for murine yolk sac angiogenesis. *Development* 129(2):361-372.
16. Kim PG, *et al.* (2013) Signaling axis involving Hedgehog, Notch, and Scl promotes the embryonic endothelial-to-hematopoietic transition. *Proc Natl Acad Sci U S A* 110(2):E141-150.
17. Gong W, *et al.* (2017) Dpath software reveals hierarchical haemato-endothelial lineages of Etv2 progenitors based on single-cell transcriptome analysis. *Nat Commun* 8:14362.
18. Byrd N & Grabel L (2004) Hedgehog signaling in murine vasculogenesis and angiogenesis. *Trends Cardiovasc Med* 14(8):308-313.
19. Ferreira R, Ohneda K, Yamamoto M, & Philipsen S (2005) GATA1 function, a paradigm for transcription factors in hematopoiesis. *Mol Cell Biol* 25(4):1215-1227.

20. Goodrich LV, Milenkovic L, Higgins KM, & Scott MP (1997) Altered neural cell fates and medulloblastoma in mouse patched mutants. *Science* 277(5329):1109-1113.
21. Hoffmann AD, *et al.* (2014) Foxf genes integrate tbx5 and hedgehog pathways in the second heart field for cardiac septation. *PLoS Genet* 10(10):e1004604.
22. Ibarra-Soria X, *et al.* (2018) Defining murine organogenesis at single-cell resolution reveals a role for the leukotriene pathway in regulating blood progenitor formation. *Nat Cell Biol* 20(2):127-134.
23. Yuan L, *et al.* (2011) RhoJ is an endothelial cell-restricted Rho GTPase that mediates vascular morphogenesis and is regulated by the transcription factor ERG. *Blood* 118(4):1145-1153.
24. Cui M, Wang Z, Bassel-Duby R, & Olson EN (2018) Genetic and epigenetic regulation of cardiomyocytes in development, regeneration and disease. *Development* 145(24).
25. Montel-Hagen A, Van Handel B, & Mikkola H (2013) [An unexpected repressive role for Scl in the embryonic endothelium]. *Med Sci (Paris)* 29(3):257-259.
26. Feng D, Nagy JA, Pyne K, Dvorak HF, & Dvorak AM (2004) Ultrastructural localization of platelet endothelial cell adhesion molecule (PECAM-1, CD31) in vascular endothelium. *J Histochem Cytochem* 52(1):87-101.
27. Wareing S, Eliades A, Lacaud G, & Kouskoff V (2012) ETV2 expression marks blood and endothelium precursors, including hemogenic endothelium, at the onset of blood development. *Dev Dyn* 241(9):1454-1464.
28. Palstra RJ, *et al.* (2003) The beta-globin nuclear compartment in development and erythroid differentiation. *Nat Genet* 35(2):190-194.
29. Rowton M, *et al.* (2018) Hedgehog signaling controls progenitor differentiation timing during heart development. *bioRxiv*.
30. Choi K (2002) The hemangioblast: a common progenitor of hematopoietic and endothelial cells. *J Hematother Stem Cell Res* 11(1):91-101.
31. Robb L & Elefanty AG (1998) The hemangioblast--an elusive cell captured in culture. *Bioessays* 20(8):611-614.
32. Wang H, Zhuang Z, & Chan CC (2018) Hemangioblast: origin of hemangioblastoma in von Hippel-Lindau (VHL) syndrome. *Oncoscience* 5(7-8):212-213.
33. Amaya E (2013) The hemangioblast: a state of competence. *Blood* 122(24):3853-3854.
34. Nishikawa S (2012) Hemangioblast: an in vitro phantom. *Wiley Interdiscip Rev Dev Biol* 1(4):603-608.
35. Kennedy M, D'Souza SL, Lynch-Kattman M, Schwantz S, & Keller G (2007) Development of the hemangioblast defines the onset of hematopoiesis in human ES cell differentiation cultures. *Blood* 109(7):2679-2687.
36. Lawson ND, Vogel AM, & Weinstein BM (2002) sonic hedgehog and vascular endothelial growth factor act upstream of the Notch pathway during arterial endothelial differentiation. *Dev Cell* 3(1):127-136.

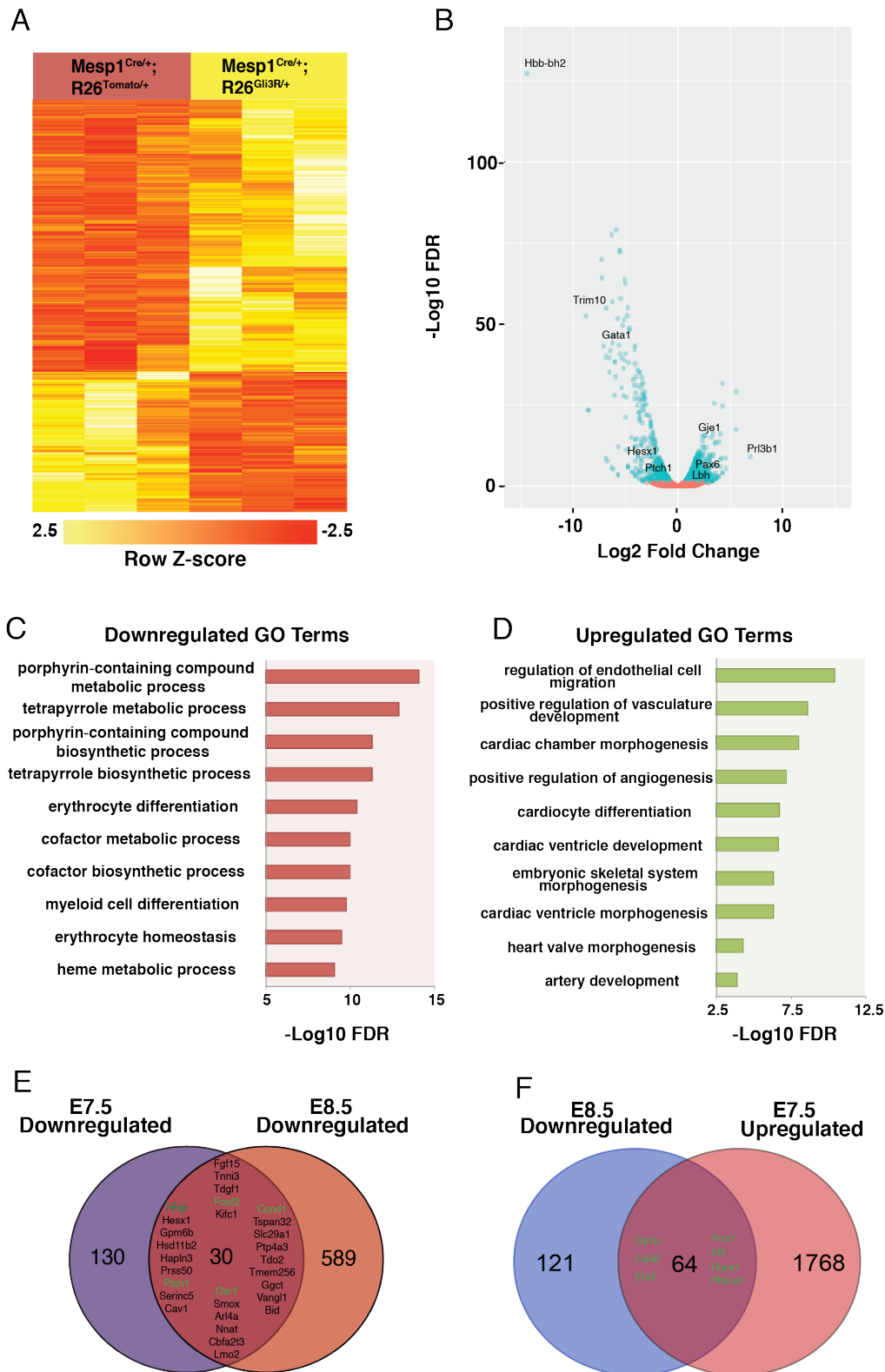


Fig. 4.1. Hh mutants reveal an absence of blood gene expression after organogenesis. (A) Heat map for differentially-expressed Hh-dependent genes (A) shows consistency of gene expression

(Fig. 4.1, Continued)

between replicates majority and that downregulated genes comprise the bulk of differential expression. (B) A volcano plot for Hh-dependent genes shows classic determinants of blood development and blood differentiation products are greatly reduced in expression. (C and D) Gene ontology (GO) analysis for downregulated genes (C) reveals almost exclusive enrichment for blood terms while GO analysis for upregulated genes (D) are represented mainly by terms for vascular development. (E) Shows overlap of downregulated genes between E7.5 and E8.5 *Mesp1-Gli3R* mutants with overlapping Hh-dependent genes highlighted in green while (F) shows overlap between upregulated E7.5 and downregulated E8.5 *Mesp1-Gli3R* mutants with overlapping blood development genes highlighted in green.

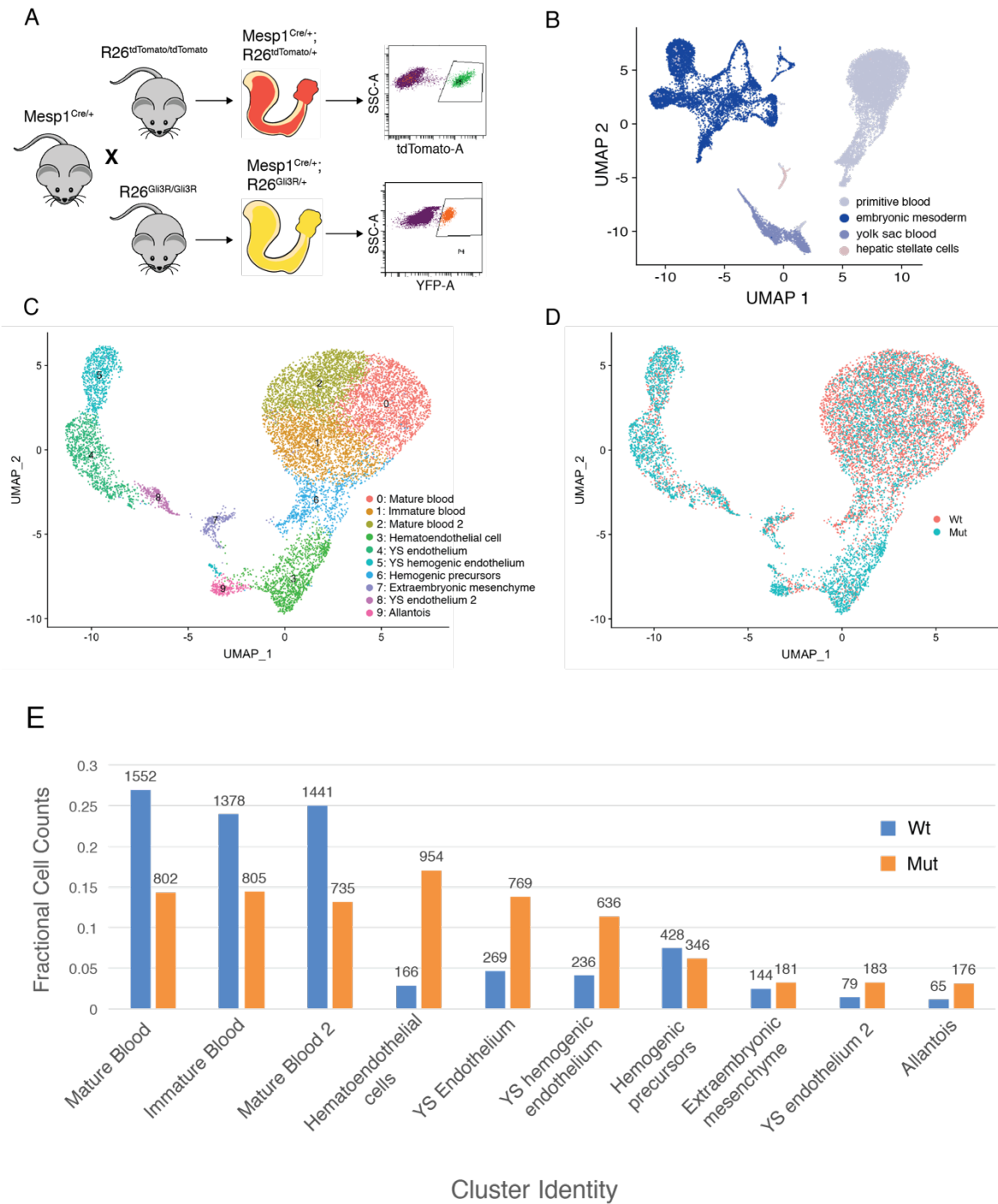


Fig. 4.2. scRNA-seq of *Mesp1*-Gli3R mutant mesoderm during organogenesis reveals increase in endothelial populations at the expense of blood: (A) *Mesp1*^{Cre}-labeled cells from

(Fig. 4.2, Continued)

both Wt (*Mesp1-tdTomato*) and Mut (*Mesp1-Gli3R*) were isolated by FACS and processed for scRNA-sequencing using Drop-seq. (B) UMAP projections of single-cell transcriptomes revealed that the majority of cells are comprised of extraembryonic tissues which are responsible for early embryonic blood production. (C) Re-clustering blood cells after removing embryonic mesoderm reveals two distinct populations of extraembryonic tissues consisting of yolk sac endothelium and an active blood-producing hematoendothelial lineage. (D and E) Marking cells by genotype on UMAP projections (D) revealed that mutant cells (orange) are enriched within the endothelial population and dis-enriched in blood populations compared to Wt controls (blue); this is confirmed by cell proportion graphs (E).

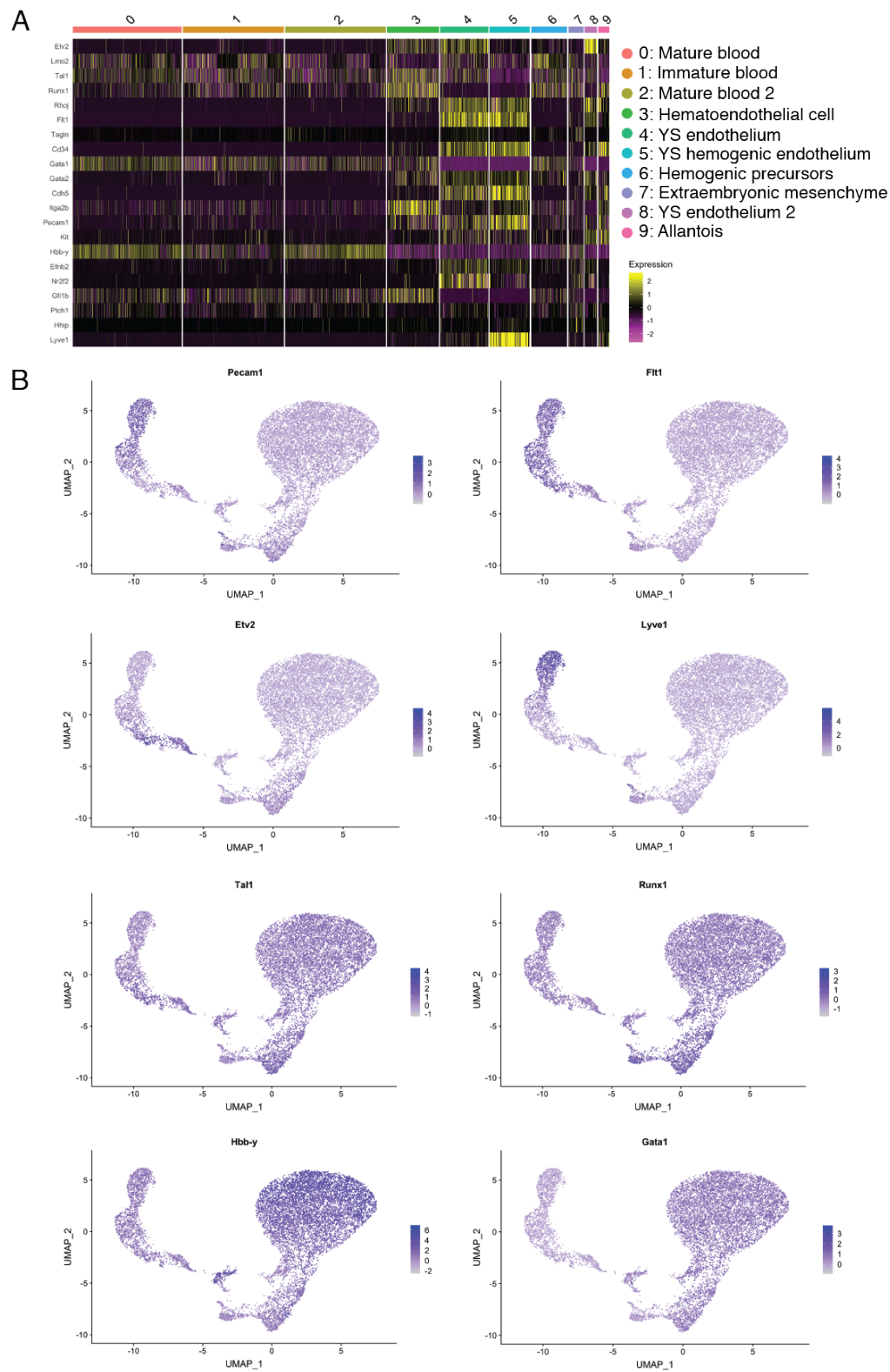


Fig. 4.3. Specific sub-lineages for blood development are identified by expression of canonical markers. (A) Heatmap for gene expression in single cells revealed discrete gene expression

(Fig. 4.3, Continued)

differences between clusters representing three general cell types including endothelium, hemogenic endothelium, and embryonic blood. (B) Heatmaps for individual gene expression confirmed this finding however general cell-type markers do not explain the left-right bifurcation of cells across the UMAP1 axis. Expression of general endothelial genes *Pecam1*, *Flt1*, and *Etv2* are represented in both branches while a marker specific to definitive YS hemogenic endothelium, *Lyve1*, is only represented on the left branch. By exclusion, the right branch is likely to represent early hemogenic precursors from first wave hematopoiesis which are the first cells to produce blood in the embryo. These cells express general hemogenic endothelium markers such as *Tall* and selectively express *Runx1* which is a known marker of hematoendothelial cells. Finally, only right-branch lineages significantly express *Gata1* and *Hbb-y* which represent maturing and mature erythrocytes respectively.

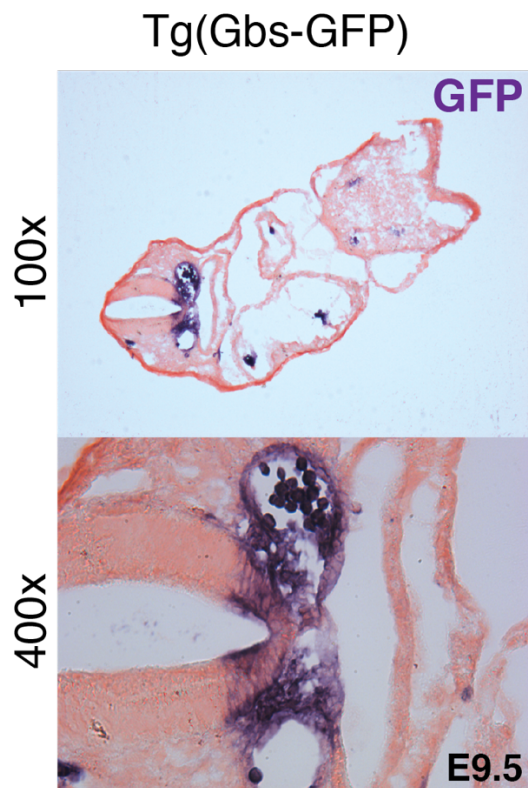


Fig. S4.1. Transverse embryo section displaying ISH for GFP expressed under a Hh-dependent reporter allele. Staining of a Hh-dependent reporter transgene in transverse sections of otherwise wild-type E9.5 embryos.

CHAPTER 5: SYNTHESIS AND FUTURE DIRECTIONS

A new role for Hh signaling in A-P Patterning

Although Hh signaling has been shown to be necessary for the patterning of diverse tissues in mammals, it has not been previously shown to pattern the A-P axis. In this study, I identified a major mechanism for anterior-specific developmental defects, which involves the Hh dependence of *Fgf4/8* signaling to drive the genesis and morphogenetic movements of the nascent mesoderm during gastrulation. Additionally, I found that a critical subset of genes for anterior mesoderm development are Hh-dependent in the mesoderm of the early mouse gastrula. Genes such as *Hnf3 β* (*FoxA2*), and *Brachyury* (*T*) are downregulated in early Hh mutants and are critically important for the formation of embryonic organizers that drive the development of anterior mesoderm (1-3). This suggests that Hh signaling may be an upstream component in a general pathway for coordinating anterior mesoderm morphogenesis and furthermore, may be a signaling component for a classic embryonic organizer.

Much of A-P axis determination and patterning is determined by embryonic organizers

The first mention of an embryonic organizer was by Victor Henson who noted the ability of the leading edge of the primitive streak to organize tissues around itself (4). Perhaps the first mechanistic experiment to address axis formation and patterning in vertebrates was performed by Spemann and Mangold where they identified a cluster of cells in amphibian embryos that could induce ectopic axis in orthografts (5). Since the discovery of this gastrula organizer, similar Spemann-Mangold-type organizers were discovered in other amphibians along with analogous structures such as the 'shield' in zebrafish (6, 7). The organization of the mammalian embryonic axis however, has been a more contentious topic due in part to the baked-in difficulties of internal

fertilization which made embryos inaccessible to classic transplantation/explantation experiments until the development of modern ex-vivo embryonic culture systems (8). Even then, fundamental limitations to the length of time mouse embryos can be cultured successfully constrain the developmental windows open to be assayed.

To make matters more difficult, murine tissues with organizing capability behave in a manner unconventional to most classic models. For instance, the mouse node, which bears morphologic resemblance to Hensen's node in the chick, does not in itself suffice to induce anterior neuroectoderm markers at ectopic sites in orthotopic transplantation experiments (9). However, additional transient embryonic organizers were identified in the posterior midline of the embryo during early to mid-gastrulation and were identified as the early gastrula organizer (EGO) and mid-gastrula organizer (MGO) respectively (10). Interestingly, although both organizers occupy the same relative posterior-midline embryonic position immediately distal to the advancing primitive streak, they have different organizing potential. While the MGO alone has been shown to induce ectopic neuroectoderm fates, the EGO requires co-transplantation of the primitive streak, anterior epiblast, and anterior visceral endoderm to achieve the same end (11). Needless to say, the specification of axes requires the communication of many tissues expressing genes in a spatiotemporally restricted manner.

In addition to axis formation, embryonic organizers play a role in axis patterning. For example, physical resection of the mouse node at late gastrulation causes failure to establish asymmetry across the L-R axis although supposedly leaves the A-P axis intact as anterior neuroectoderm markers continue to be expressed (12). Although the A-P axis itself was established, it was not determined whether the distribution of tissues across the A-P axis was effected due to short time course of development post-resection, the lack of sagittal histology, and the near

singular focus on L-R patterning (12). In order to determine the necessity of this tissue on A-P axis patterning, closer attention must be paid to anterior-specific gene expression and organ formation.

Genetic ablations of the node have arguably yielded far more useful information as to its role in embryonic patterning. For instance, deletion of *Foxa2* results in the absence of axial tissues including the node and notochord in conjunction with severe deficits to anterior mesoderm formation—although anterior axis formation is not completely lost due to the preservation of certain anterior neuroectoderm markers (2, 3). Additional genes such as *Mixl1* and *Tdgl1* also result in node agnesis concomitant with selective defects to anterior tissue development (13, 14). These data suggest that not only is A-P patterning more sensitive to perturbation, but also that the node likely plays a critical role in this process.

The question then stands as to how the node, which is comprised of few cells and contributes to relatively few adult tissues, exerts patterning information on nascent tissues arising from the primitive streak. This must require some communication with tissues in the primitive streak, which are actively involved with the generation and migratory potential of nascent mesendoderm. In chapter 3, I identified a crucial link between these two tissues where Hh pathway activity in the node seems to exert influence over the *Fgf4/8* migratory pathway within the primitive streak. Although many studies have identified factors that influence both node and primitive streak function, unlike the studies I present in chapter 3 concerning the role of Hh signaling exclusively in the node, all other extant studies involve genes that are expressed in both the primitive streak and the node (15, 16)—making it impossible to definitively answer whether their effect on anterior structure development is the result of direct action within primitive streak or through tissue communication between the node and primitive streak.

The Nodal and Hh pathways have shared function in A-P patterning

One way to go about studying the intersection of influences from the node and primitive streak on anterior mesoderm morphogenesis is to identify genes that are 1) expressed in the node and 2) produce anterior-specific mesoderm defects in loss-of-function experiments. Although several candidate pathways fulfill this requirement, the Nodal pathway is by far the most represented in the literature (16). Through deletion of various pathway components, it has been shown that the most severe mutants completely fail to generate mesoderm while moderate mutants have anterior lineage truncations and mild pathway mutants reveal selective defects to the anterior mesoderm relative to posterior mesoderm (16-18). Interestingly, although most Nodal pathway components do not seem to be downregulated in Hh mutant mesoderm, there does seem to be a shared downstream network between both pathways consisting of *FoxA2*, *T*, *Tdgf1*, and *Fgf4* (17, 19-21). Furthermore, the Hh and Nodal pathways intersect within the node during the onset of anterior mesoderm migration and activate similar downstream genes. This reveals the potential for a shared downstream network between the Hh and Nodal pathways in embryonic midline for mesoderm allocation across the A-P axis.

Although there is only mild evidence that Hh signaling directly regulates *Nodal* itself (22), Hh signaling may be directly upstream of downstream of Nodal pathway components that modulate the level of Nodal pathway activity (23, 24). In E7.5 *Mesp1-Gli3R* mutants, both *Tdgf1* and *Smad3* are significantly dysregulated (FDR \leq 0.10) where both genes produce anterior mesoderm defects of varying severity (Fig. 3.4). TDGF1 is a co-receptor for NODAL ligand and greatly increases downstream pathway signal transduction while SMAD3 acts as an important transcriptional co-activator in the nucleus (18, 23). Another mechanism for Hh and nodal pathway interaction may be through a shared genetic network for mesoderm formation downstream of both

Hh and Nodal signaling. In Chapter 3, I found that a primary explanation for the role of Hh signaling anterior mesoderm patterning was through an *Fgf4/8* signaling pathway for cell migration during gastrulation. *Fgf4* is a common downstream target of both pathways as is *T*, which is part of a well-described positive feedback loop for *Fgf8* expression (25-29). Based on gene expression alone this may describe a shared role of Nodal and Hh signaling for anterior mesoderm migration.

One pressing question is whether Nodal signaling shares a common developmental mechanism with Hh signaling for anterior mesoderm development. In Zebrafish it was recently identified that a novel signaling event through the *toddler-apelin* pathway drives mesendoderm cell migration during gastrulation and functions downstream of Nodal signaling (30, 31). However, the role for directing cell movements in mammalian gastrulation is far less clear. One study attempted to address this by creating chimeric mouse embryos by injecting labeled *Nodal*^{-/-} stem cells into unlabeled Wt blastocysts and analyzing the resultant cell fates. Due to *Nodal*'s selective role in directing anterior mesoderm formation, it was hypothesized that cells lacking *Nodal* would demonstrate insufficient contribution to anterior tissues—however, *Nodal*^{-/-} cells preferentially populated the anterior embryonic pole after gastrulation (17). It may still be possible that *Nodal* does have an impact on influencing anterior mesoderm development through control of migration but likely involves more complex regulation than originally conceived.

Finally, shared pathway interaction between Hh and nodal signaling may be mediated through the proper formation and function of the axial mesoderm. Hh pathway activity, *Nodal*, *T*, and *FoxA2* are all localized to the node (2, 3, 21, 32). Interestingly, deletion of *Smo* and perturbations to Nodal signaling through conditional deletion of *Nodal* or *Smad3* in the posterior streak does not eliminate the formation of axial organizers such as the node or notochord yet causes

anterior-specific phenotypes and perturbs the expression of *FoxA2* and *T(17, 18, 21, 33, 34)*. *FoxA2* and *T* are required for the formation of both anterior mesoderm and axial tissues where deletions to *T* interrupt node and notochord formation and deletions to *FoxA2* result in complete agenesis (2, 3, 35, 36). Additionally, development of axial mesoderm itself appears to be responsible for anterior mesoderm development as *Mix11*^{-/-} mutants fail to form axial mesoderm and display severe anterior mesoderm defects independent of Hh or Nodal pathways (14). In summary, it appears that upstream signaling from Hh or Nodal pathways may induce anterior-specific defects by blunting important gene expression within the axial mesoderm while shared downstream genes control anterior mesoderm development through the proper development of the axial mesoderm tissues.

Differential roles for Hh signaling in embryonic and extraembryonic mesoderm development

One lingering question is whether Hh signaling functions through separate mechanisms for extraembryonic and embryonic mesoderm formation. Although both tissues derive from cells that migrate through the primitive streak during gastrulation, they arise from spatiotemporally distinct populations within the epiblast (37, 38). Additionally, it has been shown that the generation of these two populations of cells does not necessarily share the same gene network for gastrulation. For example, disruptions to Nodal signaling through *Tdglf1* deletion severely affect embryonic mesoderm formation while extraembryonic structures such as the allantois and yolk sac are preserved (39).

Although the detection of blood defects by RNA-seq is delayed compared to the detection of defects to the embryonic mesoderm, it is entirely possible that the defects to gastrulation may

also influence the development in extraembryonic tissues. For example, blood and endothelial defects seem to be more severe in *Smo*^{-/-} and *Ihh*^{-/-};*Shh*^{-/-} mutants, which have impaired gastrulation, compared to *Ihh*^{-/-} embryos which have milder blood defects and unimpeded gastrulation despite *Ihh* being the only ligand expressed in the yolk sac (22, 40-42). However, my analysis of single-cell RNA-seq from E8.25 *Mesp1-Gli3R* mutants revealed an increase of Runx1+ hematoendothelial precursors relative to *Mesp1-tdTomato* controls, which are generated directly from gastrulation during first wave hematopoiesis. This suggests that either the dysfunction to gastrulation eventually affects the ability of hemogenic precursors to differentiate into erythrocytes days later in development, or that *Shh* is able to compensate for a loss of *Ihh* signaling in the yolk sac during blood development. Due to the technical challenges of parsing between these two scenarios, I focused my studies on the role of Hh signaling in endothelial and hemogenic precursor development as it relates to the differentiation of erythrocytes.

The role of Hh signaling in blood and endothelial development

Endothelial precursors, called angioblasts, migrate to the extraembryonic tissues of the yolk sac during gastrulation around the same time that the first hemogenic precursors emerge (43). Both populations share common developmental ontogeny and gene expression which was originally interpreted to mean that these lineages shared a common bipotential progenitor called the hemangioblast (44, 45). Although the hemangioblast was postulated decades earlier, the first experimental evidence to give credence to its existence was derived from *in vitro* differentiation experiments (44-47). Despite decades of work, this cell type was never isolated *in vivo* and through various fate maps it was shown that the closest identified common progenitor was a cell type that was competent to give rise to additional mesoderm lineages such as smooth muscle (48, 49).

Additionally, careful fate mapping of the nascent mesoderm identified discrete populations in the primitive streak that give rise to either endothelial cells or blood cells, but not both (43).

The role of Hh signaling in vertebrate vascular endothelial development is perhaps best studied in the context of the yolk sac. Early studies revealed that *Ihh* ligand was expressed by the extraembryonic endoderm and received by the nascent extraembryonic mesoderm during gastrulation as evidence by *Ptch1* expression (40, 50). The absence of either extraembryonic endoderm or Hh pathway activity revealed profound defects within the vascular mesoderm where vascular reorganization was severely impaired (51, 52). Additionally, it was shown that vascular reorganization could be sufficiently induced through the re-introduction of Hh ligand to angioblasts (51). Although Hh-dependent vessel remodeling defects are observed concomitant with embryonic anemia, it should be noted that the yolk sac vascular bed is fully formed through neovasculogenesis in early Hh mutants but fails to undergo further angiogenic remodeling (40, 53).

Despite the uninterrupted specification of the vascular endothelium, one study postulated that disruption to Hh signaling resulted in blood defects secondary to the failure to specify endothelium and hemogenic endothelium (54). Although this study demonstrated severe effects to blood differentiation *in vitro*, defects to either endothelium or hemogenic endothelium were modest. Additionally, the authors' own *in vivo* data from zebrafish partially contradict the main claims of their paper as note that Hh inhibition through cyclopamine disrupted arterial specification of the dorsal aorta but preserved *Runx1*+ hemogenic endothelial cell populations. This reinforced the importance of Hh signaling in endothelial function but not to the specification of hemogenic endothelium (54). This result is more in-line with my *in vivo* mouse data where the specification

of endothelial lineages are either unaffected or increased despite the presence of an anemic phenotype.

In summary, Hh signaling seems to be critical to the formation of organized vascular development through angiogenesis in the early blood-forming tissues. Although the current dogma states that the role of Hh signaling in early blood development is inextricably linked to its role in blood development, there does not appear to be a definitive link between endothelial tube in the early vascular system and blood development independent of Hh signaling.

Alternative links between Hh signaling, endothelial development, and erythrocyte differentiation.

There does seem to be a surprising link between the vascular developmental phenotypes of Hh mutants and those of embryos with phenotypes that impaired blood flow. Embryos with deletions to the gene *Mlc2a* result in impaired circulation due to contractile deficiencies of the primitive heart tube are capable of forming the primitive bed of vascular endothelium within the early yolk sac yet fail to undergo angiogenic remodeling at E9.5 (55). Although the obvious link between Hh pathway and *Mlc2a* mutants is the impairment of early embryonic circulation due to cardiac dysfunction, it has also been clearly demonstrated that Hh signaling acts independent of blood flow to induce angiogenic remodeling of yolk sac vasculature (56).

It unlikely that shear forces caused by circulation in the yolk sac activate the Hh pathway directly due to the uniform expression pattern of *Ihh* in Hh-sending tissues within the yolk sac which precede the onset of circulation (50). However, Hh signaling and shear stresses may work through a common pathway to arrange the embryonic vasculature. Yolk sac vessel remodeling seems to be dependent upon the activation of the eNOS pathway which works in concert with the

Vegf pathway for angiogenesis (57). There has also been past evidence demonstrating the direct action of Hh signaling on the Vegf pathway through modulating the expression of the ligand *Vegfa* (51, 58-60).

While the Vegf pathway is best known for its role in angiogenesis, it plays a lesser known role in hematopoiesis during early embryogenesis (61, 62). In zebrafish, it has been shown that Vegf pathway activity has a positive effect erythrocyte production during embryonic hematopoiesis (61). Although bulk E8.5 RNA-seq in my study didn't identify disruptions to *Vegfa* expression in E8.5 *Mesp1-Gli3R* embryos, this data was derived from embryonic tissue while the majority of blood production is relegated to the extraembryonic yolk sac at this developmental stage (47). Furthermore, disrupted Vegf signaling in Hh mutants would explain the fact that both angiogenesis and blood differentiation are disrupted while preserving the initial specification of both hemogenic and non-hemogenic endothelium.

Conclusion and Future Directions

The Hh signaling pathway is one of the most well known in development and yet there is still much to be learned about its ability to pattern and specify tissues within the early embryo. Perhaps the most well-known function of the pathway is the ability to pattern tissues across their axes (63-65). In this thesis, I have presented evidence that Hh signaling from the node in gastrulating embryos is a major factor in determining A-P patterning. Additionally, I discovered a mechanism for Hh signaling for blood development in the yolk sac.

One of the most exciting prospects of this work is that it opens the possibility to find a common gene regulatory network for A-P patterning within a classic embryonic organizer, the mammalian node. Although the node has been well studied in its role as an organizer of the L-R

axis, its role in determining the A-P axis has been largely ignored and presents ample opportunity for further study. Several genes arise as obvious candidates for A-P patterning from the node including *Foxa2*, *T*, *Mixl1*, and multiple members of the Nodal pathway including: *Nodal*, *Smad2/3*, *Tdgf1*, and *FoxH1*—all of which have overlapping expression domains in the node (2, 3, 14, 20, 21, 32). Hh signaling is likely not upstream of *Nodal* expression itself yet two downstream genes, *Tdgf1* and *Smad3*, are viable candidates for direct regulation by Hh signaling since they are downregulated within the mesoderm in *Mesp1-Gli3R* mutants.

One major challenge in proving direct targets for Hh signaling in the node is the tissue-input limitation of chromatin assays such as ChIP-seq which ideally require millions of cells (66). Recently, a new Assay for Transposase-Accessible Chromatin (ATAC)-seq was scaled down for single-cell measurements yet the ability to find TF-specific binding events at this input level is yet to be achieved (67, 68). Mouse Embryonic Stem Cells (mESCs) can be utilized to model the role of Hh signaling in early embryogenesis and overcome tissue input limitations of various assays yet they do not endogenously experience active Hh signaling throughout mesoderm induction (69). Additionally, these cells are recalcitrant to exogenous pathway activation through SHH and small molecule Smoothed agonists. Bypassing upstream signaling by expressing activating Hh-dependent TFs such as Gli1 during mesoderm development is a potential option to overcome this technical challenge yet introduces the caveat that overexpression systems introduce ectopic binding events that are not present *in vivo*.

Another, perhaps more fruitful approach would be to look for pathway interdependence for A-P patterning through genetic interaction studies. The requirement for Hh and Nodal pathways in A-P patterning can be studied through progressive loss of function allelic series mutants using extant mouse lines. For one, *Mox^{Cre}* can conditionally delete Hh or Nodal pathway genes from the

epiblast to produce hypomorphic signaling from either or both pathways (17). Additionally, both *Nodal*^{+/-} and *Smo*^{+/-} mutants have been shown to provide effective sensitized backgrounds in genetic interaction studies (24, 70). It would be interesting to first confirm whether Nodal and Hh signaling share a common mechanism for A-P patterning—for example by observing whether *Smo*^{-/-};*Nodal*^{+/-} embryos demonstrate a worsened anterior phenotype compared to *Smo*^{-/-} embryos. Additionally, putative downstream pathway components such as *FoxA2* or *T* can be analyzed by creating heterozygous null mutants on sensitized backgrounds lacking portions of the Hh or Nodal pathways.

Genetic interaction studies may also uncover whether the Hh-dependent defects to both the embryonic and extraembryonic mesoderm share a common mechanism. Although Hh-mutants demonstrate clear defects to erythrocyte production, the phenotype is not completely penetrant and can be exacerbated by perturbing additional genes in a common pathway. If there is a common pathway for the development of both tissues, it would be most interesting to test whether genetic interactions disrupt erythrocyte differentiation from both first and second wave hematopoiesis, as seems to be the case in Hh mutants, or if there is a disparate effect on the two processes.

Lastly, it has been known for many decades that *Smo*^{-/-} and *Shh*^{-/-};*Ihh*^{-/-} mutants produce vastly different phenotypes than individual ligand knockouts (22, 41). However, there has been a failure to investigate this phenomenon beyond defects to L-R patterning and endothelial tube formation. Through extensive phenotyping and an array of independent assays, I have shown that these defects stem primarily from improper gastrulation due to signaling dysfunction for the development of both embryonic and extraembryonic mesoderm. Additionally, these studies may implicate a general mechanism for anterior axis patterning through the action of a conserved signaling network within the embryonic midline.

REFERENCES

1. Beddington RSP, Rashbass P, & Wilson V (1992) Brachyury - a Gene Affecting Mouse Gastrulation and Early Organogenesis. *Development*:157-165.
2. Ang SL & Rossant J (1994) HNF-3 beta is essential for node and notochord formation in mouse development. *Cell* 78(4):561-574.
3. Weinstein DC, *et al.* (1994) The winged-helix transcription factor HNF-3 beta is required for notochord development in the mouse embryo. *Cell* 78(4):575-588.
4. Selleck MA & Stern CD (1991) Fate mapping and cell lineage analysis of Hensen's node in the chick embryo. *Development* 112(2):615-626.
5. Spemann H & Mangold H (2001) Induction of embryonic primordia by implantation of organizers from a different species. 1923. *Int J Dev Biol* 45(1):13-38.
6. Shih J & Fraser SE (1996) Characterizing the zebrafish organizer: microsurgical analysis at the early-shield stage. *Development* 122(4):1313-1322.
7. De Robertis EM (2006) Spemann's organizer and self-regulation in amphibian embryos. *Nat Rev Mol Cell Biol* 7(4):296-302.
8. Hsu YC (1979) In vitro development of individually cultured whole mouse embryos from blastocyst to early somite stage. *Dev Biol* 68(2):453-461.
9. Beddington RS (1994) Induction of a second neural axis by the mouse node. *Development* 120(3):613-620.
10. Robb L & Tam PP (2004) Gastrula organiser and embryonic patterning in the mouse. *Semin Cell Dev Biol* 15(5):543-554.
11. Tam PP & Steiner KA (1999) Anterior patterning by synergistic activity of the early gastrula organizer and the anterior germ layer tissues of the mouse embryo. *Development* 126(22):5171-5179.
12. Davidson BP, Kinder SJ, Steiner K, Schoenwolf GC, & Tam PP (1999) Impact of node ablation on the morphogenesis of the body axis and the lateral asymmetry of the mouse embryo during early organogenesis. *Dev Biol* 211(1):11-26.
13. Ding J, *et al.* (1998) Cripto is required for correct orientation of the anterior-posterior axis in the mouse embryo. *Nature* 395(6703):702-707.
14. Hart AH, *et al.* (2002) Mix11 is required for axial mesendoderm morphogenesis and patterning in the murine embryo. *Development* 129(15):3597-3608.
15. Arnold SJ & Robertson EJ (2009) Making a commitment: cell lineage allocation and axis patterning in the early mouse embryo. *Nat Rev Mol Cell Biol* 10(2):91-103.
16. Tam PP & Loebel DA (2007) Gene function in mouse embryogenesis: get set for gastrulation. *Nat Rev Genet* 8(5):368-381.
17. Lu CC & Robertson EJ (2004) Multiple roles for Nodal in the epiblast of the mouse embryo in the establishment of anterior-posterior patterning. *Dev Biol* 273(1):149-159.

18. Dunn NR, Vincent SD, Oxburgh L, Robertson EJ, & Bikoff EK (2004) Combinatorial activities of Smad2 and Smad3 regulate mesoderm formation and patterning in the mouse embryo. *Development* 131(8):1717-1728.
19. Perea-Gomez A, *et al.* (2002) Nodal antagonists in the anterior visceral endoderm prevent the formation of multiple primitive streaks. *Dev Cell* 3(5):745-756.
20. Yamamoto M, *et al.* (2001) The transcription factor FoxH1 (FAST) mediates Nodal signaling during anterior-posterior patterning and node formation in the mouse. *Genes Dev* 15(10):1242-1256.
21. Zhou X, Sasaki H, Lowe L, Hogan BL, & Kuehn MR (1993) Nodal is a novel TGF-beta-like gene expressed in the mouse node during gastrulation. *Nature* 361(6412):543-547.
22. Zhang XM, Ramalho-Santos M, & McMahon AP (2001) Smoothed mutants reveal redundant roles for Shh and Ihh signaling including regulation of L/R symmetry by the mouse node. *Cell* 106(2):781-792.
23. Xu C, Liguori G, Persico MG, & Adamson ED (1999) Abrogation of the Cripto gene in mouse leads to failure of postgastrulation morphogenesis and lack of differentiation of cardiomyocytes. *Development* 126(3):483-494.
24. Waldrip WR, Bikoff EK, Hoodless PA, Wrana JL, & Robertson EJ (1998) Smad2 signaling in extraembryonic tissues determines anterior-posterior polarity of the early mouse embryo. *Cell* 92(6):797-808.
25. Evans AL, *et al.* (2012) Genomic targets of Brachyury (T) in differentiating mouse embryonic stem cells. *PLoS One* 7(3):e33346.
26. Draper BW, Stock DW, & Kimmel CB (2003) Zebrafish fgf24 functions with fgf8 to promote posterior mesodermal development. *Development* 130(19):4639-4654.
27. Griffin KJ & Kimelman D (2003) Interplay between FGF, one-eyed pinhead, and T-box transcription factors during zebrafish posterior development. *Dev Biol* 264(2):456-466.
28. Fletcher RB & Harland RM (2008) The role of FGF signaling in the establishment and maintenance of mesodermal gene expression in *Xenopus*. *Dev Dyn* 237(5):1243-1254.
29. Isaacs HV, Pownall ME, & Slack JM (1994) eFGF regulates Xbra expression during *Xenopus* gastrulation. *EMBO J* 13(19):4469-4481.
30. Norris ML, *et al.* (2017) Toddler signaling regulates mesodermal cell migration downstream of Nodal signaling. *Elife* 6.
31. Pauli A, *et al.* (2014) Toddler: an embryonic signal that promotes cell movement via Apelin receptors. *Science* 343(6172):1248636.
32. Amin S, *et al.* (2016) Cdx and T Brachyury Co-activate Growth Signaling in the Embryonic Axial Progenitor Niche. *Cell Rep* 17(12):3165-3177.
33. Concepcion D, Hamada H, & Papaioannou VE (2018) Tbx6 controls left-right asymmetry through regulation of Gdf1. *Biol Open* 7(5).

34. Conlon FL, *et al.* (1994) A primary requirement for nodal in the formation and maintenance of the primitive streak in the mouse. *Development* 120(7):1919-1928.
35. Showell C, Binder O, & Conlon FL (2004) T-box genes in early embryogenesis. *Dev Dyn* 229(1):201-218.
36. Gruneberg H (1958) Genetical studies on the skeleton of the mouse. XXIII. The development of brachyury and anury. *J Embryol Exp Morphol* 6(3):424-443.
37. Kinder SJ, *et al.* (1999) The orderly allocation of mesodermal cells to the extraembryonic structures and the anteroposterior axis during gastrulation of the mouse embryo. *Development* 126(21):4691-4701.
38. Tam PP, Parameswaran M, Kinder SJ, & Weinberger RP (1997) The allocation of epiblast cells to the embryonic heart and other mesodermal lineages: the role of ingression and tissue movement during gastrulation. *Development* 124(9):1631-1642.
39. Jin JZ, Zhu Y, Warner D, & Ding J (2016) Analysis of extraembryonic mesodermal structure formation in the absence of morphological primitive streak. *Dev Growth Differ* 58(6):522-529.
40. Byrd N, *et al.* (2002) Hedgehog is required for murine yolk sac angiogenesis. *Development* 129(2):361-372.
41. Astorga J & Carlsson P (2007) Hedgehog induction of murine vasculogenesis is mediated by Foxf1 and Bmp4. *Development* 134(20):3753-3761.
42. Tsukui T, *et al.* (1999) Multiple left-right asymmetry defects in Shh(-/-) mutant mice unveil a convergence of the shh and retinoic acid pathways in the control of Lefty-1. *Proc Natl Acad Sci U S A* 96(20):11376-11381.
43. Padron-Barthe L, *et al.* (2014) Clonal analysis identifies hemogenic endothelium as the source of the blood-endothelial common lineage in the mouse embryo. *Blood* 124(16):2523-2532.
44. Choi K (2002) The hemangioblast: a common progenitor of hematopoietic and endothelial cells. *J Hematother Stem Cell Res* 11(1):91-101.
45. Robb L & Elefanty AG (1998) The hemangioblast--an elusive cell captured in culture. *Bioessays* 20(8):611-614.
46. Wang H, Zhuang Z, & Chan CC (2018) Hemangioblast: origin of hemangioblastoma in von Hippel-Lindau (VHL) syndrome. *Oncoscience* 5(7-8):212-213.
47. Lacaud G & Kouskoff V (2017) Hemangioblast, hemogenic endothelium, and primitive versus definitive hematopoiesis. *Exp Hematol* 49:19-24.
48. Azzoni E, *et al.* (2014) Hemogenic endothelium generates mesoangioblasts that contribute to several mesodermal lineages in vivo. *Development* 141(9):1821-1834.
49. Nishikawa S (2012) Hemangioblast: an in vitro phantom. *Wiley Interdiscip Rev Dev Biol* 1(4):603-608.

50. Dyer MA, Farrington SM, Mohn D, Munday JR, & Baron MH (2001) Indian hedgehog activates hematopoiesis and vasculogenesis and can respecify prospective neurectodermal cell fate in the mouse embryo. *Development* 128(10):1717-1730.
51. Vokes SA, *et al.* (2004) Hedgehog signaling is essential for endothelial tube formation during vasculogenesis. *Development* 131(17):4371-4380.
52. Vokes SA & Krieg PA (2002) Endoderm is required for vascular endothelial tube formation, but not for angioblast specification. *Development* 129(3):775-785.
53. Byrd N & Grabel L (2004) Hedgehog signaling in murine vasculogenesis and angiogenesis. *Trends Cardiovasc Med* 14(8):308-313.
54. Kim PG, *et al.* (2013) Signaling axis involving Hedgehog, Notch, and Scl promotes the embryonic endothelial-to-hematopoietic transition. *Proc Natl Acad Sci U S A* 110(2):E141-150.
55. Lucitti JL, *et al.* (2007) Vascular remodeling of the mouse yolk sac requires hemodynamic force. *Development* 134(18):3317-3326.
56. Nagase M, Nagase T, Koshima I, & Fujita T (2006) Critical time window of hedgehog-dependent angiogenesis in murine yolk sac. *Microvasc Res* 71(2):85-90.
57. Kroll J & Waltenberger J (1998) VEGF-A induces expression of eNOS and iNOS in endothelial cells via VEGF receptor-2 (KDR). *Biochem Biophys Res Commun* 252(3):743-746.
58. Pinter M, *et al.* (2013) Hedgehog inhibition reduces angiogenesis by downregulation of tumoral VEGF-A expression in hepatocellular carcinoma. *United European Gastroenterol J* 1(4):265-275.
59. Chen W, *et al.* (2011) Canonical hedgehog signaling augments tumor angiogenesis by induction of VEGF-A in stromal perivascular cells. *Proc Natl Acad Sci U S A* 108(23):9589-9594.
60. Lawson ND, Vogel AM, & Weinstein BM (2002) sonic hedgehog and vascular endothelial growth factor act upstream of the Notch pathway during arterial endothelial differentiation. *Dev Cell* 3(1):127-136.
61. Liang D, *et al.* (2001) The role of vascular endothelial growth factor (VEGF) in vasculogenesis, angiogenesis, and hematopoiesis in zebrafish development. *Mech Dev* 108(1-2):29-43.
62. Gerber HP & Ferrara N (2003) The role of VEGF in normal and neoplastic hematopoiesis. *J Mol Med (Berl)* 81(1):20-31.
63. Briscoe J & Therond PP (2013) The mechanisms of Hedgehog signalling and its roles in development and disease. *Nat Rev Mol Cell Biol* 14(7):416-429.
64. Robbins DJ, Fei DL, & Riobo NA (2012) The Hedgehog signal transduction network. *Sci Signal* 5(246):re6.
65. Ingham PW & Placzek M (2006) Orchestrating ontogenesis: variations on a theme by sonic hedgehog. *Nat Rev Genet* 7(11):841-850.

66. Park PJ (2009) ChIP-seq: advantages and challenges of a maturing technology. *Nat Rev Genet* 10(10):669-680.
67. Stuart T, *et al.* (2019) Comprehensive Integration of Single-Cell Data. *Cell* 177(7):1888-1902 e1821.
68. Buenrostro JD, Giresi PG, Zaba LC, Chang HY, & Greenleaf WJ (2013) Transposition of native chromatin for fast and sensitive epigenomic profiling of open chromatin, DNA-binding proteins and nucleosome position. *Nat Methods* 10(12):1213-1218.
69. Rowton M, *et al.* (2018) Hedgehog signaling controls progenitor differentiation timing during heart development. *bioRxiv*.
70. Xie L, *et al.* (2012) Tbx5-hedgehog molecular networks are essential in the second heart field for atrial septation. *Dev Cell* 23(2):280-291.